





This is to certify that the  
 dissertation entitled  
 SPECTROSCOPIC AND COMPUTATIONAL STUDIES OF THE EFFECTS OF INTERMOLECULAR  
 INTERACTIONS AND VIBRATIONAL ENERGY TRANSFER ON THE OPTICAL RESPONSE  
 OF LARGE CHROMOPHORES IN SOLUTION  
 presented by  
 Patty K McCarthy

has been accepted towards fulfillment  
 of the requirements for  
 Ph. D. degree in Chemistry

  
 Major professor

Date 11/18/96

**PLACE IN RETURN BOX to remove this checkout from your record.  
TO AVOID FINES return on or before date due.**

<b>DATE DUE</b>	<b>DATE DUE</b>	<b>DATE DUE</b>
_____	_____	_____
_____	_____	_____
_____	_____	_____
_____	_____	_____
_____	_____	_____
_____	_____	_____
_____	_____	_____

**MSU is An Affirmative Action/Equal Opportunity Institution**

c:\cric\datedue.pm3-p.

**SPECTROSCOPIC AND COMPUTATIONAL STUDIES OF THE EFFECTS OF  
INTERMOLECULAR INTERACTIONS AND VIBRATIONAL ENERGY TRANSFER  
ON THE OPTICAL RESPONSE OF LARGE CHROMOPHORES IN SOLUTION**

**By**

**Patty K McCarthy**

**A DISSERTATION**

**Submitted to  
Michigan State University  
in partial fulfillment of the requirements  
for the degree of**

**DOCTOR OF PHILOSOPHY**

**Department of Chemistry**

**1996**

## ABSTRACT

### SPECTROSCOPIC AND COMPUTATIONAL STUDIES OF THE EFFECTS OF INTERMOLECULAR INTERACTIONS AND VIBRATIONAL ENERGY TRANSFER ON THE OPTICAL RESPONSE OF LARGE CHROMOPHORES IN SOLUTION

By

Patty K McCarthy

A key step in developing predictive power over reaction mechanisms and macroscopic properties of solutions and materials is to understand how dissimilar molecules interact with one another. One means to characterize this interaction is by observing the transfer of energy between donor and acceptor molecules that comprise the system. The energy transfer process is related to the interactive distance of the donor and acceptor species, the IR vibrational optical and electronic responses and the dielectric response of any intervening medium. In addition, the donor and acceptor relative orientations determine the efficiency of energy transfer and, in the liquid phase, the orientational distribution sampled by such processes is assumed to be random. For electronic energy transfer this assumption is typically valid because of the characteristically large distances over which such processes proceed. For vibrational energy transfer, however, this is not necessarily the case. We monitored the degenerate vibrational energy transfer from the  $\sim 1370\text{ cm}^{-1}$  solute (donor) ring distortion modes of perylene, 1-methylperylene, and tetracene to the  $1378\text{ cm}^{-1}$  solvent acceptor  $\text{CH}_3$  rocking modes of alkanes and alkenes using an ultrafast stimulated emission pump-probe laser spectroscopic technique. Three series of donor and acceptor species were utilized to determine the

dependence of vibrational energy transfer efficiency on solvent aliphatic chain length (inter-acceptor spacing), acceptor density, donor-acceptor molecular alignment, coupling mechanism, and detuning effects. These data point to the central role of solvent local organization about solutes in defining the efficiency of energy transfer events.

The observed optical response of a system is influenced not only by intermolecular interactions but also by the intramolecular characteristics of the probe molecule. Using AM1 semi-empirical calculations, the dependence of the former two properties on substituent group identity, placement and geometry were investigated for family of substituted coumarins. Experimentally, the transient spectral shift behavior of coumarin 153 in a series of polar solvents was interrogated using ultrafast spontaneous emission spectroscopy. Since coumarin 153 exhibits an excitation energy dependence as well as a dynamic Stokes shift, there are multiple excited electronic states within the spontaneous emission envelope that contribute to the measured dynamics. This complexity, indicated by experiment and calculation, renders these derivatives inappropriate for direct examination of solvation dynamics. Comparing the results of experimental and computational methods, an understanding of cyanine photoisomerization has been achieved for two cyanine molecules 3,3'-diethylthiadicarbocyanine iodide (DTDCI) and 3,3'-diethyloxadicarbocyanine iodide (DODCI). Although these species are similar in structure, differing only in the presence of an oxygen or sulfur at two heteroatom sites, they yield different equilibrium geometries as inferred from their radiative and nonradiative population relaxation kinetics. The difference in the equilibrium geometries is attributed to steric hindrance in the excited state, caused by the oxygen and sulfur heteroatoms, as predicted by calculations of the isomerization coordinate and verified by experiment.

**To Dad, Mom, Tamie, and Corky:  
for helping me through both the good and the bad times.**

## ACKNOWLEDGMENTS

Over the course of four years I have seen many people come and go. Those of you who have played an important role in my life and education deserve recognition. First of all, I would like to thank Professor Gary J. Blanchard for providing substantial insight and patience as I expanded my intellect. I would also like to thank the Blanchard group members with whom I have worked over the years: Selezion, Ying, Wendy, Jennifer, Joe, Sandjaja, Scott, Punit, Dave, and Jeff. I would also like to thank my committee members for giving me the chance and encouragement to prove myself: Professors Marcos Dantus, Greg Baker, Robert Cukier, and Gerald T. Babcock. Without the wisdom and craftsmanship of the machine shop the majority of my research would not be possible, for this I would like to thank Russell Geyer, Samuel M. Jackson, and Richard Menke for their helpful suggestions and design of several sample mounts. I would also like to thank Dr. Tom Carter and Dr. Long Lee for their insight, expertise, and help in obtaining Raman and NMR spectra, respectively, and Dr. Rui Huang for performing analysis on my “pure” compounds. Of course, without the available funding from the National Science Foundation, Michigan State University Center for Fundamental Materials Research, and Michigan State University College of Natural Science Fellowship (1993), I would not have had sufficient time to reach my goals. Most importantly, I would like to thank Michael Wagner for the encouragement, understanding, and never-ending patience to help

me conquer the rough roads throughout these years. Finally, I would like to express my deepest appreciation to the people that helped me for a few days in June of 1992.

## TABLE OF CONTENTS

LIST OF TABLES	ix
LIST OF FIGURES	xi
CHAPTERS	
I. INTRODUCTION	1
A. Background Information	1
B. References	7
II. EXPERIMENTAL	10
A. Ultrafast Stimulated Spectroscopy	10
1. Experimental Design	10
2. Vibrational Relaxation Measurements	15
3. Rotational Diffusion Measurements	17
B. Steady State Spectroscopies	20
C. References	20
III. SOLVENT METHYL GROUP DENSITY DEPENDENCE OF VIBRATIONAL POPULATION RELAXATION IN 1- METHYLPERYLENE: EVIDENCE FOR SHORT RANGE ORGANIZATION IN BRANCHED ALKANES	22
A. Introduction	22
B. Experimental	23
1. Chemicals and Sample Handling	23
C. Results and Discussion	25
D. Vibrational Population Relaxation Measurements	26
E. Rotational Diffusion Measurements	35
F. Conclusions	38
G. References	40

IV. AN EXPERIMENTAL EXAMINATION OF THE COMPETITION BETWEEN POLAR COUPLING AND LOCAL ORGANIZATION IN DETERMINING VIBRATIONAL POPULATION RELAXATION	42
A. Introduction	42
B. Experimental	43
1. Chemicals and Sample Handling	43
C. Results and Discussion	45
1. Vibrational Relaxation	49
2. Rotational Diffusion Dynamics	55
D. Conclusions	59
E. References	59
V. VIBRATIONAL POPULATION RELAXATION OF TETRACENE IN <i>N</i> -ALKANES. EVIDENCE FOR SHORT-RANGE MOLECULAR ALIGNMENT	62
A. Introduction	62
B. Experimental	62
1. Chemicals and Sample Handling	63
C. Results and Discussion	63
D. Conclusion	76
E. References	77
VI. CAN A CHEMICAL REACTION PROCEED ON A TIMESCALE RELEVANT TO VIBRATIONAL POPULATION RELAXATION? AN EXAMINATION OF 1-METHYLPERYLENE IN ALKENE SOLVENTS	79
A. Abstract	79
B. Introduction	80
C. Experimental	82
1. Time Resolved Spectroscopies	82
2. Steady State Spectroscopies	83
3. Photoreaction Product Studies	83
4. Chemicals and Sample Handling	83
D. Results and Discussion	85
E. Conclusion	96
F. References	97
VII. EVALUATION OF COUMARIN 153 AS A PROBE MOLECULE FOR SOLVATION DYNAMICS STUDIES	101

A. AM1 Study of the Electronic Structure of Coumarins	101
1. Abstract	101
2. Introduction	101
3. Calculations	103
4. Results and Discussion	106
5. Conclusions	119
6. References and Notes	120
B. The Role of Multiple Electronic States in the Dissipative Energy Dynamics of Coumarin 153	122
1. Abstract	122
2. Introduction	122
3. Background	126
A. Spectroscopy of the coumarins	126
B. Transient Stokes Shift Spectroscopies	127
4. Experimental	129
A. Time-Domain Spectroscopies	129
B. Steady State Spectroscopies	130
C. Chemicals and Sample Handling	130
D. Calculations	132
5. Results and Discussion	132
6. Conclusion	151
7. References	152
VIII. PHOTOISOMERIZATION OF CYANINES. A COMPARATIVE STUDY OF OXYGEN- AND SULFUR- CONTAINING SPECIES	156
A. Abstract	156
B. Introduction	156
C. Experimental Results	158
D. Results and Discussion	161
1. DODCI	161
2. DTDCI	167
E. Conclusion	174
F. References and Notes	175
IX. OVERVIEW	178
A. Conclusion	178
BIBLIOGRAPHY	180

## LIST OF TABLES

CHAPTER		PAGE
II.1	Operating wavelength ranges and dye solution recipes, as well as the optimal mirror sets for the dye lasers.	13
III.1	1370cm <sup>-1</sup> mode vibrational relaxation and rotational diffusion times for the 1-methylperylene in alkane solvents. a) Data Book on the Viscosity of Liquids, D. S. Viswanath and G. Natarajan, Hemisphere Publishing Corporation, 1989. b) CRC Handbook of Chemistry and Physics, 71 <sup>st</sup> Edition, 1991, Ed. By D. R. Lide.	29
IV.1	Vibrational population relaxation time constants, T <sub>1</sub> , zero-time anisotropies, R(0), and reorientation time constants, τ <sub>OR</sub> , for perylene and 1-methylperylene in toluene and benzene. T <sub>1</sub> times for perylene are for the ν <sub>7</sub> mode at 1375 cm <sup>-1</sup> and for 1-methylperylene are for the 1370 cm <sup>-1</sup> mode.	50
V.1	T <sub>1</sub> lifetimes of selected tetracene vibrations in <i>n</i> -alkanes. a) Sum of two exponential decays. See text for a discussion of these data.	69
VI.1	Vibrational relaxation, rotational diffusion, and acceptor density for 1-methylperylene 1370 cm <sup>-1</sup> mode in the alkene solvents. * Jiang, Y.; Blanchard, G. J.; <i>J. Phys. Chem.</i> , <b>99</b> , 7904 (1995).	95
VII.A.1	Calculated properties of several coumarins. ΔH <sub>f</sub> is the heat of formation and the quantities μ and the calculated dipole moments for the states indicated. Units are D, (1D = 3.336 x10 <sup>-30</sup> C·m).	107
VII.A.2	Comparison of experimental and calculated 0-0 transition energies. The planar amino group heading refers to a calculation where the amino group dihedral angle with respect to the coumarin ring system was optimized and ~0°. The twisted amino group refers to calculations where a stable conformation of the amino group was at ~90° with respect to the coumarin ring system. Experimental data were taken from:	

	Ernsting, N. P.; Asimov, M.; Schafer, F. P. <i>Chem. Phys. Lett.</i> <b>91</b> , 231 (1982).	110
VII.A.3	Calculated triplet-triplet absorption energies, and the energetic displacement of the T <sub>1</sub> state from the S <sub>0</sub> ground state.	111
VII.A.4	Calculated atomic charges, expressed as decimal fractions of an electron charge, for coumarin 1. The atom numbers corresponding to this table appear in Figure VII.A.3.	113
VII.B.1	Reorientation times of coumarin 153 at two excitation wavelengths. Jiang, Y.; McCarthy, P. K.; Blanchard, G. J.; <i>Chem. Phys.</i> , <b>183</b> , 249 (1994).	142
VII.B.2	Decay and build-up time constants for spontaneous emission data. These times were determined from the data presented in Figures VII.B.5-VII.B.7. N/A indicates that a build-up was not detected or resolvable.	148
VIII.1	Ground state recovery times and stimulated emission decay times for DODCI in 1-propanol and ethylene glycol. The double exponential decay function is given by $f(t) = a_1 \exp\left(-t/\tau_1\right) + a_2 \exp\left(-t/\tau_2\right)$ , $a_1 + a_2 = 1$ . The N/A listed for stimulated emission times indicates the best fit of these data is to a single exponential decay. These data represent averages of six individual determinations of each quantity. For each of the fits to the six determinations, the value of $\chi^2 = \frac{\sum_{i=1}^N (f(x_i) - y_i)^2}{N - n} \leq 10^{-4}.$	166
VIII.2	Ground state recovery times and stimulated emission decay times for DTDCI in 1-propanol and ethylene glycol. The double exponential decay function is the same as given in the caption to Table VIII.1.	169

## LIST OF FIGURES

CHAPTER		PAGE
I.1	a) Electronic energy transfer between two dissimilar molecules. b) Vibrational energy transfer between two dissimilar species, where excitation of the donor vibrational resonance is effected either by a Raman population scheme (1) or a direct absorption approach (2).	2
II.1	Ultrafast stimulated emission laser spectrometer used to measure the vibrational relaxation and rotational diffusion of various chromophore-solvent systems. The time resolution of this system is ~10 ps.	11
II.2	Coupled three-level system depicting the experimental design.	16
II.3	Comparison of oblate and prolate rotor shapes and decay patterns.	19
III.1	Linear absorption and emission spectra of 1-methylperylene in 3-methylhexane.	24
III.2	$T_1$ relaxation times of 1-methylperylene in the $C_7$ alkane homologous series as a function of solvent methyl carbon density.	27
III.3	Atomic displacement vectors for the 1-methylperylene $1370\text{ cm}^{-1}$ mode determined by semi-empirical calculation. The arrows are not indication of the amplitudes of oscillation.	33
III.4	Boiling points of solvents as a function of solvent methyl carbon density. Boiling point data taken from the CRC Handbook of Chemistry and Physics, 71 <sup>st</sup> Edition.	34
III.5	$T_1$ relaxation of the 1-methylperylene $1370\text{ cm}^{-1}$ resonance in the $C_7$ alkane homologous series plotted vs. solvent boiling point. Boiling point data taken from the CRC Handbook of Chemistry and Physics, 71 <sup>st</sup> Edition.	36

III.6	Rotational diffusion time, $\tau_{OR}$ , for 1-methylperylene as a function of solvent methyl group density.	39
IV.1	Absorption and emission spectra of (a) 1-methylperylene in toluene and (b) perylene in toluene	44
IV.2	Experimental pump-probe signal intensity-dependence for $2 \times 10^{-5}$ M perylene in benzene. The probed vibrational resonance is $1375 \text{ cm}^{-1}$ . The instrumental response function is shown with the data. Individual traces have been offset from $\Delta T/T = 0$ for clarity of presentation only. Top trace; $I_{probe} = I_{pump} \sim 10 \text{ mW}$ average power. Second trace from the top; $I_{probe} = 0.1 I_{pump}$ . Third trace; $I_{probe} = 0.01 I_{pump}$ . Fourth (bottom) trace; $I_{probe} = 0.001 I_{pump}$ . While $\Delta T/T$ scale is arbitrary, the signals have not been normalized, and are of the same magnitude for all conditions.	46
IV.3	IR spectra of (a) benzene and (b) toluene.	52
IV.4	Raman spectra of (a) benzene and (b) toluene.	54
IV.5	(a) $I_{  }(t)$ and $I_{\perp}(t)$ and (b) $R(t)$ for 1-methylperylene in toluene.	56
IV.6	(a) $I_{  }(t)$ and $I_{\perp}(t)$ and (b) $R(t)$ for 1-methylperylene in benzene.	57
V.1	Normalized absorption and emission spectra of tetracene in <i>n</i> -nonane. The arrow denotes the 0-0 transition ( $\lambda_{pump}$ ) and the boxed region indicates the spectral region containing the vibrational modes studied here ( $\lambda_{probe}$ ).	64
V.2	Schematic atomic displacements for the vibrational modes studied here. Frequencies and activities are indicated for each mode. The arrows are directional indicators only and are not meant to indicate the amplitudes of the displacements.	66
V.3	$T_1$ times of tetracene as a function of solvent aliphatic chain length. (a) $1383 \text{ cm}^{-1}$ mode, (b) $1293 \text{ cm}^{-1}$ mode, and (c) $1462 \text{ cm}^{-1}$ mode. For the $1462 \text{ cm}^{-1}$ mode, the relaxation behavior in <i>n</i> -hexadecane is anomalous and is not included in the figure. See text for a discussion of this point.	68
V.4	Time scans for tetracene $1462 \text{ cm}^{-1}$ mode in (a) <i>n</i> -dodecane and (b) <i>n</i> -hexadecane. For both measurements the probe laser electric field is oriented at $54.7^\circ$ with respect to the pump laser electric field.	73

VI.1	Absorption and emission spectra of 1-methylperylene in <i>cis</i> -2-heptene.	84
VI.2	a) Absorption spectra of 1-methylperylene in <i>cis</i> -2-heptene at various stages of photoreaction: — 0 minutes, — 25 minutes, ... 36 minutes, --- 49 minutes, ---- 24 hours. b) Absorption spectra of 1-methylperylene in <i>n</i> -heptane at various stages of photoreaction: — 0 minutes, — 15 minutes, ... 30 minutes, -- 80 minutes.	88
VI.3	Solvent dependence of photoreaction products as manifested in the absorption response of the system: • <i>n</i> -heptane, ▲ <i>cis</i> -2-heptene. The absorption bands centered at 425 nm and 325 nm are representative of the 1-methylperylene and 7H-benz[ <i>de</i> ]anthracene chromophores, respectively.	89
VI.4	Reaction mechanism of 1-methylperylene with O <sub>2</sub> and alkene, indicating resonance structures for the radical intermediate and site of alkene photo-addition.	90
VI.5	Changes in the <sup>1</sup> H-NMR spectra of 1-methylperylene (a) before and (b) after the photoreaction. The peak at 2.91 ppm in (a) is the methyl group resonance of 1-methylperylene.	92
VII.A.1	Structures of the coumarin molecules for which AM1 calculations were performed. Only one resonance structure is shown for each molecule. (a) coumarin, (b) coumarin 4, (c) coumarin 138, (d) X = S for coumarin 6, X = NCH <sub>3</sub> for coumarin 30, (e) R = H for coumarin 120, R = F for coumarin 151, (f) R = H for coumarin 102, R <sub>1</sub> = CF <sub>3</sub> for coumarin 152, (g) R <sub>1</sub> = CH <sub>3</sub> and R <sub>2</sub> = H for coumarin 102, R <sub>1</sub> = CF <sub>3</sub> and R <sub>2</sub> = H for coumarin 153, R <sub>1</sub> = H and R <sub>2</sub> = COCH <sub>3</sub> for coumarin 334, R <sub>1</sub> = H and R <sub>2</sub> = CN for coumarin 337, R <sub>1</sub> = H and R <sub>2</sub> = COOH for coumarin 343.	104
VII.A.2.	Comparison of experimental absorption maxima ( <u>Optical Products</u> , <i>Publication JJ-169</i> , Eastman Kodak Co., pp. 12-36.) to the calculated 0-0 transition energies for the coumarins shown in Figure VII.A.1. a = coumarin 153, b = coumarin 337, c = coumarin 6, d = coumarin 343, e = coumarin 334, f = coumarin 152, g = coumarin 102, h = coumarin 151, i = coumarin 30, j = coumarin 138, k = coumarin 1, l = coumarin 120, m = coumarin 4.	108

VII.A.3	Structure and atom number assignment for coumarin 1. Partial charges are given for each atom for the $S_0$ and $S_1$ states in Table VII.A.4.	114
VII.A.4	Calculated energy-dependence of the dimethylamino group rotation for the $S_0$ , $T_1$ and $S_1$ states of coumarin 1. The dihedral angle is the angle made by the amino group with respect to the coumarin chromophore. Missing points indicate a failure of the calculated structure to converge at the given dihedral angle.	117
VII.A.5	Calculated energy-dependence of the benzothiazolyl group rotation for the $S_0$ , $T_1$ and $S_1$ states of coumarin 6. The dihedral angle is for the angle made by the benzothiazolyl group with respect to the coumarin chromophore. Missing points indicate a failure of the calculated conformation to converge at the given dihedral angle.	118
VII.B.1	Absorption and spontaneous emission spectra of coumarin 153 in 1-butanol. Both spectra have been normalized to appear as the same intensity.	131
VII.B.2	Time resolved spontaneous emission spectra of coumarin 153 in 1-butanol. Spectra were reconstructed from individual time scans. See text for a discussion of the data processing. The times after excitation are: (●) 30 ps, (▲) 90 ps, (▼) 210 ps, (◆) 500 ps, (⊕) 3000 ps, (⊗) 8000 ps. Excitation wavelengths are indicated for each family of spectra.	135
VII.B.3	Time resolved spontaneous emission spectra of coumarin 153 in DMSO. Spectra were reconstructed from individual time scans. See text for a discussion of the data processing. The times after excitation are: (●) 30 ps, (▲) 90 ps, (▼) 210 ps, (◆) 500 ps, (⊕) 3000 ps, (⊗) 8000 ps. Excitation wavelengths are indicated for each family of spectra.	136
VII.B.4	Time resolved spontaneous emission spectra of coumarin 153 in DMF. Spectra were reconstructed from individual time scans. See text for a discussion of the data processing. The times after excitation are: (●) 30 ps, (▲) 90 ps, (▼) 210 ps, (◆) 500 ps, (⊕) 3000 ps, (⊗) 8000 ps. Excitation wavelengths are indicated for each family of spectra.	137

VII.B.5	Spontaneous emission time scans of coumarin 153 in 1-butanol detected at 470 nm. The three excitation wavelengths are indicated beside the time scans.	139
VII.B.6	Spontaneous emission time scans of coumarin 153 in DMSO detected at 470 nm. The three excitation wavelengths are indicated beside the time scans. Note the build-up in intensity subsequent to decay of the fast response for excitation at 427 nm.	140
VII.B.7	Spontaneous emission time scans of coumarin 153 in DMF detected at 460 nm. The three excitation wavelengths are indicated beside the time scans. Note the build-up in intensity subsequent to decay of the fast response for excitation at 427 nm.	141
VII.B.8	Energy levels calculated for excited electronic states of coumarin 153. The configuration interaction energies depend on the excitation calculated, but the relative ordering remains the same. Details of the calculation are reported in the text. $\mu(S_0)$ is calculated to be 5.2 D, $\mu(S_1) = 11.0$ D, and $\mu(S_2) = 8.4$ D.	146
VII.B.9	Schematic of energy surfaces consistent with the spontaneous and stimulated emission data reported here.	148
VIII.1	(a) Structure of 3, 3'-diethyloxadecarbocyanine iodide (DODCI). (b) Structure of 3, 3'-diethylthiadecarbocyanine iodide (DTDCI). For each molecular the iodide counter ion has been omitted and only one resonance structure is shown.	159
VIII.2	Schematic of the dependence of isomerization surface energy for the $S_0$ and $S_1$ . This model was developed initially by Rulliere (Rulliere, C.; <i>Chem. Phys. Letters</i> , <b>43</b> , 303 (1976)). Constants and quantities shown on the diagram are described in the text.	162
VIII.3	(a) Ground-state recovery signal for DODCI in 1-propanol. (b) Stimulated emission decay signal for DODCI in 1-propanol. For both data sets the best fit parameters are given in Table VIII.1.	165
VIII.4	(a) Ground state recovery signal for DTDCI in 1-propanol. (b) Stimulated emission decay signal for DTDCI in 1-propanol. For both data sets the best fit parameters are given in Table VIII.2.	168

- VIII.5      Calculated isomerization surfaces for  $S_0$  and  $S_1$  DODCI. Molecular structures indicate progressive isomerization about succeeding polyene bonds. The integrated rotation angle indicates the total extent of rotation, *i.e.* the sum of the rotation angles for the rotated bonds. For each bond rotated,  $180^\circ$  was the maximum rotation, and the indices for each bond are indicated in parentheses. 171
- VIII.6      Calculated isomerization surfaces for  $S_0$  and  $S_1$  DTDCI. Molecular structures indicate progressive isomerization about succeeding polyene bonds. The integrated rotation angle indicates the total extent of rotation, *i.e.* the sum of the rotation angles for the rotated bonds. For each bond rotated,  $180^\circ$  was the maximum rotation, and the indices for each bond are indicated in parentheses. We indicate the local minima on the two potential surfaces that are responsible for the second component of the DTDCI stimulated emission decay. 172

# I. INTRODUCTION

## I.A. Background Information

Understanding how dissimilar molecules interact and exchange energy is essential for developing a molecular understanding of materials and solution properties. How efficiently dissimilar species interact to effect this exchange plays a significant role in determining the properties of solutions and materials as well as playing a key role in mediating photochemical and thermal reaction pathways. To provide a frame of reference for what follows in this thesis a brief description of the mechanisms of energy transfer from one moiety to another is provided here.

An energy transfer process is initiated when a ground state donor molecule is excited to an excited vibrational and / or electronic state (Figure I.1). Relaxation of the excited donor state population occurs either by radiative or nonradiative pathways to the ground state. If a second species is present that possesses a resonance in close energetic proximity to that amount of excess energy contained by the donor, then transfer of the energy from the donor to the acceptor may occur (Figure I.1). The first time that energy transfer was observed was in 1923 by Cario and Franck.<sup>[1]</sup> In Cario and Franck's experiment, a container of mercury and thallium vapors produced two emission lines upon selective excitation of the mercury absorption line. This result indicated that the thallium atoms acquired electronic energy from the excited mercury atoms. Several decades after

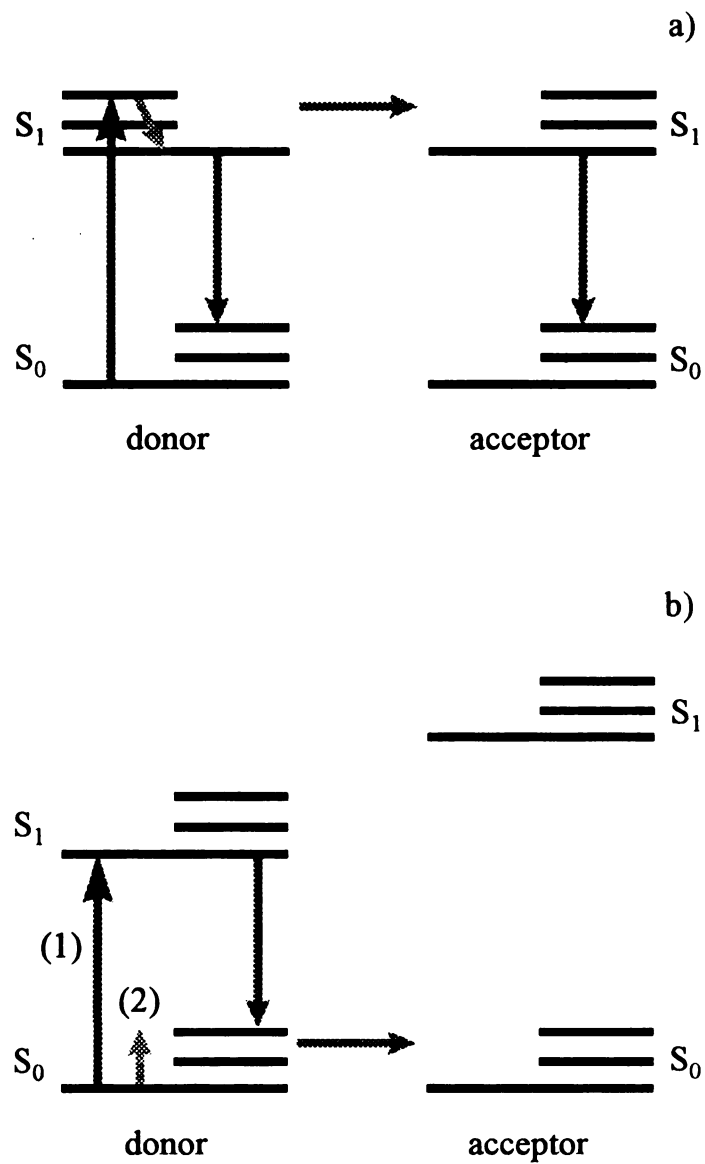


Figure I.1. a) Electronic energy transfer between two dissimilar molecules. b) Vibrational energy transfer between two dissimilar species, where excitation of the donor vibrational resonance is effected either by a Raman population scheme (1) or a direct absorption approach (2).

this initial experiment, the mechanisms of energy transfer are still investigated widely.

Depending on the system under consideration, the experimental method used to interrogate intermolecular energy transfer will vary substantially. Specifically, for a vibrational dephasing process, which is dominated by quasi-elastic collisional interactions between molecules, the characteristic distance between the donor and acceptor is very short (i.e. less than one Ångström at the point of collision). In contrast, vibrational population transfer processes can occur either by collisional or long-range mechanisms, with the highest probability of a v-v energy transfer occurring when the donor and acceptor resonances are degenerate.<sup>[3]</sup>

Electronic excitation transport occurs over distances characterized by a critical transfer radius of  $\sim 25\text{-}50\text{Å}$  for electric dipole allowed transitions, owing to the relatively large oscillator strengths of the donor and acceptor transitions.<sup>[2-4]</sup> For rotational diffusion measurements,<sup>[5-28]</sup> the intermolecular interactions that dominate the observed response are mediated by the dielectric properties of the solvent and the length scale sensed by such interactions is determined significantly by the hydrodynamic volume of the probe molecule. The type of energy transfer process described in this thesis is degenerate vibrational energy transfer between dissimilar species, (Figure I.1b). In the vibrational relaxation measurements we perform, the interactive distance of the donor and acceptor needs to be calibrated by a second measurement method. We use rotational diffusion dynamics for this purpose because of the combined experimental and theoretical maturity of this measurement. The rotational diffusion dynamics of the probe molecules perylene and 1-methylperylene are sensitive to local organization on a  $\sim 10\text{ Å}$  length scale. Correlation of the rotational diffusion and vibrational relaxation data can help to estimate

the length scale sensed by the  $T_1$  measurements at least in cases where the two times correlate.<sup>[29]</sup> The short interactive distances characteristic of vibrational energy transfer processes can thus be inferred by vibrational population relaxation times where the molecular-scale structural properties of the acceptor environment can be varied systematically.

Vibrational energy transfer measurements<sup>[30-41]</sup> are limited in information content in the sense that only the depopulation of a selected state is monitored, and not the various channels into which the vibrational energy relaxes. In addition, because vibrational transitions possess, typically, smaller transition cross-sections than electronic transitions, most  $T_1$  measurement schemes are characterized by small signals. By virtue of these small cross-sections, however, the characteristic length over which these relaxation processes operate is much shorter than the electronic transitions, and thus a non-random orientational distribution of acceptors about the donor is sensed. An added advantage of  $T_1$  measurements is the IR intrinsic “directionality”. Through careful selection of the donor and acceptor vibrational modes, the directionality of the energy transfer coordinate relative to the donor orientation can be selected.

We used the Förster energy transfer model as our theoretical basis because the essential physics of energy transfer is the same for both electronic and vibrational transfer events. The Förster energy transfer model describes the dipole-dipole interaction between an excited state donor and a ground state acceptor. The rate constant ( $k_{DA}$ ) for excited state energy transfer between donor and acceptor depends on the donor excited state lifetime ( $\tau_D$ ), the intermolecular distance ( $R$ ), the critical transfer radius ( $R_o$ ) and the

spatial alignment of the donor with respect to the acceptor species ( $\kappa^2$ ).<sup>[42]</sup>

$$k_{DA} = \frac{3\kappa^2}{2\tau_D} \left( \frac{R_o}{R} \right)^6 \quad [I.1]$$

The  $\kappa^2$  term describes the alignment of the donor and acceptor dipole moments<sup>[3,43]</sup> with respect to one another. For dipole-dipole interactions, the orientation dependence of the energy transfer process is:

$$\kappa^2 = (\sin \theta_D \sin \theta_A \cos \phi - 2 \cos \theta_D \cos \theta_A)^2 \quad [I.2]$$

where  $\theta_A$  and  $\theta_D$  are the angles of the acceptor and donor transition dipole moments relative to the vector connecting them and  $\phi$  is the torsional angle between donor and acceptor transition moments. The value of  $\kappa^2$ , for dipole-dipole interactions, ranges between 0 and 1, and for a fully random orientational distribution,  $\langle \kappa^2 \rangle = \frac{2}{3}$ .

The critical transfer radius,  $R_o$ , is related to the spectral overlap of the donor and acceptor species as described in the Förster energy transfer model by<sup>[3,41]</sup>:

$$R_o^6 = \frac{9000 \ln 10 \Phi_D}{128 \pi^5 n^4 N} \frac{2}{3} \int_0^\infty \frac{F_D(\bar{\nu}) \epsilon_A(\bar{\nu})}{\bar{\nu}^4} d\bar{\nu} \quad [I.3]$$

with the variables representing the refractive index of the intervening medium ( $n$ ), Avogadro's number ( $N$ ), the molar extinction coefficient ( $\epsilon_A(\bar{\nu})$ ) of the acceptor species at wavenumber  $\bar{\nu}$ , and the donor fluorescence intensity ( $F_D(\bar{\nu})$ ). In order to employ the Förster energy transfer model for electronic processes in vibrational energy transfer, replacement of the donor emission-acceptor absorption spectral overlap integral by an integral that describes the overlap of the donor and acceptor vibrational resonances would be required. Vibrational energy transfer is more sensitive to detuning effects than

electronic energy transfer processes because of the different bandwidths of the transition involved. Thus, the influence of acceptor resonances proximal to the primary donor-acceptor vibration must be incorporated into the critical transfer radius equation. Finally, consideration of the vibrational energy emission directionality should be included in the modified equation, *i.e.* whether or not the emitted vibrational energy occurs parallel or perpendicular to the major symmetry axis of the donor species. We have approached these effects experimentally rather than theoretically.

To elucidate information on donor-acceptor local organization in solution, we investigated the efficiency of vibrational energy transfer for three probe molecules and a series of organic solvents where the donor and acceptor vibrations are degenerate. The specific variables under consideration were the acceptor density (Chapter III: 1-methylperylene in a series of branched alkanes), order of polar interaction and detuning effects (Chapter IV: perylene and 1-methylperylene in benzene and toluene), the relationship of the relaxation and reaction coordinates for a photoreactive system (Chapter VI: 1-methylperylene in alkenes), and the interactive distances of the donors and acceptors (Chapter V: tetracene in *n*-alkanes). Additional information contained in this thesis describes how the intramolecular relaxation behavior of polar solute molecules influences the observed optical response. Specifically, a series of coumarin derivatives was evaluated computationally for their electronic state ordering, dipole moments and charge distribution dependence upon substituents identity and location on the base chromophore (Chapter VII.A). Couarmin 153 was evaluated experimentally by spontaneous emission spectroscopy (Chapter VII.B) to determine the role of intramolecular relaxation processes in the observed transient spectral dynamics. The

interest in this particular probe molecule stems from its use in solvation dynamics studies.<sup>[44-46]</sup> Another intramolecular property that can influence the optical response of probe molecules is photoisomerization. Two similar cyanine molecules, DODCI and DTDCI, were studied in solvents with different viscosities. The ground state recovery and stimulated emission responses of these molecules, in conjunction with semi-empirical calculations, demonstrated the importance of steric effects in mediating photoisomerizations (Chapter VIII). The final chapter (Chapter IX) in this thesis discusses possible future directions for the vibrational relaxation investigations under way in the Blanchard group laboratory.

## **I.B           References**

1. Cario, G.; Franck, J.; *Z. Physik*, **17**, 202 (1923).
2. Förster, Th; *Ann. Phys. Leipzig*, **2**, 55 (1948).
3. Yardley, J. T.; Introduction to Molecular Energy Transfer, Academic Press, New York, 1980.
4. Fleming, G. R.; Chemical Applications of Ultrafast Spectroscopy, Oxford University Press, New York 1986.
5. Sanders, M. J.; Wirth, M. J.; *Chem. Phys. Lett.*, **101**, 361 (1983).
6. Gudgin-Templeton, E. F.; Quitevis, E. L.; Kenney-Wallace, G. A.; *J. Phys. Chem.*, **89**, 3238 (1985).
7. Von Jena, A.; Lessing, H. E.; *Chem. Phys.*, **40**, 245 (1979).
8. Von Jena, A.; Lessing, H. E.; *Ber. Bunsen-Ges. Phys. Chem.*, **83**, 181 (1979).
9. Von Jena, A.; Lessing, H. E.; *Chem. Phys. Lett.*, **78**, 187 (1981).
10. Eissenthal, K. B.; *Acc. Chem. Res.*, **8**, 118 (1975).

11. Fleming, G. R.; Morris, J. M.; Robinson, G. W.; *Chem. Phys.*, **17**, 91 (1976).
12. Shank, C. V.; Ippen, E. P.; *Appl. Phys. Lett.*, **26**, 62 (1975).
13. Millar, D. P.; Shah, R.; Zewail, A. H.; *Chem. Phys. Lett.*, **66**, 435 (1979).
14. Gudgin-Templeton, E. F.; Kenney-Wallace, G. A.; *J. Phys. Chem.*, **90**, 2896 (1986).
15. Blanchard, G. J.; Wirth, M. J.; *J. Phys. Chem.*, **90**, 2521 (1986).
16. Blanchard, G. J.; *J. Chem. Phys.*, **87**, 6802 (1987).
17. Blanchard, G. J.; Cihal, C. A.; *J. Phys. Chem.*, **92**, 5950 (1988).
18. Blanchard, G. J.; *J. Phys. Chem.*, **92**, 6303 (1988).
19. Blanchard, G. J.; *J. Phys. Chem.*, **93**, 4315 (1989).
20. Blanchard, G. J.; *Anal. Chem.*, **61**, 2394 (1989).
21. Alavi, D. S.; Hartman, R. S.; Waldeck, D. H.; *J. Phys. Chem.*, **95**, 6770 (1991).
22. Hartman, R. S.; Alavi, D. S.; Waldeck, D. H.; *J. Phys. Chem.*, **95**, 7872 (1991).
23. Hu, C. M.; Zwanzig, R.; *J. Chem. Phys.*, **60**, 4354 (1974).
24. Youngren, G. K.; Acrivos, A.; *J. Chem. Phys.*, **63**, 3846 (1975).
25. Zwanzig, R.; Harrison, A. K.; *J. Chem. Phys.*, **83**, 5861 (1985).
26. Ben-Amotz, D.; Scott, T. W.; *J. Chem. Phys.*, **87**, 3739 (1987).
27. Ben-Amotz, D.; Drake, J. M.; *J. Chem. Phys.*, **89**, 1019 (1988).
28. Jiang, Y.; Blanchard, G. J.; *J. Phys. Chem.*, **98**, 6436 (1994).
29. Jiang, Y.; Blanchard, G. J.; *J. Phys. Chem.*, **99**, 7904 (1995).
30. Elsaesser, T.; Kaiser, W.; *Annu. Rev. Phys. Chem.*, **42**, 83 (1991).
31. Lingle, R., Jr.; Xu, X.; Yu, S. C.; Zhu, H.; Hopkins, J. B.; *J. Chem. Phys.*, **93**, 5667 (1990).

32. Anfinrud, P. A.; Han, C.; Lian, T.; Hochstrasser, R. M.; *J. Phys. Chem.*, **94**, 1180 (1990).
33. Heilweil, E. J.; Casassa, M. P.; Cavanagh, R. R.; Stephenson, J. C.; *Ann. Rev. Phys. Chem.*, **40**, 143 (1989).
34. Heilweil, E. J.; Cavanagh, R. R.; Stephenson, J. C.; *Chem. Phys. Lett.*, **134**, 181 (1987).
35. Heilweil, E. J.; Cavanagh, R. R.; Stephenson, J. C.; *J. Chem. Phys.*, **89**, 230 (1989).
36. Heilweil, E. J.; Casassa, M. P.; Cavanagh, R. R.; Stephenson, J. C.; *J. Chem. Phys.*, **85**, 5004 (1986).
37. Chang, T. C.; Dlott, D. D.; *Chem. Phys. Lett.*, **147**, 18 (1988).
38. Hill, J. R.; Dlott, D. D.; *J. Chem. Phys.*, **89**, 830 (1988).
39. Hill, J. R.; Dlott, D. D.; *J. Chem. Phys.*, **89**, 842 (1988).
40. Chang, T. C.; Dlott, D. D.; *J. Chem. Phys.*, **90**, 3590 (1989).
41. Kim, H.; Dlott, D. D.; *J. Chem. Phys.*, **94**, 8203 (1991).
42. K. B. Eisenthal and S. Siegel, *J. Chem. Phys.*, **41**, 652 (1964).
43. Gray, C. G.; Gubbins, K. E.; Theory of Molecular Fluids: Volume 1: Fundamentals, Clarendon Press, Oxford 1984.
44. Maroncelli, M.; Fleming, G. R.; *J. Chem. Phys.*, **86**, 6221 (1987).
45. Horng, M. L.; Gardecki, J. A.; Papazyan, A.; Maroncelli, M.; *J. Phys. Chem.*, **99**, 17311 (1995).
46. Tominaga, K.; Walker, G. C.; *J. Photochem. Photobiol. A: Chem.*, **87**, 127 (1995).

## **II. EXPERIMENTAL**

### **II.A. Ultrafast Stimulated Spectroscopy**

An ultrafast stimulated emission spectrometer was used to measure both the vibrational population relaxation and rotational diffusion of selected polycyclic aromatic hydrocarbon chromophores. The specific attributes of the laser and detection system and the experimental methods used in Chapters III-VI of this thesis are detailed in this chapter.

#### **II.A.1 Experimental Design**

The ultrafast pump-probe laser spectrometer (Figure II.1) used to measure both the vibrational population relaxation and rotational diffusion dynamics of various solute-solvent interactions begins with a mode locked cw Nd:YAG laser (Coherent Antares 76-S). The Nd:YAG laser produces 30W of average power at 1064 nm with 100 ps pulses at a repetition rate of 76 MHz. The 1064 nm output is frequency doubled with a Type I, temperature tuned LBO crystal (7 mm x 3 mm x 3 mm) to produce  $\geq 3$  W average power at 532 nm. The second harmonic light is then mixed with residual fundamental light using a Type I angle tuned BBO crystal (7 mm x 3 mm x 3 mm) to produce approximately 1.1 W of third harmonic light (354.7 nm) with same repetition rate and pulse characteristics as the fundamental.

The third harmonic light is split using a beam splitter ( $R = 0.56$ ) and used to pump

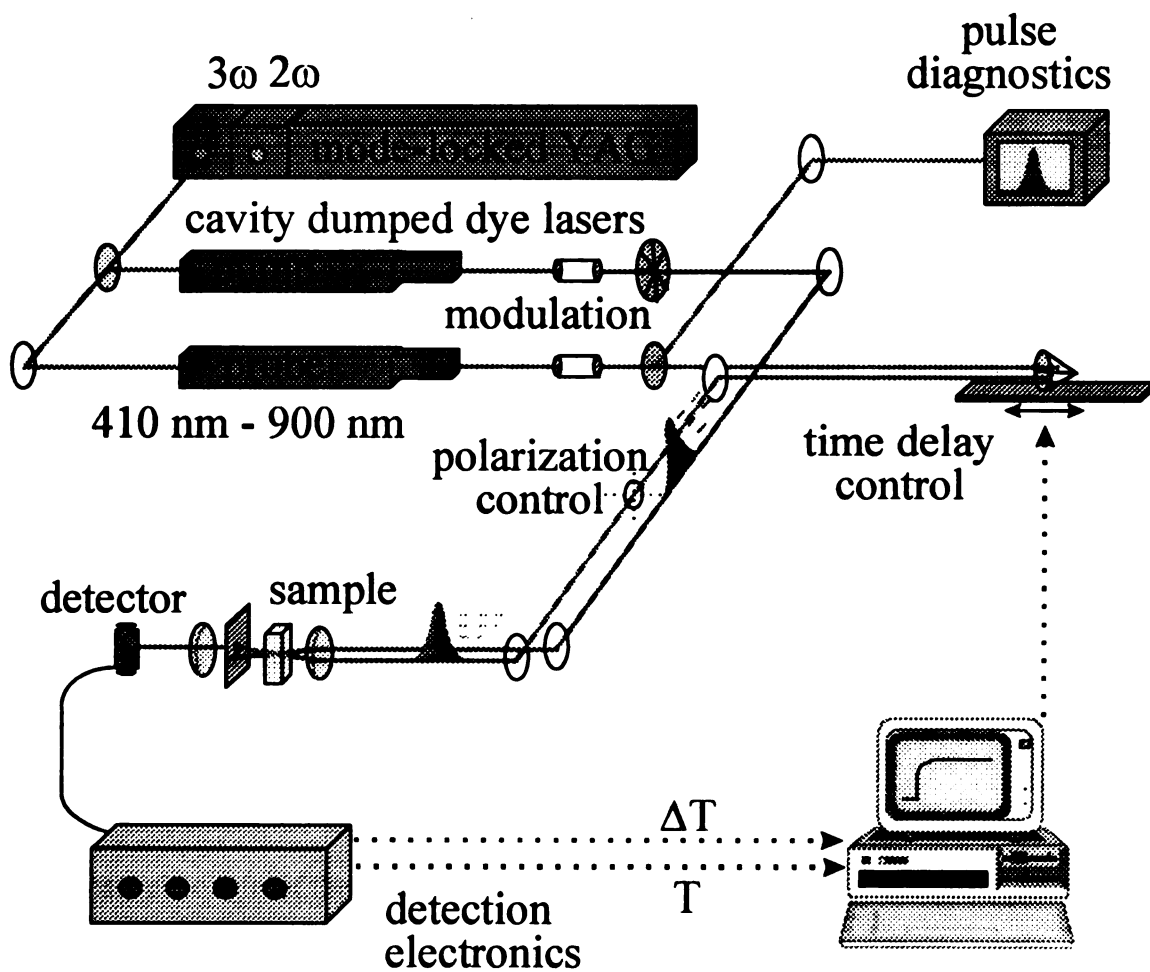


Figure II.1. Ultrafast stimulated emission laser spectrometer used to measure the vibrational relaxation and rotational diffusion of various chromophore-solvent systems. The time resolution of this system is  $\sim 10$  ps.

synchronously two cavity dumped dye lasers (pump and probe) (Coherent 701-3). To enhance the useful lifetime, viscosity, and stability of the laser dye solutions, they were cooled to  $\sim 2$  °C (Neslab RTE-110). The repetition rate of the dye lasers was set to 8 MHz to ensure autocorrelation traces free of substructure.<sup>[1]</sup> The tuning range of our dye lasers is 405 nm to 555 nm with a conversion efficiency of  $\sim 1$ -25 %, which depends on both the laser wavelength and the identity of the dye.<sup>[1]</sup> The  $\sim 7$  ps dye laser pulses can be modeled by the noise-burst model.<sup>[2]</sup> The dye laser linewidth is  $\sim 4$  cm<sup>-1</sup>.<sup>[1]</sup> The time resolution of this pump-probe system is determined by the cross correlation of the two laser pulse trains and is  $\sim 10$  ps FWHM. The maximum of the cross correlation establishes time zero for the pump-probe measurements.

The dye solutions used in the pump and probe dye lasers depend on both the absorption and emission spectra of the system under investigation and the vibrational mode of interest. The dye solutions used in this thesis are shown in Table II.1. For the  $T_1$  measurements, discussed below, the pump dye laser operating wavelength is set to the spectroscopic origin of the chromophore, ( $S_0^{v=0} \rightarrow S_1^{v=0}$ ), and the probe dye laser is set to one vibrational resonance lower in energy than the pump dye laser, ( $S_1^{v=0} \rightarrow S_0^{v=\nu}$ ).

The signals inherent to the pump-probe measurement approach we use are small; often the changes in intensity of the probe beam associated with the signal of interest are in the nanowatt range. To eliminate background noise contributions to the measured experimental signal, we use a shot noise limited detection scheme.<sup>[3-5]</sup> This method of detection shifts the signal away from the most significant portion of the noise spectrum, *i.e.* low frequencies, where  $N \propto 1/f$  dominates, to higher frequencies, where the dominant

<b>Dye</b>	<b>Preparation</b>	<b>Operation Range</b>	<b>Coherent Optics Coating Code</b>
stilbene 420	2 g in 150 mL benzyl alcohol (heating may be required). Dilute to 1.2 L ethylene glycol.	425 - 470 nm	03
coumarin 460	same as above	460 - 490 nm	04

**Table II.1.** Operating wavelength ranges and dye solution recipes, as well as the optimal mirror sets for the dye lasers.

noise contribution is laser shot noise. For our system, this noise is  $\sim 10^{-6}$ - $10^{-9}$  of the laser beam intensity. To shift the signal away from low frequency  $1/f$  noise, we employed radio and audio frequency triple modulation, using electro-optic and mechanical modulators. The operating frequency for the pump and probe electro-optic modulators are 3.011 MHz ( $\omega_\alpha$ ) and 2.110 MHz ( $\omega_\beta$ ), respectively. For our detection system, a mechanical chopper, set at  $\sim 100$  Hz ( $\omega_\gamma$ ), is also used to modulate the pump laser. The experimental signal is detected as a gain or loss on the probe beam after it is passed through the sample. The probe is separated from the pump beam with a monochromator (ISA 8422-5-86), and focusing it on a photodiode detector. The signal resulting from this modulation and associated demodulation scheme has the form:

$$\frac{I_{\text{probe}}(\text{pump on}) - I_{\text{probe}}(\text{pump off})}{I_{\text{probe}}} \quad [\text{II.1}]$$

where  $I_{\text{probe}}(\text{pump on}) \sim I_{\text{probe}}(\text{pump off})$ . Because, for these experiments, the sample interacts linearly with each laser pulse, the sample is acting as a molecular mixer of the pump and probe modulations. The signal is detected at either the sum or the difference of the electro-optic modulation frequencies:

$$\cos \omega_\alpha \cos \omega_\beta = \frac{1}{2} \cos(\omega_\alpha + \omega_\beta) + \frac{1}{2} \cos(\omega_\alpha - \omega_\beta) \quad [\text{II.2}]$$

Experimentally, we detect the sum of the modulation frequencies, ( $\omega_\alpha + \omega_\beta$ ). The mechanical audio frequency modulation has the effect of applying side-bands offset from the ( $\omega_\alpha + \omega_\beta$ ) modulation frequency by ( $\omega_\gamma$ ).

## II.A.2 Vibrational Relaxation Measurements

In pump-probe measurements, the time evolution of the stimulated signal is measured as a gain of intensity of the probe laser beam and contains the population dynamics of the vibration accessed in the ground electronic state. The time evolution of this signal can be modeled using a coupled three level system (Figure II.2), where a small fraction of the ground state population ( $A_3$ ) is excited by a  $\delta(t)$  function (pump dye laser) to the excited state manifold ( $A_1$ ).<sup>[6]</sup> For our experiments, we excite  $\sim 7\%$  of the ground state chromophores with each pump laser pulse. The population of  $A_2$  is achieved by both spontaneous and stimulated processes, with the steady state population being given approximately by  $(k_{12}/k_{23})$ . The rate at which this steady state condition is achieved is characterized by a rate constant  $(1/T_1)$ , for  $(k_{23} \gg k_{21} \approx k_{12})$ . The population dynamics for the system shown in Figure II.2 are given by:

$$A_1(0) = 1$$

$$A_1 + A_2 + A_3 = 1$$

$$\frac{dA_1}{dt} = -k_{12}A_1 + k_{21}A_2$$

$$\frac{dA_2}{dt} = k_{12}A_1 - (k_{21} + k_{23})A_2$$

$$\frac{dA_3}{dt} = k_{23}A_2$$

[II.3]

The signal we obtain from this experimental set-up is of the form (stimulated gain - absorptive loss). However, due to the nature of the pump and probe dye laser modulation scheme, the populations in states  $A_1$  and  $A_2$  (Figure II.2) are out of phase with one

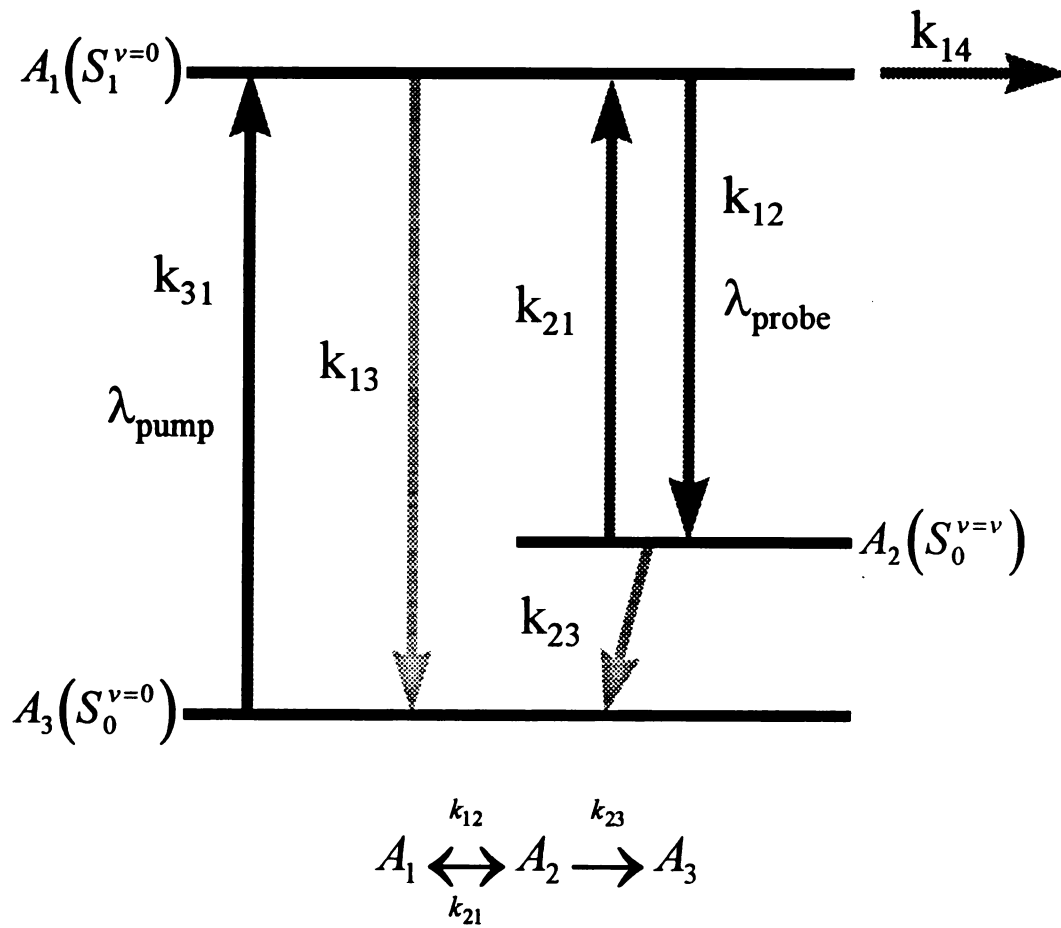


Figure II.2. Coupled three-level system depicting the experimental design.

another. Through the use of trigonometric substitution, the net result of this phase mismatch is that our signal is represented by sum of the populations in states  $A_1$  and  $A_2$ .<sup>[6]</sup>

$$S(\omega_m t) = A_1(t) \sin(\omega_m t) - A_2(t) \sin(\omega_m t - \pi) \quad [\text{II.4}]$$

$$\sin(\omega_m t) = -\sin(\omega_m t - \pi)$$

$$S(\omega_m t) = A_1(t) \sin(\omega_m t) + A_2(t) \sin(\omega_m t) \quad [\text{II.5}]$$

The equation describing the experimental signal is:

$$S(t) = \left[ \frac{k_{21} + k_{23}}{k_{23} - k_{12}} \right] A_1(0) \exp(-k_{12}t) - \left[ \frac{k_{21} + k_{12}}{k_{23} - k_{12}} \right] A_1(0) \exp(-k_{23}t) \quad [\text{II.6}]$$

where  $A_1(0)$  is the initial excited state population and the  $k_{ij}$  are the rate constants for the  $i \rightarrow j$  transitions.  $T_1$  is the inverse of  $k_{23}$ . Equation II.6 can be simplified to:

$$S(t) \approx \exp(-k_{12}t) - \left( \frac{1}{k_{23}} \right) \exp(-k_{23}t) \quad [\text{II.7}]$$

for fitting of our experimental data, in the limit that  $(k_{23} \gg k_{12})$ .

The simulated pump-probe signals we obtain contain information on both vibrational population relaxation and orientational relaxation. To separate these two different types of information, the polarization of the probe laser is controlled with respect to the polarization of the pump laser. For  $T_1$  measurements the probe polarization is set to be  $54.7^\circ$ <sup>[7]</sup> with respect to that of the pump to eliminate reorientation contributions to the data and for the rotational diffusion measurements, data are acquired for both parallel and perpendicular probe polarizations.

### II.A.3 Rotational Diffusion Measurements

As stated in Chapter I, vibrational relaxation measurements do not have an inherent length-scale calibration and a second measurement must be performed to calibrate the operative length scale of the relaxation process. Rotational diffusion dynamics provide a convenient means of estimating these interactions because the operative length scale of such measurements is determined largely by size of the reorienting molecule.

The reorientation dynamics information from our pump-probe measurements is determined by measuring the orientational anisotropy induced in the chromophore population by the absorption of the pump laser. The decay of this anisotropy is extracted from the experimental signals for probe polarizations parallel ( $I_{\parallel}(t)$ ) and perpendicular ( $I_{\perp}(t)$ ) to the pump:<sup>[7]</sup>

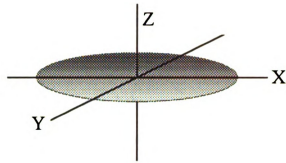
$$R(t) = \frac{I_{\parallel}(t) - I_{\perp}(t)}{I_{\parallel}(t) + 2I_{\perp}(t)} \quad \text{[II.8]}$$

The form of the anisotropy decay determines the rotor shape of the probe molecules within the specific solvent system. When the transition dipole of the probe molecule is located parallel to the major symmetry axis, the anisotropic decay is fitted by a single exponential decay function:

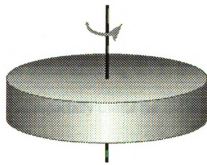
$$R(t) = (\%_0) \exp(-6D_z t)$$

$$D_x > D_y = D_z \quad \text{[II.9]}$$

The resulting reorientation shape of the probe is a prolate rotor (Figure II.3). In contrast, a double exponential is recovered when the transition dipole lies perpendicular to the symmetry axis:



prolate rotor:  $R(t) = \left(\frac{1}{2}\right) \exp(-6D_z t)$   
 $D_x \neq D_y = D_z$



oblate rotor:  $R(t) = \left(\frac{1}{2}\right) \exp(-(2D_x + 4D_z)t) + \left(\frac{1}{2}\right) \exp(-6D_x t)$   
 $D_z \neq D_x = D_y$

Figure II.3. Comparison of oblate and prolate rotor shapes and decay patterns.

$$R(t) = \left(\frac{3}{10}\right) \exp\left(- (2D_x + 4D_z)t\right) + \left(\frac{1}{10}\right) \exp(-6D_x t)$$

$$D_z > D_x = D_y \quad \text{[II.10]}$$

In this situation the probe molecule behaves as an oblate rotor (Figure II.3). The differences in the effective rotor shape of the probe molecule provides insight to the constraints imposed by the solvent molecules onto the solute molecules.

## II.B Steady State Spectroscopies

The linear absorption and emission spectra of the chromophores in the solvents used in this thesis were taken to determine the appropriate laser wavelengths to be used in the time resolved measurements. Absorption and emission spectra were taken with approximately 1 nm resolution with a Hitachi U-4001 and Hitachi F-4500 spectrometers, respectively. For systems that were sensitive to photo-oxidation, had their absorption spectra taken before and after the laser experiments were performed to determine the extent of photoreaction that had occurred during the  $T_1$  and / or  $\tau_{OR}$  measurements. These measurements have proven to be especially useful for the work described in Chapter VI of this thesis.

## II.C References

1. Jiang, Y.; Hambir, S. A.; Blanchard, G. J.; *Optics Communications*, **99**, 216 (1993).
2. Pike, H. A.; Hercher, M.; *J. Appl. Phys.*, **41**, 4562 (1970).
3. Bado, L.; Wilson, S. B.; Wilson, K. R.; *Rev. Sci. Instrum.* **53**, 706 (1982).

4. Andor, L.; Lorinez, A.; Siemion, D.; Smith, D.; Rice, S. A.; *Rev. Sci. Instrum.*, **55**, 64 (1984).
5. Blanchard, G. J.; Wirth, M. J.; *Anal. Chem.*, **58**, 532 (1986).
6. Blanchard, G. J.; *Rev. Sci. Instruments*, in press.
7. Gordon, R. G.; *J. Chem. Phys.*, **45**, 1643 (1966).

### **III. SOLVENT METHYL GROUP DENSITY DEPENDENCE OF VIBRATIONAL POPULATION RELAXATION IN 1-METHYLPERYLENE: EVIDENCE FOR SHORT RANGE ORGANIZATION IN BRANCHED ALKANES**

#### **III.A. Introduction**

We report on the vibrational population relaxation and rotational diffusion dynamics of 1-methylperylene in a series of  $C_7H_{16}$  branched alkanes. Using the  $1370\text{ cm}^{-1}$  ring breathing resonance of 1-methylperylene as the donor state and the  $1378\text{ cm}^{-1}$  methyl rocking resonances of the solvents as the acceptor states, we have found that the  $T_1$  times of 1-methylperylene vary from 10 ps to 24 ps and the rotational diffusion times in these same solvents range from 10 ps to 23 ps, but the two relaxation time constants do not correlate directly. For these systems, the time constant for vibrational population relaxation,  $T_1$ , is directly proportional to solvent  $CH_3$  group density, counter to the expected behavior for a statistical orientational distribution of solvent molecules about the solute. The experimental  $T_1$  times are also inversely proportional to the boiling point of the solvent, indicating that the ability of the solvent to form organized assemblies around the solute determines the coupling between the solute donor mode coordinate and the solvent acceptor vibrational mode. These data indicate that bath density considerations are less important than intermolecular alignment in determining the efficiency of energy transfer over molecular length scales.

### **III.B. Experimental**

The experimental system used for measurements of 1-methylperylene  $T_1$  or  $\tau_{OR}$  times in a series of branched  $C_7H_{16}$  alkane solvents is described in Chapter II. The 0-0 transition energy for each solute-solvent system was determined by the spectral overlap of the normalized absorption and emission spectra (Figure III.1). Since no spectral shifts outside the resolution of the linear response measurements were observed as a result of changing solute identity, both dye lasers were operated with Stilbene 420 laser dye (Exciton), at 430.5 nm for the pump laser and 457.5 nm for the probe laser.

#### **III.B.1. Chemicals and Sample Handling**

The alkanes used here (*n*-heptane, 2-methylhexane, 3-methylhexane, 2,3-dimethylpentane and 2,4-dimethylpentane) were purchased from Aldrich Chemical Company at the highest available purity and were used without further purification. 1-methylperylene was synthesized according to a published procedure<sup>[1]</sup>. The identity and purity of 1-methylperylene was verified using  $^1H$  NMR, mass spectrometry and UV-visible spectrometry<sup>[2]</sup>. All 1-methylperylene solutions used for dynamical measurements were  $\sim 10\mu M$ . The samples were held in a sealed 1 cm path length cuvette and stirred to minimize thermal lensing contributions to the experimental signal. The sample cuvette was supported in a jacketed mount (brass block) with the temperature of the brass block maintained at  $300 \pm 0.2$  K (Neslab EX-100-DD).

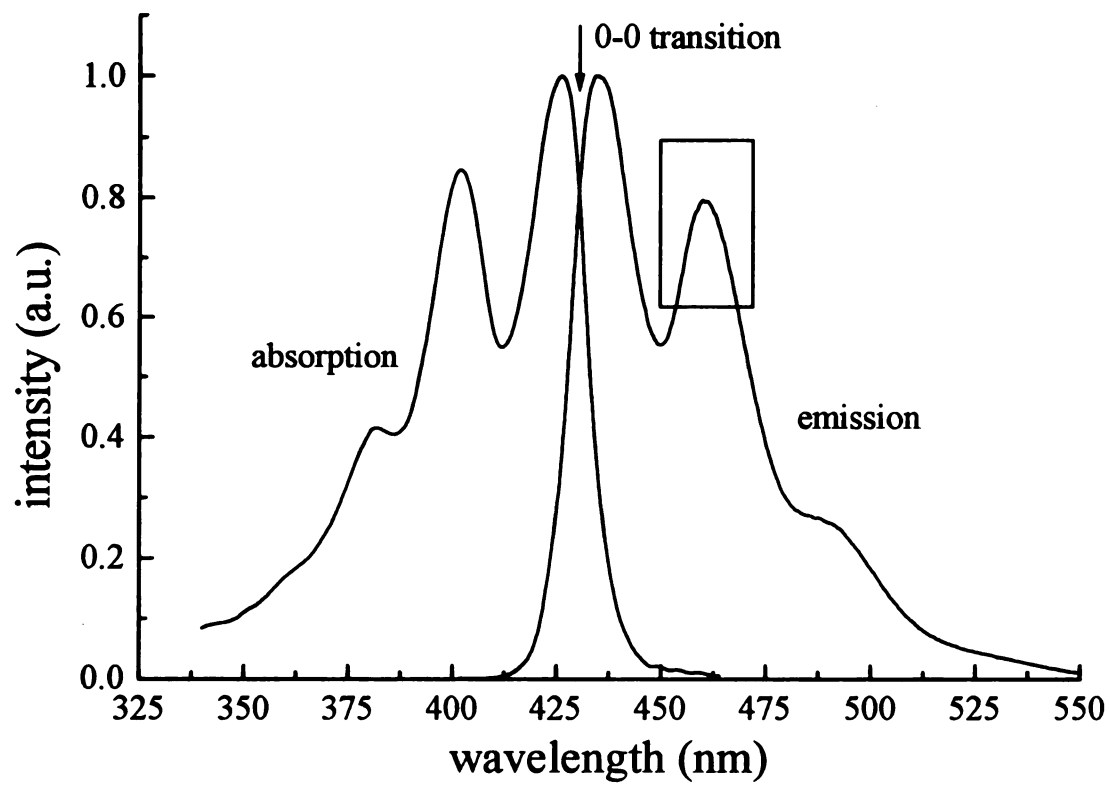


Figure III.1. Linear absorption and emission spectra of 1-methyperylene in 3-methylhexane.

### III.C. Results and Discussion

A significant motivation for doing this research is to understand local organization in liquid and fluid media and to determine the length scales over which polar coupling processes operate to mediate intermolecular vibrational energy transfer in solution.<sup>[3]</sup> An important advantage of our experimental approach to this problem is that we can perform v-v relaxation measurements on systems where the donor and acceptor resonance frequencies are degenerate by virtue of the Raman-based excitation scheme we use (Chapter II). The initial focus of this work was on degenerate vibrational energy transfer between perylene and *n*-alkanes<sup>[4]</sup> because of the apparent structural simplicity of the constituents. For that work, using the perylene 1375 cm<sup>-1</sup>  $\nu_7$  Raman-active  $a_g$  mode as the donor species and the solvent terminal CH<sub>3</sub> group rocking vibration as the acceptor moiety, we found that there was, indeed, organization in room temperature *n*-alkanes, with a characteristic persistence length of several Å. To verify that the efficiency of vibrational energy transport in solution depends on the order of the polar modulation imposed on the donor and acceptor molecules by the vibrational motion of the modes involved, we demonstrated that the analogous v-v energy transfer process between 1-methylperylene and the same *n*-alkanes operated over a significantly longer (~10 Å) range.<sup>[5]</sup> For 1-methylperylene, there is a discontinuous dependence of the T<sub>1</sub> relaxation time constant for the 1370 cm<sup>-1</sup> vibration in the same *n*-alkanes. Further, this T<sub>1</sub> behavior correlates directly with rotational diffusion dynamics, in contrast to the results for perylene.<sup>[6]</sup> We believe that the dynamical data for 1-methylperylene in the *n*-alkanes are consistent with local organization of the solvent about the solute molecule and, specifically, for the longer *n*-alkanes ( $\geq C_{10}$ ), that the 1-methylperylene solute resides in

quasi-lamellar solvent cages. We are interested in achieving a more detailed understanding of local organization in these comparatively simple systems and, accordingly, it is important to determine whether or not the  $T_1$  relaxation dynamics of the 1-methylperylene  $1370\text{ cm}^{-1}$  mode can be explained simply in stoichiometric terms for cases where the solvent is not expected to form well-organized local environments. We have investigated the  $T_1$  relaxation behavior of 1-methylperylene in a series of  $C_7$  alkanes, where we can control both the density of  $\text{CH}_3$  groups and, at the same time, introduce sufficient structural irregularity to the system to minimize the possibility of forming significantly structured local environments. In order to estimate the length scale over which these relaxation processes operate, we have examined the rotational diffusion dynamics of 1-methylperylene in these same solvents. We discuss the results of these two bodies of experimental data separately.

#### **III.D. Vibrational Population Relaxation Measurements**

The details of how we measure  $T_1$  have been presented before<sup>[4,7]</sup> and we recap only the salient aspects of these measurements here. Briefly, the pump dye laser is tuned to the 1-methylperylene 0-0 transition so that there is no contribution to the stimulated response from excited state vibrational relaxation.<sup>[8]</sup> The probe dye laser is tuned to couple the vibrationless excited electronic state with the ground state vibrational resonance of interest (the  $1370\text{ cm}^{-1}$  mode here). The experimental stimulated signal is modeled in the context of the four wave mixing response of a strongly coupled three level system (Figure II.2). The form of the stimulated response,  $S(t)$ , detected in these experiments is

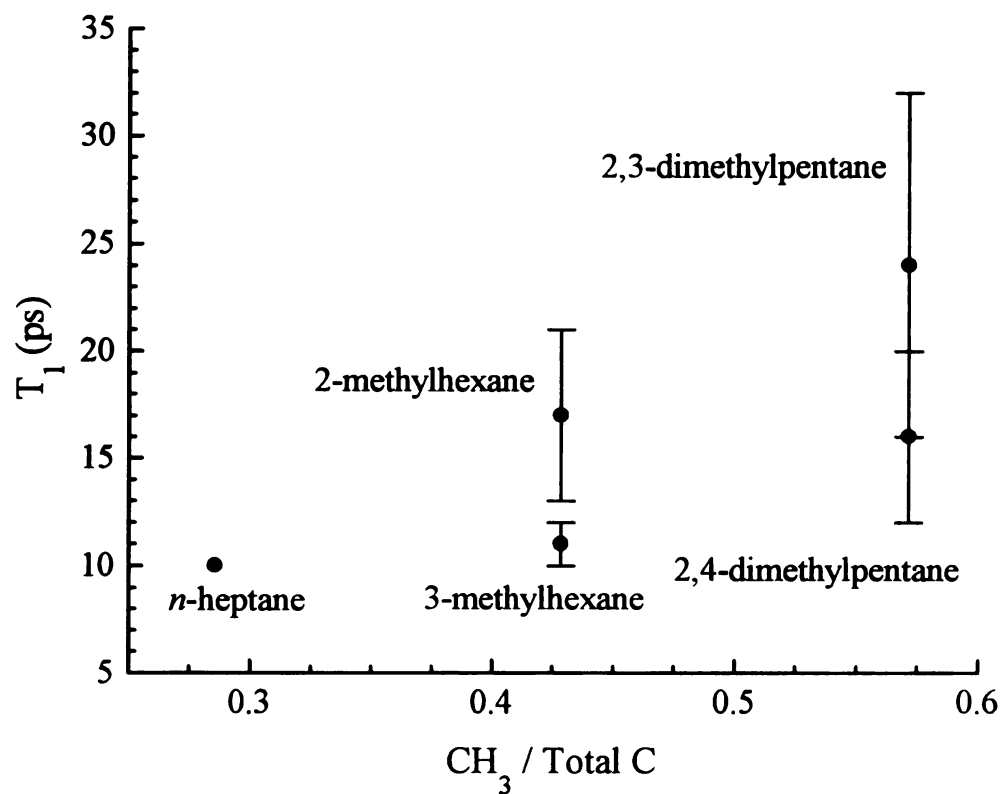


Figure III.2.  $T_1$  relaxation times of 1-methylperylene in  $C_7$  alkane homologous series as a function of solvent methyl carbon density.

$$S(t) \approx A \exp(-k_{12}t) - B \exp(-k_{23}t), \quad \text{[III.1]}$$

where the prefactors  $A$  and  $B$  are functions of the rate constants indicated in Figure II.2,  $k_{12}$  is the sum of the spontaneous and stimulated emission rate constants and  $k_{23}$  is the vibrational population relaxation rate constant for the mode of interest. As discussed in Chapter II, the form of the experimental signal is the difference between two exponential functions and not the sum of the two functions because of the way the detection system applies modulations to the electronic and vibrational state populations.<sup>[4]</sup> The dependence of  $T_1$  on solvent identity is shown in Figure III.2 and Table III.1. There are several important points to note regarding these data. The first is that the  $T_1$  times are comparatively fast, consistent with our earlier report on the  $T_1$  relaxation dynamics of 1-methylperylene in *n*-alkanes.<sup>[5]</sup> The reason that relaxation from the  $1370 \text{ cm}^{-1}$  mode of 1-methylperylene is fast compared to relaxation of the perylene  $\nu_7$  mode in the same solvents is that the intermolecular coupling responsible for excitation transfer proceeds over a longer range for 1-methylperylene than for perylene.<sup>[3]</sup> We note that the  $T_1$  relaxation time we report here for 1-methylperylene in *n*-heptane is slightly faster than that we reported previously. This reproducible difference between the two experiments arises from a (small) local heating effect encountered for the sample handling apparatus we have used in this work. Specifically, in the earlier report we used a 1 mm path length flow cell and held the temperature at 300 K. For this work we could not flow the sample because of solvent volume limitations, and instead used a 1 cm path length stirred cuvette. For these experiments, thermal lensing effects were significant, in contrast to the measurements made using a flow cell. We believe the sample temperature in the overlap volume of the two laser beams was slightly and consistently higher in the stirred-cell measurements than

solvent	viscosity ( $\eta$ ) (cP)	$T_1 \pm 1\sigma$ (ps)	$R(0) \pm 1\sigma$ (ps)	$\tau_{OR} \pm 1\sigma$ (ps)
<i>n</i> -heptane	0.38 <sup>a</sup>	<10	$0.23 \pm 0.03$	$13 \pm 1$
2-methylhexane	0.35 <sup>a</sup>	$17 \pm 4$	$0.44 \pm 0.12$	$10 \pm 2$
3-methylhexane	0.34 <sup>a</sup>	$11 \pm 1$	$0.30 \pm 0.05$	$13 \pm 1$
2,3-dimethylpentane	0.44 <sup>b</sup>	$16 \pm 4$	$0.19 \pm 0.02$	$23 \pm 2$
2,4-dimethylpentane	0.36 <sup>b</sup>	$24 \pm 8$	$0.26 \pm 0.03$	$15 \pm 1$

Table III.1.  $1370\text{cm}^{-1}$  mode vibrational relaxation and rotational diffusion times for the 1-methylperylene in alkane solvents. a) Data Book on the Viscosity of Liquids, D. S. Viswanath and G. Natarajan, Hemisphere Publishing Corporation, 1989. b) CRC Handbook of Chemistry and Physics, 71<sup>st</sup> Edition, 1991, Ed. By D. R. Lide.

for the flow cell measurements. The data we report here were taken under a single set of experimental conditions and the data in the earlier report were taken under a slightly different set of conditions, and thus a direct, quantitative comparison of the two bodies of data is not possible without correcting for this temperature difference. The second important point regarding these data is that the  $T_1$  relaxation times depend on the identity of the solvent in a way that is *not* consistent with random organization of the solvent about the solute. Finally, the measured solvent-dependence of  $T_1$  relaxation correlates directly with the boiling points of the solvents, providing insight into the competition between acceptor density and intermolecular orientation effects in determining the efficiency of energy transfer in liquids.

There is evidence in the literature that the relaxation times of C-H stretching resonances in liquid *n*-alkanes depend on the relative abundance of terminal  $\text{CH}_3$  groups.<sup>[9]</sup> In other words, the terminal  $\text{CH}_3$  groups of *n*-alkanes serve as the energy transfer points for intermolecular vibrational population relaxation. The  $T_1$  relaxation time for C-H stretching resonances in *n*-alkanes scales inversely with the density of terminal  $\text{CH}_3$  groups. For short chain *n*-alkanes, the methyl C-H stretching mode relaxes more rapidly than it does for long chain *n*-alkanes.<sup>[5]</sup> While the experimental data we present here are for relaxation between dissimilar molecules and are significantly different than those reported for *n*-alkane relaxation, it is important to compare these two bodies of data. The most important piece of information from the *n*-alkane relaxation measurements is that the energy relaxation occurs primarily through the  $\text{CH}_3$  groups, which we use as acceptor moieties in our experiments. These data suggest that the efficiency of 1-methylperylene  $T_1$  relaxation should scale with the density of solvent methyl groups, counter to our

experimental finding.

The efficiency of relaxation of the 1-methylperylene  $1370\text{ cm}^{-1}$  mode should scale with the  $\text{CH}_3$  (acceptor) group concentration *if* the orientational distribution of solvent  $\text{CH}_3$  groups is random with respect to the donor mode coordinate. This is a simple statement of the expected acceptor concentration dependence of polar excitation transport processes. Our experimental data show the opposite trend, *i.e.* the branched alkanes with the highest relative density of  $\text{CH}_3$  groups give rise to the longest  $T_1$  times for 1-methylperylene. This observation indicates that local organization of the solvent molecules about the solute is not random, but rather, is such that the  $\text{CH}_3$  group rocking mode(s) are either not well aligned with the 1-methylperylene  $1370\text{ cm}^{-1}$  mode coordinate or are separated by a significant distance from the donor mode coordinate. The latter possibility cannot be true because of the size of the solvent alkane molecules and the density of the bulk liquids. Our data must necessarily be consistent with some alignment of the branched alkane solvents around the 1-methylperylene chromophore. It is important to note that the  $T_1$  relaxation times we measure are significantly longer than the Debye relaxation times of the solvents. Thus the  $T_1$  times we measure are effectively averaged over many solvent molecule reorientation times, and there remains evidence for solvent organization on a molecular length scale.

It is instructive to examine the vibrational coordinate of the 1-methylperylene  $1370\text{ cm}^{-1}$  mode to gain an understanding of how the probed coordinate relates to the structure of the molecule. Because we observe an inverse relationship between  $T_1$  relaxation time for this mode and the solvent  $\text{CH}_3$  group concentration, we postulate that the solvent molecules are, on average, arranged in such a way as to minimize the orientational overlap

between the CH<sub>3</sub> group IR transition dipole moments and the 1-methylperylene 1370 cm<sup>-1</sup> mode dipole moment. We show in Figure III.3 the atomic displacement vectors for the 1370 cm<sup>-1</sup> mode of 1-methylperylene, determined from a semi-empirical calculation. These data indicate that the dominant atomic displacements of this mode are along the short axes of the naphthalene and methylnaphthalene moieties, *i.e.* the primary coordinate of this mode is along the 1-methylperylene long axis. For the solvents, the terminal methyl group rocking mode coordinate(s) are nominally perpendicular to the C-C bond axis between the CH<sub>3</sub> group and the  $\alpha$ -CH<sub>2</sub> group. For an all *trans* alkane chain, the rocking motion of this mode occurs in the plane in which the *trans* chain resides. Thus, to optimize coupling between the solute donor mode coordinate and the solvent acceptor mode coordinate, the orientation of the solvent should be perpendicular to the 1370 cm<sup>-1</sup> mode coordinate and the solvent molecule dominant *trans* axis should be parallel to the 1-methylperylene  $\pi$  system. The observation that the donor-acceptor coupling is less than optimum (the measured 1-methylperylene T<sub>1</sub> times in the branched alkanes are slower than in *n*-heptane) can be ascribed to an unresolved combination of two factors; the solvent molecules exhibit some amount of orientational preference for the 1-methylperylene long axis and some “misalignment” occurs due to the large number of solvent conformers present in solution. The primary conclusion of these data is that the distribution of solvent CH<sub>3</sub> group orientations about the 1-methylperylene molecule is not sufficiently random to yield a simple CH<sub>3</sub> density-dependent T<sub>1</sub> response.

To test this assertion, we show in Figure III.4 the boiling points of the solvents as a function of solvent methyl group density. *n*-heptane, the solvent used here for which intermolecular alignment is expected to be comparatively optimum, exhibits the highest

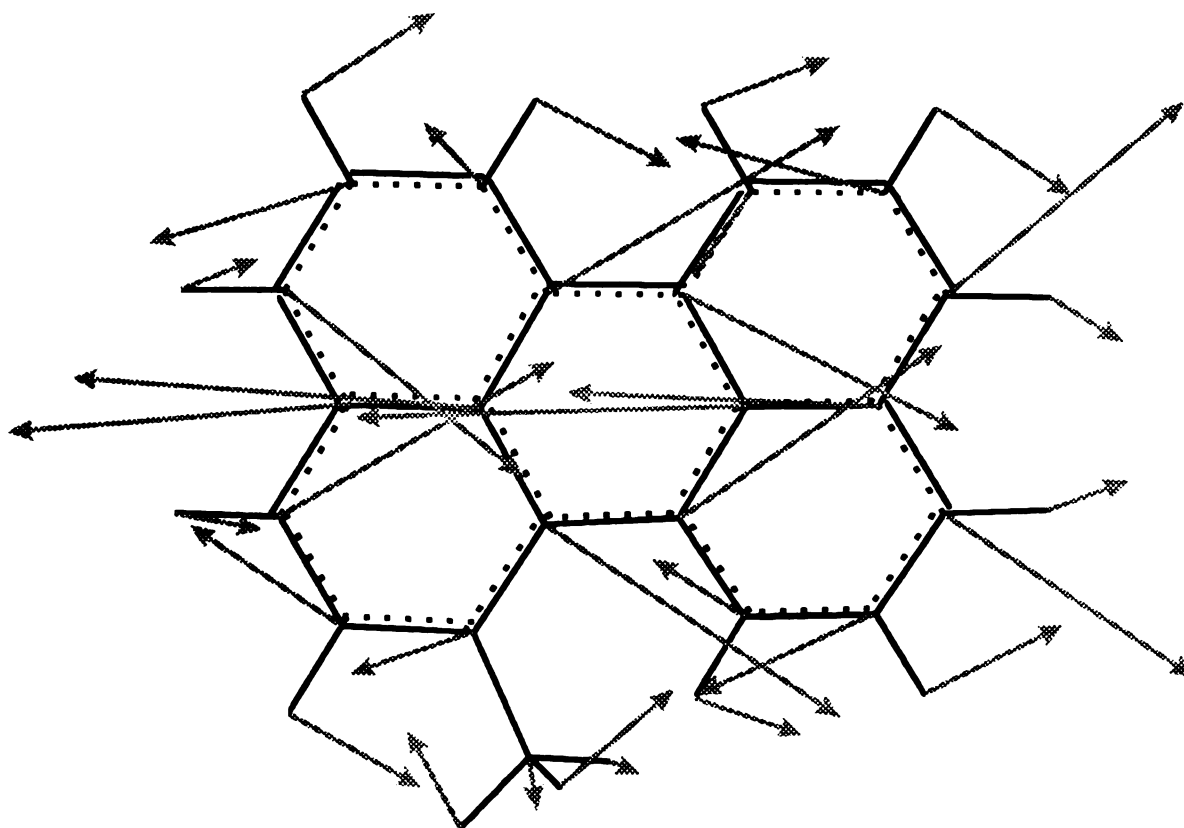


Figure III.3. Atomic displacement vectors for the 1-methylperylene  $1370\text{ cm}^{-1}$  mode determined by semi-empirical calculation. The arrows are not indication of the amplitudes of oscillation.

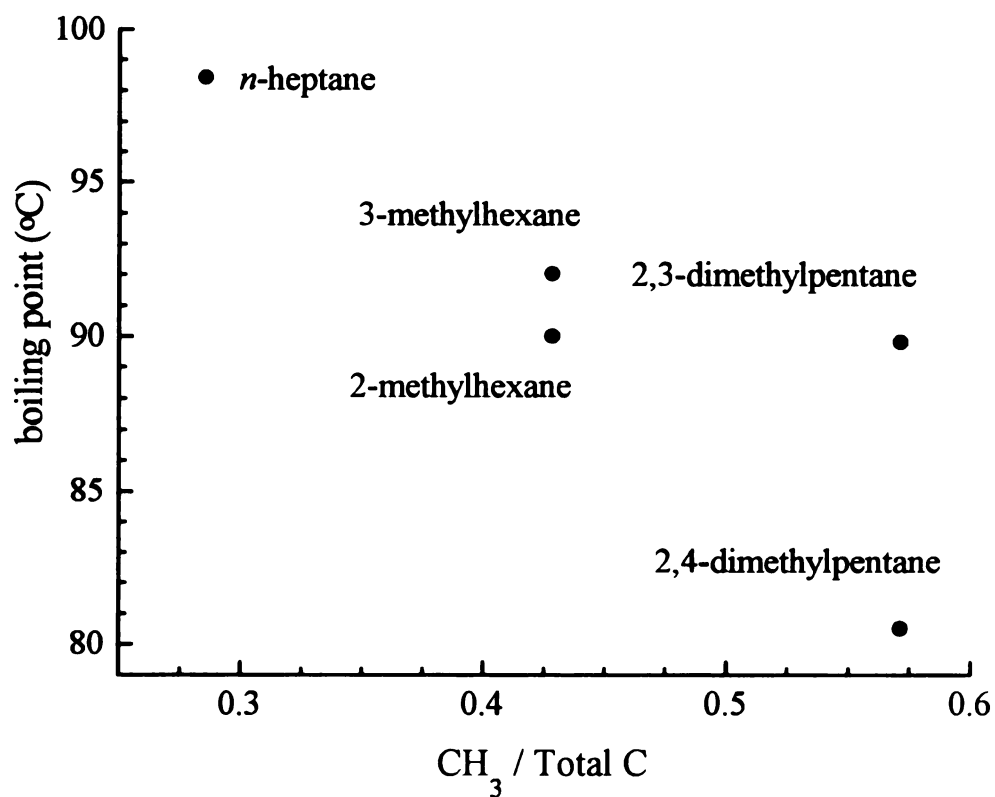


Figure III.4. Boiling points of solvents as a function of solvent methyl carbon density. Boiling point data taken from the CRC Handbook of Chemistry and Physics, 71<sup>st</sup> Edition.

boiling point in the homologous series, with the boiling points of the other solvents decreasing with increasing number and proximity of branch points. We expect, based on molecular structure arguments, that the solvent molecule alignment with 1-methylperylene will be less favorable for branched alkanes than for *n*-alkanes. Thus, there are two competing factors in determining the relative efficiency of vibrational energy transfer in solution; donor-acceptor stoichiometry, as controlled by solvent CH<sub>3</sub> group density, and alignment, controlled by the extent and proximity of solvent branching points. Because of the complexity of these systems, it is not possible, absent experimental data, to determine *a priori* which factor plays the dominant role in vibrational energy transport. Our experimental T<sub>1</sub> data (Figure III.2) correlate well with boiling point data<sup>[10]</sup> (Figure III.4), indicating that *alignment dominates over acceptor density in determining the efficiency of vibrational energy transfer*. Plotting the experimental T<sub>1</sub> times vs. solvent boiling point (Figure III.5) underscores the dependence of vibrational energy transfer on the relative alignment of the solvent and solute molecules. An important factor in determining which contribution, either alignment or acceptor density, dominates is the distance over which the energy transfer event takes place. We consider next our estimate of the length scale over which the T<sub>1</sub> relaxation measured here operates.

### III.E. Rotational Diffusion Measurements

The rotational diffusion motion of a chromophore provides a (crude) calibration of the length scale over which dipolar T<sub>1</sub> processes operate. The rotational diffusion behavior of a solute molecule in a given solvent can be approximated by the modified Debye-Stokes-Einstein (DSE) equation,<sup>[11]</sup>

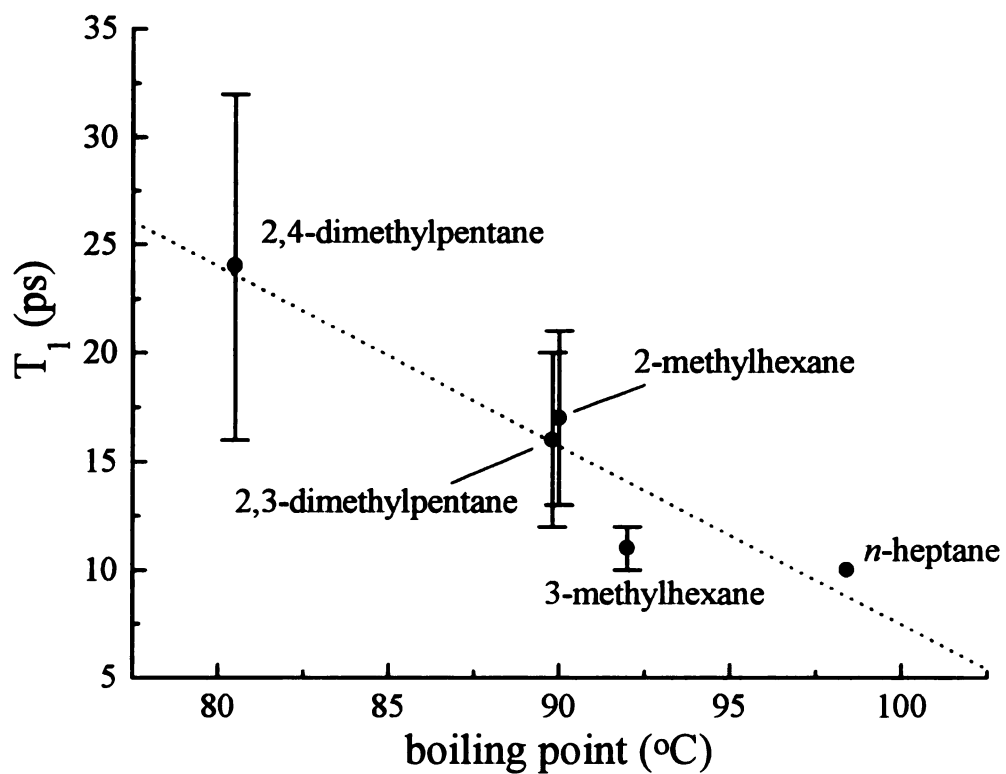


Figure III.5.  $T_1$  relaxation times of the 1-methylperylene  $1370\text{ cm}^{-1}$  resonance in the  $\text{C}_7$  alkane homologous series plotted vs. solvent boiling point. Boiling point data taken from the CRC Handbook of Chemistry and Physics, 71<sup>st</sup> Edition.

$$\tau_{OR} = \frac{\eta V}{k_B T} \left( \frac{f}{S} \right), \quad [\text{III.2}]$$

where  $\eta$ ,  $V$ ,  $k_B$ , and  $T$  represent the solvent viscosity, solute hydrodynamic volume, the Boltzmann constant, and temperature, respectively. In the original DSE equation, the solute is assumed to be spherical and imbedded in a continuous medium. In this model, the interaction between the solvent and solute is presumed to be purely frictional. Despite these limiting assumptions, the DSE equation has proven to be quite useful as a qualitative predictor of molecular reorientation, and modifications have been made to account for the generally nonspherical shape of the solute<sup>[12]</sup> and the nature of the frictional interactions between dissimilar molecules.<sup>[13-15]</sup> These modifications were realized by incorporation of the proportionality constants  $f$  (friction) and  $S$  (shape) into the DSE equation. The motivation behind using rotational diffusion measurements as a gauge of length scale is that the processes that dominate the frictional interactions between molecules arise not only from dielectric friction contributions but also from dipolar coupling. In addition, the volume of the reorienting molecule is considered explicitly so that a lower limit for the length scale of the measurement is the dimensions of the probe molecule.

We measured the rotational diffusion dynamics of 1-methylperylene in the same linear and branched alkanes for which we report  $T_1$  data. For all of the data we report here, we observe a single exponential decay of the induced orientational anisotropy, consistent with our earlier report on 1-methylperylene reorientation in *n*-heptane.<sup>[5]</sup> In that work we observed, for *n*-alkanes longer than  $C_9$ , 1-methylperylene exhibits a double exponential decay functionality for  $R(t)$  and for shorter chain solvents  $R(t)$  decays as a single exponential. We interpreted those data in the context of solute confinement by the

solvent and observed that the  $T_1$  and  $\tau_{OR}$  data were correlated closely. The reorientation data we report here (Figure III.6) do not correlate with the  $T_1$  relaxation data, providing a further indication that the interactions between 1-methylperylene and branched alkanes are less regular than they are for 1-methylperylene and the *n*-alkanes. This finding is in agreement with chemical intuition but provides little direct insight into the organization of the solvent about the solute. We are therefore left to conclude that the  $T_1$  data are indicative of local organization because of their dependence on solvent  $\text{CH}_3$  group density, but a more detailed understanding, augmented by reorientation data, as for 1-methylperylene in the *n*-alkanes, is not possible.

### III.F. Conclusions

We have studied the  $T_1$  and rotational diffusion dynamics of 1-methylperylene in a series of branched alkanes using ultrafast stimulated spectroscopy. There are two possible contributions to the efficiency of  $T_1$  relaxation in these solvents. Specifically, the density of methyl group acceptors or the relative donor-acceptor alignment could, in principle, dominate the solvent-dependence of the measured  $T_1$  times. The  $T_1$  relaxation data reveal a dependence on solvent  $\text{CH}_3$  group density that is counter to that expected from statistical arguments, but the experimental  $T_1$  times correlate well with solvent boiling points. These data point to local organization in solution, and plausibility arguments can be made that the solvent aligns predominantly along the 1-methylperylene long molecular axis. Perhaps more important, however, is that the  $T_1$  data indicate the dominance of intermolecular alignment effects over simple density considerations. These results imply that statistical treatments of energy transfer do not necessarily yield accurate predictions

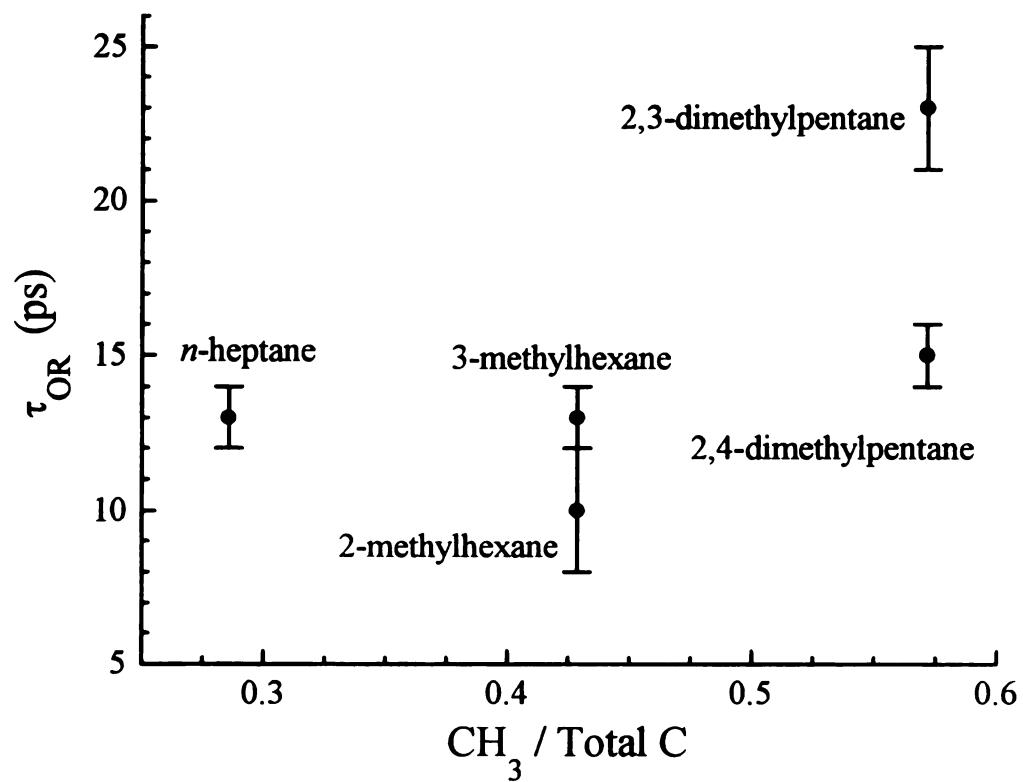


Figure III.6. Rotational diffusion times,  $\tau_{OR}$ , for 1-methylperylene as a function of solvent methyl group density.

over length scales sufficiently short that an incomplete subset of solvent orientations is sampled. Comparison of the  $T_1$  data to rotational diffusion data can, in some cases, provide a qualitative means to calibrate the coupling distance for the energy transfer from 1-methylperylene to the solvent. For the branched alkanes, the relationship between reorientation time and  $T_1$  time is not apparent, indicating that the local organization exhibited by the solvent about the solute is more complex than that seen for the *n*-alkanes. The examination of more intermolecular coupling pathways in these systems is likely to reveal a more complete "picture" of the probe molecule local environment.

### III.G. References

1. Zieger, H. E.; Laski, E. M.; *Tetrahedron Lett.* **32**, 3801 (1966).
2. Jiang, Y.; Ultrafast Stimulated Spectroscopy Studies of Vibrational Relaxation and Short Range Solvent Organization in Organic Solutions, Michigan State University, 1995.
3. Gray, C. G.; Gubbins, K. E.; Theory of Molecular Fluids, Vol. 1: Fundamentals, Oxford Science, 1984, pp. 91-100.
4. Jiang, Y.; Blanchard, G. J.; *J. Phys. Chem.*, **98**, 9411 (1994).
5. Jiang, Y.; Blanchard, G. J.; *J. Phys. Chem.*, **99**, 7904 (1995).
6. Jiang, Y.; Blanchard, G. J.; *J. Phys. Chem.*; **98**, 6436 (1994).
7. Hambir, S. A.; Jiang, Y.; Blanchard, G. J.; *J. Phys. Chem.*, **98**, 6075 (1993).
8. Jiang, Y.; Blanchard, G. J.; *J. Phys. Chem.*, **98**, 9417 (1994).
9. Monson, P. R.; Patumtevipal, S.; Kaufmann, K. J.; Robinson, G. W.; *Chem. Phys. Lett.*, **28**, 312 (1974).
10. CRC Handbook of Chemistry and Physics, 71st Edition, 1991, Ed. By D. R. Lide.
11. Debye, P.; Polar Solvents, Chemical Catalog Co., New York, 1929, p. 84.

12. Perrin, F.; *J. Phys. Radium*, **7**, 1 (1936).
13. Hu., C. M.; Zwanaig, R.; *J. Chem. Phys.*, **60**, 4354 (1974).
14. Youngren, G. K.; Acrivos, A.; *J. Chem. Phys.*, **63**, 3846 (1975).
15. Zwanzig, R.; Harrison, A. K.; *J. Chem. Phys.*, **83**, 5861 (1985).

## **IV. AN EXPERIMENTAL EXAMINATION OF THE COMPETITION BETWEEN POLAR COUPLING AND LOCAL ORGANIZATION IN DETERMINING VIBRATIONAL POPULATION RELAXATION**

### **IV.A. Introduction**

We report on the vibrational population relaxation and rotational diffusion dynamics of perylene and 1-methylperylene in benzene and toluene. For these experiments, the naphthalene-like ring distortion modes of both perylene ( $1375\text{ cm}^{-1}$ ) and 1-methylperylene ( $1370\text{ cm}^{-1}$ ) were excited selectively using a stimulated emission population scheme, and the efficiency of depopulation of these modes was measured in each solvent. For these systems, there is an IR-active acceptor vibrational mode at the same frequency and the order of the dominant intermolecular vibrational energy transfer process depends on the identity of the solute. For 1-methylperylene, dipole-dipole coupling is operative and for perylene, quadrupole-dipole coupling determines the transfer. The importance of solvent organization about the solute can be evaluated by comparing solute  $T_1$  times in the two solvents. In the limit of fast solvent cage exchange, the solute  $T_1$  relaxation times should increase with increasing order of the polar coupling process and decrease with increasing intermolecular alignment. Our experimental data indicate that the  $T_1$  times are similar for all systems studied, implying the importance of persistent intermolecular interactions in determining the efficiency of vibrational population

exchange in solution.

## IV.B. Experimental

The ultrafast pump-probe laser system used to measure the vibrational relaxation and rotational diffusion dynamics of the probe molecules has been described in Chapter II. Both dye lasers were operated with Stilbene 420 laser dye (Exciton). Due to small solvent-dependent shifts of the probe molecule absorption and emission spectra (Figure IV.1), the pump dye laser, set to excite the  $S_0^{v=0} \leftrightarrow S_1^{v=0}$  transition, was operated at fixed wavelengths between 435.8 nm and 442.2 nm. The probe dye laser was operated within the wavelength range of 463.5 nm to 470.9 nm. For the 1-methylperylene and perylene measurements  $\nu_{\text{pump}} - \nu_{\text{probe}} = 1370 \text{ cm}^{-1}$  and  $1375 \text{ cm}^{-1}$ , respectively.

### IV.B.1. Chemicals and Sample Handling

Perylene, benzene, and toluene were purchased from Aldrich Chemical Co. at the highest purity available and were used as received. 1-Methylperylene was synthesized according to a literature preparation from perylene and  $\text{CH}_3\text{Li}$ .<sup>[1]</sup> This reaction methylates perylene at the 1- position with >95 % selectivity. Methyllithium and 10% Pd on C catalyst were purchased from Aldrich and used as received. Following purification by plate chromatography, the identity of 1-methylperylene was confirmed by mass spectrometry,  $^1\text{H}$  NMR, UV-visible, and infrared absorption measurements. The sample concentrations were  $\sim 1 \times 10^{-5} \text{ M}$  in the probe molecule to minimize the possibility of aggregation effects, concentration quenching, and excited state donor-donor energy

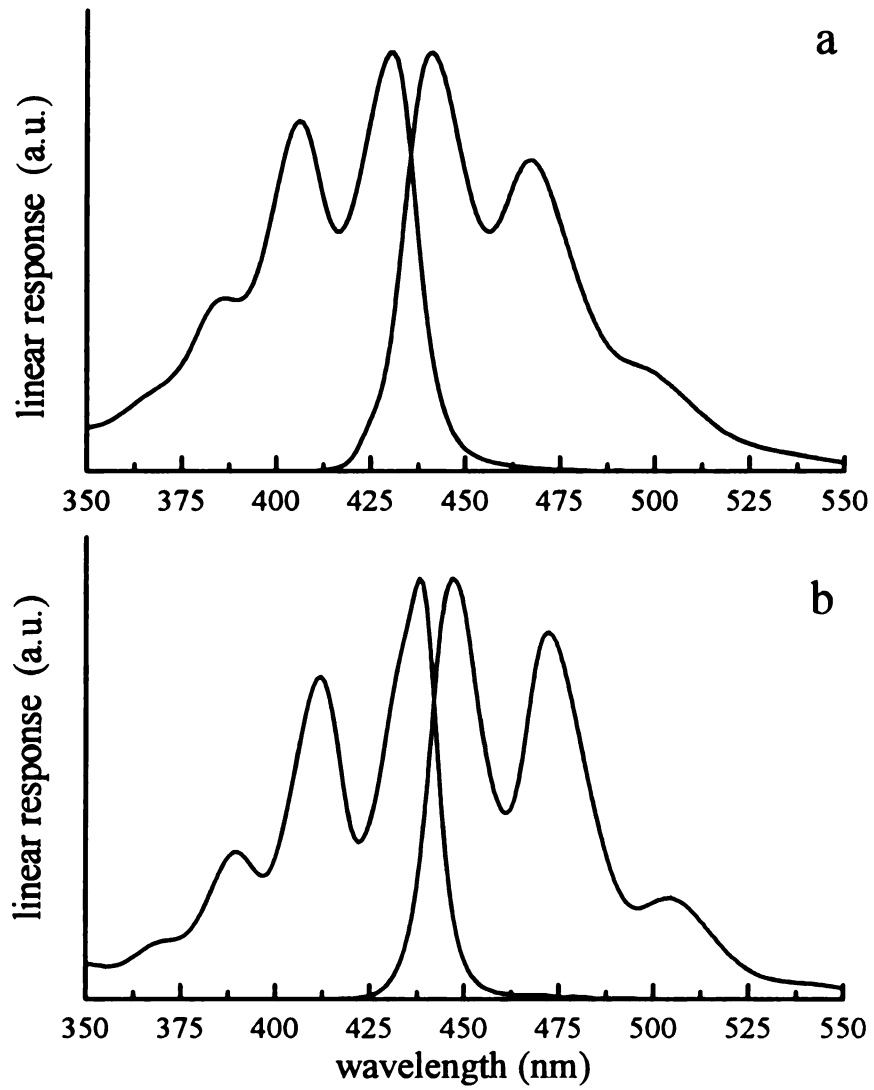


Figure IV.1. Absorption and emission spectra of (a) 1-methylperylene in toluene and (b) perylene in toluene.

transfer. The sample handling system used a flow cell with a path length of 1mm and a temperature control system set at  $300 \pm 0.1\text{K}$ .

#### IV.C. Results and Discussion

The primary focus of this work is on determining whether intermolecular alignment or type of intermolecular coupling dominates  $T_1$  relaxation. In a series of previous papers, we have discussed the foundations of the measurement scheme we use to obtain ground state  $T_1$  relaxation information.<sup>[2-8]</sup> For our technique to yield information on the ground state vibrational resonance of interest, the probe laser pulse senses both  $S_1^{v=0} \leftrightarrow S_0^{v=v}$  stimulated absorptive and emissive transitions during the time that the probe pulse is present. The time resolved data we show in Figure IV.2 for perylene in benzene demonstrate the probe laser intensity independence of the signal demonstrating that both stimulated emission and absorption contribute to the measured response.<sup>[8]</sup> We understand the temporal evolution of the experimental signal and can model these data quantitatively in the context of the probe molecule behaving as a strongly coupled three level system. A first consideration is whether the dominant process for the exchange of vibrational energy is collisional or by non-collisional resonant coupling processes. Our work on perylene in the *n*-alkanes<sup>[3]</sup> demonstrated that intermolecular collisions could not be the dominant relaxation pathway, consistent with a discussion of this point for gas phase v-v energy transfer by Yardley.<sup>[9]</sup> In that work, Yardley concluded that resonant ( $\mu$ - $\mu$ ) coupling was a factor of  $\sim 10^3$  more efficient than collisions at exact resonance, and that collisional interactions in gases did not dominate until a D-A detuning of  $\Delta_{\text{VDA}} \sim 250 \text{ cm}^{-1}$ .

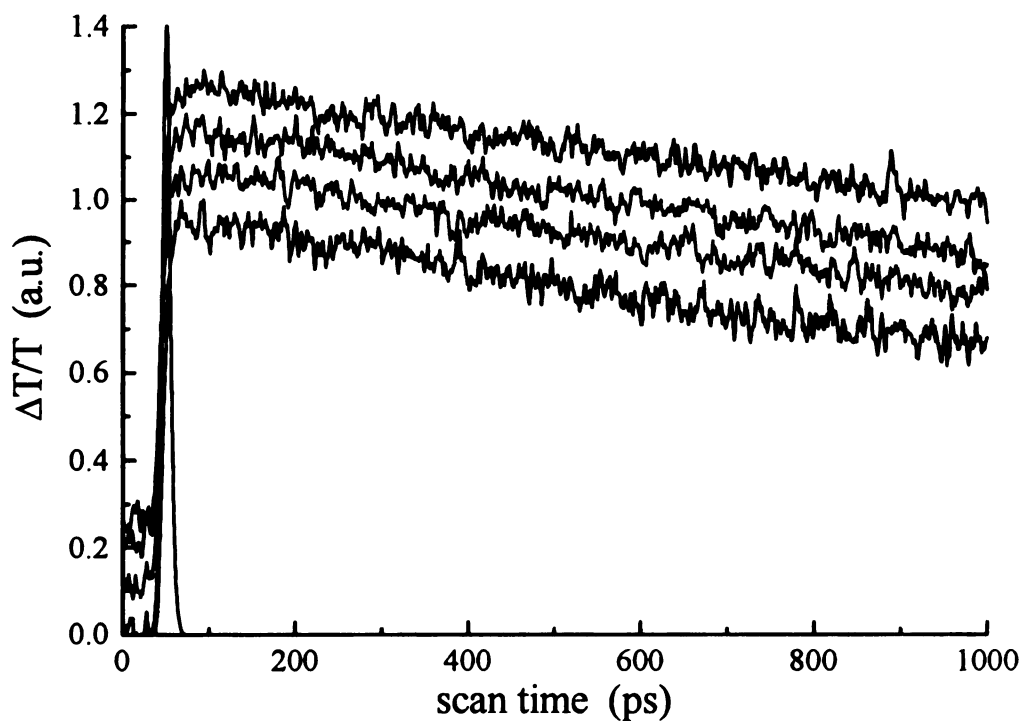


Figure IV.2. Experimental pump-probe signal intensity-dependence for  $2 \times 10^{-5}$  M perylene in benzene. The probed vibrational resonance is  $1375 \text{ cm}^{-1}$ . The instrumental response function is shown with the data. Individual traces have been offset from  $\Delta T/T = 0$  for clarity of presentation only. Top trace;  $I_{\text{probe}} = I_{\text{pump}} \sim 10 \text{ mW}$  average power. Second trace from the top;  $I_{\text{probe}} = 0.1 I_{\text{pump}}$ . Third trace;  $I_{\text{probe}} = 0.01 I_{\text{pump}}$ . Fourth (bottom) trace;  $I_{\text{probe}} = 0.001 I_{\text{pump}}$ . While  $\Delta T/T$  scale is arbitrary, the signals have not been normalized, and are of the same magnitude for all conditions.

While the D-A detuning for which this cross-over occurs may be slightly different for liquid phase systems, we work under conditions of  $\Delta\nu_{\text{DA}} \sim 0 \text{ cm}^{-1}$ , ensuring the dominance of long range resonant coupling. Our earlier comparison of the  $T_1$  relaxation dynamics of perylene in  $n\text{-C}_8\text{H}_{18}$  and  $n\text{-C}_8\text{D}_{18}$  indicates that, for significant D-A detuning, there is a background relaxation process that limits  $T_1$  for the perylene  $\nu_7$  mode to  $\sim 350 \text{ ps}$ .<sup>[3]</sup> The mechanism of this background relaxation is likely off-resonance polar coupling, but could also have contributions from intramolecular anharmonic coupling to low frequency modes or direct collisional interactions with the solvent.

For the systems we have investigated here, the donor multipole moment we sense is induced by the incident laser electric field(s) and the modulation of the acceptor moment(s) are induced by energy transfer from the donor. Thus, despite any permanent polar interactions operating in these systems, it is the moments induced in the donor and acceptor that are of consequence to these measurements, and therefore we treat these processes in the context of dispersion interactions. As discussed above, we control the order of the longest range v-v coupling process through judicious choice of the donor and acceptor molecules. We need, therefore, to consider the length scale over which these processes operate. For dispersion interactions involving induced dipole-induced dipole coupling the relative interaction energy may be written in the following manner,<sup>[10]</sup>

$$U_{\text{ds}}^{\mu-\mu} \approx - \left( \frac{-3E_{\text{D}}}{4(4\pi\epsilon_0)^2} \right) \left( \frac{\alpha_{\text{D}}\alpha_{\text{A}}}{r^6} \right) \quad [\text{IV.1}]$$

where  $E_{\text{D}}$  is the ionization energy of the donor molecule,  $\alpha_{\text{D}}$  and  $\alpha_{\text{A}}$  are the dipole-dipole polarizability tensors for the donor and acceptor species, and  $r$  is the intermolecular distance. The second term on the right hand side of Equation IV.1 is of consequence here,

with the first term acting as a scaling constant. For quadrupole-dipole interactions we approximate the interaction energy dependence on polar coupling,

$$u_{ds}^{\Theta-\mu} \propto -\frac{A_D \alpha_A}{r^7} \quad [\text{IV.2}]$$

where  $A_D$  is the quadrupole-dipole polarizability tensor for the donor and, as before,  $\alpha_A$  is the dipole-dipole polarizability tensor for the acceptor. The terms  $A$  and  $\alpha$  depend, necessarily, on the symmetry of the donor and acceptor species, and Equations IV.1 and IV.2 represent the general cases for these interactions. For molecules possessing a center of inversion, such as perylene, the  $A$  term will vanish and the next higher order terms are the longest range processes,

$$u_{ds}^{\Theta-\mu} \propto -\frac{O_D \alpha_A}{r^8} \quad [\text{IV.3}]$$

where the term  $O_D$  is the octupole-dipole polarizability tensor for the donor. From Equations IV.1 - IV.3, it is clear that the operative length scale of the coupling process depends sensitively on the order of the polar interaction. Despite the significant  $r$ -dependence for each process, we expect that intermolecular alignment can also play a role in our measurements. For example, in dipole-dipole interactions, the Förster treatment<sup>[11]</sup> shows that the probability of an excitation transport event is related to D-A alignment,<sup>[12]</sup>

$$k_{D-A} = K' \kappa^2 \left( \frac{R_0}{R} \right)^6 \quad [\text{IV.4}]$$

$$\kappa_{\mu-\mu}^2 = \left\{ \sin \theta_D \sin \theta_A \cos \phi - 2 \cos \theta_D \cos \theta_A \right\}^2$$

The terms  $\theta_D$  and  $\theta_A$  are the angles that the D and A dipole moments make with respect to the vector connecting them and  $\phi$  is the azimuthal angle between the D and A dipole

moments. For the higher order multipolar interactions, such as quadrupole-dipole interactions, the orientation dependence of  $k_{DA}$  may be described as<sup>[12]</sup>

$$\kappa_{\Theta-\mu}^2 = \left\{ \frac{3}{2} \left[ \cos \theta_D (3 \cos^2 \theta_A - 1) - 2 \sin \theta_D \sin \theta_A \cos \theta_D \cos \phi \right] \right\}^2 \quad [\text{IV.5}]$$

For higher order coupling, the form of  $\kappa^2$  is slightly different, but the general result is the same, and the essential symmetry elements of the interaction are represented in Equation IV.5. We expect, in general, that intermolecular distance,  $r$ , order of polar coupling, D-A alignment, and detuning effects all play a role in determining the  $T_1$  times we measure experimentally. We can determine the order of the polar coupling process and  $\Delta v_{DA}$ , leaving the quantities  $r$  and  $\kappa^2$  to be inferred by experiment.

#### IV.C.1 Vibrational Relaxation

We have reported previously on the dominance of intermolecular alignment over simple acceptor chromophore density.<sup>[6]</sup> In this work, the density of the acceptor chromophore is held nominally constant and the order of the coupling process is the variable. We expect, in the limit of fast exchange of solvent molecules in the cage surrounding the solute, 1-methylperylene to exhibit  $T_1$  times faster than perylene. We do not realize this expectation experimentally, (Table IV.1), and there are four possible reasons for the discrepancy between experiment and expectation. It is possible that there is density augmentation of the solvent about the solute, or that the relative strengths of the donor and acceptor vibrational transition moments vary widely and in such a way as to compensate for variations in polar coupling effects. It is also possible that contributions from non-resonant ( $\Delta v > 0 \text{ cm}^{-1}$ ) coupling processes serve to make energy transfer

solute / solvent system	$T_1 \pm 1\sigma$ (ps)	$R(0) \pm 1\sigma$	$\tau_{OR} \pm 1\sigma$ (ps)
1-methylperylene / toluene	$15 \pm 3$	$0.29 \pm 0.01$	$18 \pm 1$
1-methylperylene / benzene	$35 \pm 3$	$0.28 \pm 0.02$	$15 \pm 1$
		$0.035 \pm 0.002$	$281 \pm 16$
perylene / toluene	$16 \pm 4$	$0.26 \pm 0.03$	$16 \pm 1$
perylene / benzene	$11 \pm 2$	$0.27 \pm 0.02$	$15 \pm 1$

Table IV.1. Vibrational population relaxation time constants,  $T_1$ , zero-time anisotropies,  $R(0)$ , and reorientation time constants,  $\tau_{OR}$ , for perylene and 1-methylperylene in toluene and benzene.  $T_1$  times for perylene are for the  $\nu_7$  mode at  $1375 \text{ cm}^{-1}$  and for 1-methylperylene are for the  $1370 \text{ cm}^{-1}$  mode.

efficient for all systems we have studied, or in connection with our earlier work, vibrational energy transfer could be mediated primarily by intermolecular alignment effects.<sup>[6]</sup> We consider each of these possibilities below.

The data we report here could potentially be accounted for in terms of local density augmentation, analogous to what has been observed for supercritical fluids near their critical points.<sup>[13-21]</sup> Several factors, however, argue against this possibility. These are, first, that local density augmentation effects have not been observed previously for liquids and this effect is not seen for supercritical fluids under conditions well away from the critical temperature and pressure. In addition, we should observe a solvent-dependent trend, independent of the solute for both  $T_1$  and reorientation measurements if augmentation were operative, and we do not see this experimentally (*vide infra*).

A second possibility that could account for the experimental  $T_1$  data is that the D and A transition moments vary widely enough and in such a way as to compensate for differences in the  $r$ -dependence of the coupling processes. Again, this is not likely based on a comparative examination of perylene and 1-methylperylene  $T_1$  relaxation dynamics in  $n$ -alkanes.<sup>[3,5]</sup> In that work, the differences in  $T_1$  for the two solutes could be explained in terms of the  $r$ -dependence of the coupling processes. In addition, for the solvents we use here, the Raman active transitions we use have similar Raman scattering cross section, to within a factor of five, based on measurements made in our laboratory.<sup>[22]</sup> The IR spectra of benzene and toluene have essentially the same absorption cross sections for the 1375  $\text{cm}^{-1}$  resonance (Figure IV.3). Thus the transition moments for the solute-solvent permutations we examine are uniform enough that they cannot account for the similarities in the  $T_1$  times for all systems.

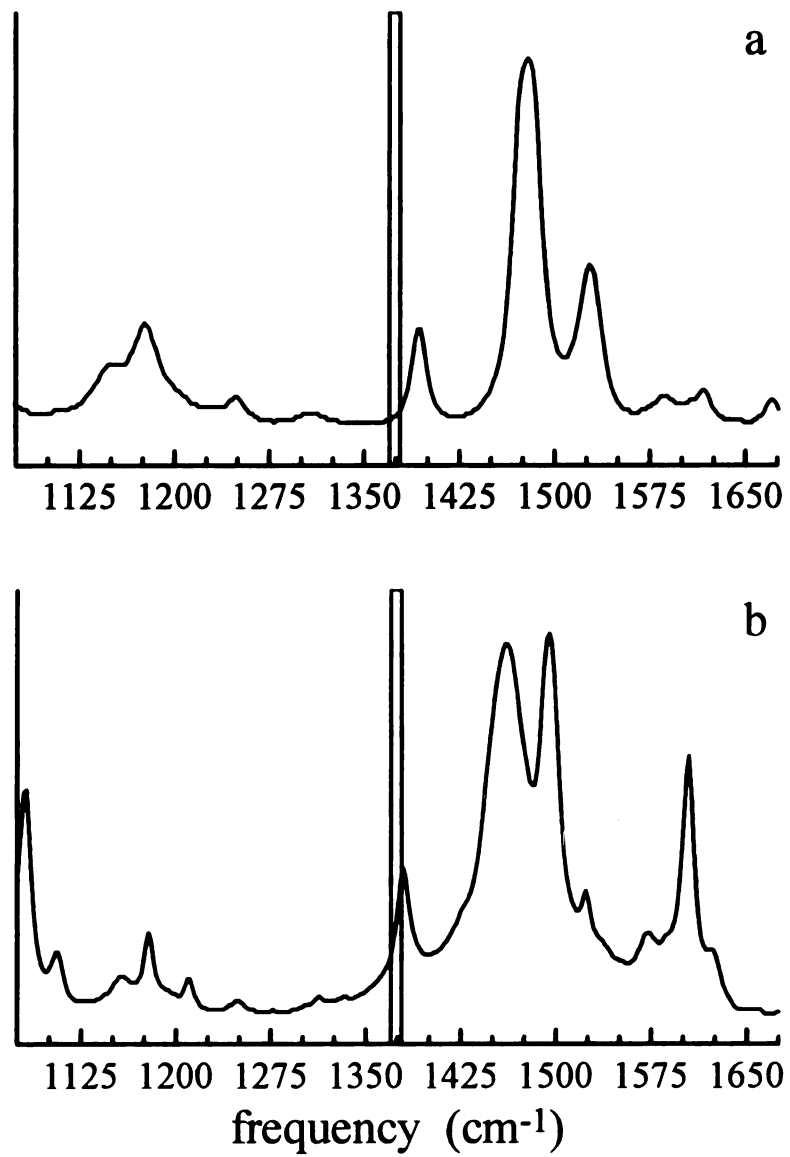


Figure IV.3. IR spectra of (a) benzene and (b) toluene.

The third factor that may influence the vibrational relaxation times are the presence of additional acceptor vibrations at  $|\Delta\nu_{DA}| > 0 \text{ cm}^{-1}$ . Specifically, both toluene and benzene have several additional IR (Figure IV.3) and Raman active vibrations (Figure IV.4) in the vicinity of the dominant acceptor vibration ( $\sim 1380 \text{ cm}^{-1}$ ). The presence of these competing acceptor modes, even for  $|\Delta\nu_{DA}| \sim 200 \text{ cm}^{-1}$ , can substantially increase the probability of an energy transfer event. Previous measurements in our laboratory indicate that the order of D-A polar coupling does affect the efficiency of vibrational energy transfer. For perylene / *n*-hexane<sup>[3]</sup> and 1-methylperylene / *n*-hexane<sup>[5]</sup> the  $T_1$  times were 300 ps and 20 ps, respectively. Since, in that work, the solvent molecules are similar in size to the solutes, changes in the donor-acceptor interactive distance could be ruled out as the cause of the different  $T_1$  times. For the solvents benzene and toluene, perylene and 1-methylperylene yield similar  $T_1$  times. The solvent-dependence of  $T_1$  in the alkanes for both solutes excludes the possibility of intramolecular relaxation dominating the relaxation of these donor modes. We attribute these effects to coupling of the solute donor resonances to several solvent acceptor resonances as well as at least some alignment of the donor and acceptor vibrational mode coordinates. Perylene, in principle, allows for better alignment of the solvent molecules with the donor coordinate because of its planar structure, where the twisted conformation of 1-methylperylene<sup>[23]</sup> inhibits an analogous degree of alignment. There is one somewhat longer  $T_1$  time in these data, that for 1-methylperylene in benzene. It is not possible to determine the origin of the longer  $T_1$  time for this system absent another, complementary means of examining solvent organization about the solute. Rotational diffusion measurements can provide this additional information and we consider reorientation data on these systems below.

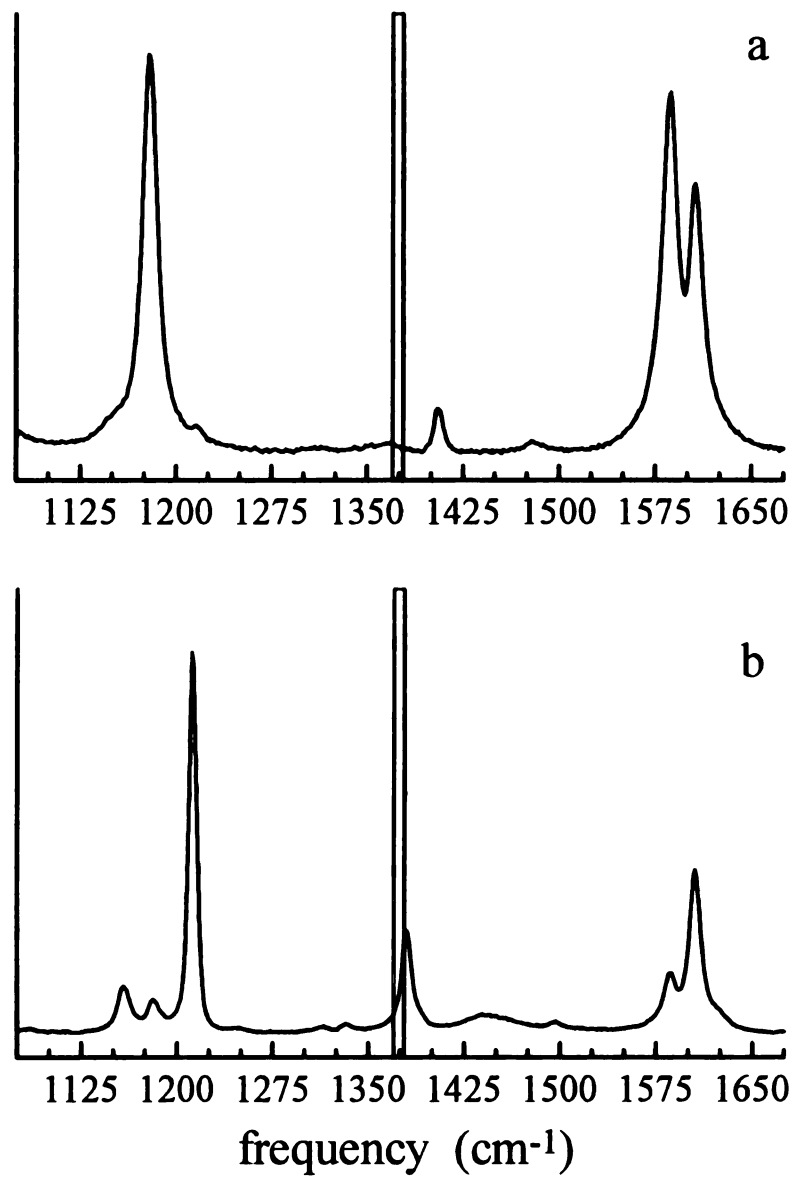


Figure IV.4. Raman spectra of (a) benzene and (b) toluene.

#### IV.C.2. Rotational Diffusion Dynamics

The  $T_1$  data for the systems studied indicate that the efficiency of vibrational energy transfer is substantially the same for perylene and 1-methylperylene in toluene, but the interactions between perylene and benzene are measurably different than they are for 1-methylperylene and benzene. Rotational diffusion measurements have proven useful in the past in helping to elucidate local organization about perylene and 1-methylperylene.<sup>[5,24]</sup> Previous data on 1-methylperylene in *n*-alkanes indicate that the probe molecule reorients as a prolate rotor in short *n*-alkanes and as an oblate rotor in *n*-alkanes longer than *n*-octane.<sup>[5]</sup> In contrast, perylene was seen to reorient as a prolate rotor in all of the same *n*-alkanes.<sup>[24]</sup> Comparison of these two bodies of data indicates that the non-planar conformation of 1-methylperylene affects its interaction with surrounding solvents significantly. The rotational diffusion data we present here for perylene in benzene and toluene both yield single exponential decays of the induced orientational anisotropy,  $R(t)$ , indicating that perylene behaves as a prolate rotor in both of these solvents.<sup>[5,24]</sup> The achievement of a single exponential anisotropy decay for these systems is not limited by the achievable signal-to-noise ratio. The reorientation behavior of 1-methylperylene is different in the two solvents. In toluene, 1-methylperylene exhibits a single exponential anisotropy decay (Figure IV.5), indicating that it reorients as a prolate rotor.<sup>[5]</sup> In benzene, a double exponential anisotropy decay is measured, indicating reorientation as an oblate rotor (Figure IV.6). The equations for  $R(t)$  for oblate and prolate rotors are useful in interpreting the  $\tau_{OR}$  data. For these equations, the long chromophore  $\pi$ -plane axis is taken as the  $x$ -axis and the  $z$ -axis is perpendicular to the chromophore  $\pi$ -plane. A prolate rotor is given by the condition  $D_x > D_y = D_z$  and an

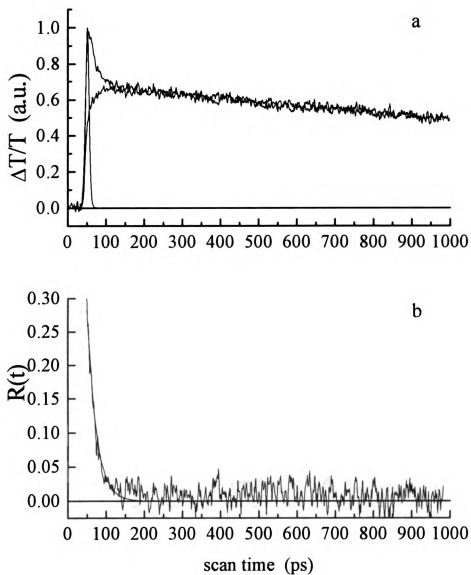


Figure IV.5. (a)  $I_1(t)$  and  $I_2(t)$  and (b)  $R(t)$  for 1-methylperylene in toluene.

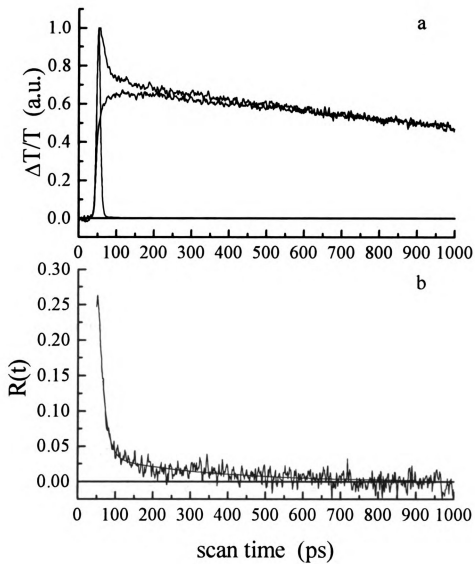


Figure IV.6. (a)  $I_0(t)$  and  $I_1(t)$  and (b)  $R(t)$  for 1-methylperylene in benzene.

oblate rotor by  $D_z > D_x = D_y$ .

$$\textit{prolate: } R(t) = \left(\frac{4}{10}\right)\exp(-6D_z t) \quad [\text{IV.6}]$$

$$\textit{oblate: } R(t) = \left(\frac{3}{10}\right)\exp(-(2D_x + 4D_z)t) + \left(\frac{1}{10}\right)\exp(-6D_x t) \quad [\text{IV.7}]$$

The single exponential decays we recover for perylene in both solvents and for 1-methylperylene in toluene yield  $\tau_{\text{OR}} = 6D_z^{-1} = 15$  ps, or  $D_z = 9.26$  GHz. Despite the fact that  $D_x$  is not determined in these measurements,  $D_x > D_z$ , yielding  $D_z/D_x < 1$ . For the double exponential decay seen for 1-methylperylene in benzene, the times  $\tau_{\text{OR}}$  correspond to  $D_z = 16.4$  GHz and  $D_x = 0.60$  GHz. Thus  $D_z/D_x \cong 27$ , implying a very significant change in the effective rotor shape of 1-methylperylene for the two solvents. Perhaps even more striking is that the limiting value for 1-methylperylene in the *n*-alkanes was found to be  $D_z/D_x = 8.5$ .<sup>[5]</sup> Correlation of the reorientation behavior with the  $T_1$  relaxation behavior indicates that the organization of benzene about 1-methylperylene is such that the alignment of the donor and acceptor modes yields a value of  $\langle \kappa^2 \rangle < \frac{2}{3}$ . While the fundamental reason for the apparently anomalous reorientation behavior of 1-methylperylene in benzene remains unclear and requires further examination, a clear implication of these data is that the efficiency of  $T_1$  relaxation for both probe molecules is mediated primarily by intermolecular alignment effects, in agreement with the relaxation behavior measured for 1-methylperylene in the branched alkanes.<sup>[6]</sup> While it is fair to question what changes in intermolecular alignment could account for these data, we do not have sufficient information to draw definitive conclusions regarding solvent local organization about the solute(s).

#### IV.D. Conclusions

We have measured the vibrational population relaxation and rotational diffusion dynamics of perylene and 1-methylperylene in benzene and toluene using pump-probe stimulated emission spectroscopy. We find that the vibrational relaxation dynamics do not correlate simply with the order of polar D-A coupling. The reorientation dynamics of 1-methylperylene in benzene are fundamentally different than for this same probe molecule in toluene or for perylene in benzene. The fundamental reason for this unexpected confinement of the 1-methylperylene motion in benzene is unclear as yet, but is strongly indicative of local organization of the solvent about the solute. The fact that the  $T_1$  time for 1-methylperylene in benzene is measurably slower than for the other systems we report indicates that the solute confinement is effected in such a way that the donor and acceptor vibrational coordinates (in-plane ring distortions) are poorly aligned. It is apparent that the organization of the solvent about the solute can play a dominant role in determining reorientation as well as vibrational population relaxation. It is also clear that the reorientation dynamics of the two probe molecules perylene and 1-methylperylene require further understanding.

#### IV.E. References

1. Zieger, H. E.; Laski, E. M.; *Tet. Lett.*, **32**, 3801 (1966).
2. Hambir, S. A.; Jiang, Y.; Blanchard, G. J.; *J. Chem. Phys.*, **98**, 6075 (1993).
3. Jiang, Y.; Blanchard, G. J.; *J. Phys. Chem.*, **98**, 9411 (1994).
4. Jiang, Y.; Blanchard, G. J.; *J. Phys. Chem.*, **98**, 9417 (1994).
5. Jiang, Y.; Blanchard, G. J.; *J. Phys. Chem.*, **99**, 7904 (1995).

6. McCarthy, P. K.; Blanchard, G. J.; *J. Phys. Chem.*, **100**, 5182 (1996).
7. Heitz, M. P.; Horne, J. C.; Blanchard, G. J.; Bright, F. V.; *Appl. Spec.*, in press.
8. Blanchard, G. J.; *Rev. Sci. Instruments.*, in press.
9. Yardley, J. T.; Introduction to Molecular Energy Transfer, Academic, New York, 1980.
10. Gray, C. G.; Gubbins, K. E.; Theory of Molecular Fluids, Vol. 1: Fundamentals, Oxford Science, 1984, pp. 91-100.
11. Förster, Th.; *Ann. Phys. Leipzig*, **2**, 55 (1948).
12. Rigby, M.; Smith, E. B.; Wakeham, W. A.; Maitland, G. C.; The Forces Between Molecules, Oxford Science, 1986, p. 7.
13. Supercritical Fluid Science and Technology; Johnston, K.P. and Penninger, J.M.L., Eds.; ACS Symposium Series 406; American Chemical Society: Washington, DC, 1989.
14. Supercritical Fluid Technology - Theoretical and Applied Approaches in Analytical Chemistry, Bright, F.V. and McNally, M.E.P., Eds.; ACS Symposium Series 488; American Chemical Society: Washington, DC, 1992.
15. Supercritical Fluid Technology - Reviews in Modern Theory and Applications; Bruno, T.J. and Ely, J.F., Eds.; CRC Press: Boca Raton, FL, 1991.
16. Supercritical Fluid Engineering Science - Fundamentals and Applications, Kiran, E. and Brennecke, J.F., Eds.; ACS Symposium Series 514; American Chemical Society: Washington, DC, 1993.
17. M. A. McHugh, and V. J. Krukoni, Supercritical Fluid Extraction - Principles and Practice, (Butterworths, Boston, MA), 1993.
18. Rhodes, T. A.; O'Shea, K.; Bennett, G.; Johnston, K. P.; Fox, M. A. *J. Phys. Chem.* **99**, 9903 (1995).
19. Zhang, J.; Lee, L. L.; Brennecke, J. F. *J. Phys. Chem.* **99**, 9268 (1995).
20. Eckert, C. A.; Ziger, D. H.; Johnston, K. P.; Ellison, T. K. *Fluid Phase Equil.*, **14**, 167 (1983).
21. Betts, T. A.; Zagrobelny, J.; Bright, F. V. *J. Am. Chem. Soc.* **114**, 8163 (1992).

22. Tjahajadiputra, S.; Hunt, K. L. C.; Blanchard, G. J.; in preparation.
23. Grimme, S.; Lohmannsroben, H.-G.; *J. Phys. Chem.*, **96**, 7005 (1992).
24. Jiang, Y.; Blanchard, G. J.; *J. Phys. Chem.*, **98**, 6436 (1994).

## **V. VIBRATIONAL POPULATION RELAXATION OF TETRACENE IN *n*-ALKANES. EVIDENCE FOR EFFICIENT COUPLING BETWEEN SOLVENT AND SOLUTE**

### **V.A. Introduction**

This study was performed to develop an understanding of solvent chain length effects on energy transfer efficiency. The transfer of energy from three vibrational modes of tetracene ( $1462\text{ cm}^{-1}$ ,  $1383\text{ cm}^{-1}$ , and  $1294\text{ cm}^{-1}$ , the first two being fundamentals and the latter is a combination mode) to a series of *n*-alkane solvents was measured. The  $T_1$  times for the vibrational energy transfer ranged from  $\leq 10$  ps through  $\sim 40$  ps, depending on the solvent and vibrational mode of interest. The solvent dependent  $T_1$  times for the fundamentals indicate that the solute-solvent coupling is much more efficient than previous measurements involving perylene in the same solvent series. However, the existence of solvent chain length dependent  $T_1$  relaxation for perylene and 1-methylperylene suggests local ordering of the solvent rather than a random orientational distribution in the proximity of the solutes.

### **V.B. Experimental**

The ultrafast pump-probe laser system used to measure the vibrational population relaxation dynamics of tetracene is detailed in Chapter II. The schematic representing the strongly coupled three level system is depicted in Figure II.2. The pump dye laser is

operated with Stilbene 420 dye (Exciton) in the range of 468 nm to 473 nm, depending on the solvent used. The probe laser is operated with Coumarin 490 dye (Exciton) between 498 nm and 508 nm. The pump dye laser wavelength was determined by the spectral overlap of the normalized absorption and emission spectra of tetracene in each solvent system (Figure V.1). The probe dye laser frequency is set to one vibrational resonance lower in energy than the pump dye laser frequency.

### **V.B.1. Chemicals And Sample Handling**

Tetracene and the *n*-alkane solvents were purchased from Aldrich Chemical Co. in the highest purity grade available and were used as received. Tetracene solution concentrations were  $\sim 10^{-5}$  M and were prepared by saturating the solution and then removing excess solid tetracene by filtration prior to the  $T_1$  measurements. The solubility of tetracene increases with increasing solvent aliphatic chain length, and thus the chromophore concentrations used in these experiments varied (by a factor of  $\sim 4$ ) over the range of solvents used. For all measurements, however, saturation was achieved at a concentration sufficiently low that no aggregation effects were observed. For the pump-probe measurements, thermal lensing contributions to the signal were minimized by flowing the sample through a 1 mm path length cell. For all measurements, the sample temperature was maintained at  $300 \pm 0.2$  K.

### **V.C. Results And Discussions**

The  $T_1$  relaxation behavior of perylene<sup>[1]</sup> and 1-methylperylene<sup>[2]</sup> in the *n*-alkanes has been examined previously. For these systems, the donor-acceptor frequency detuning

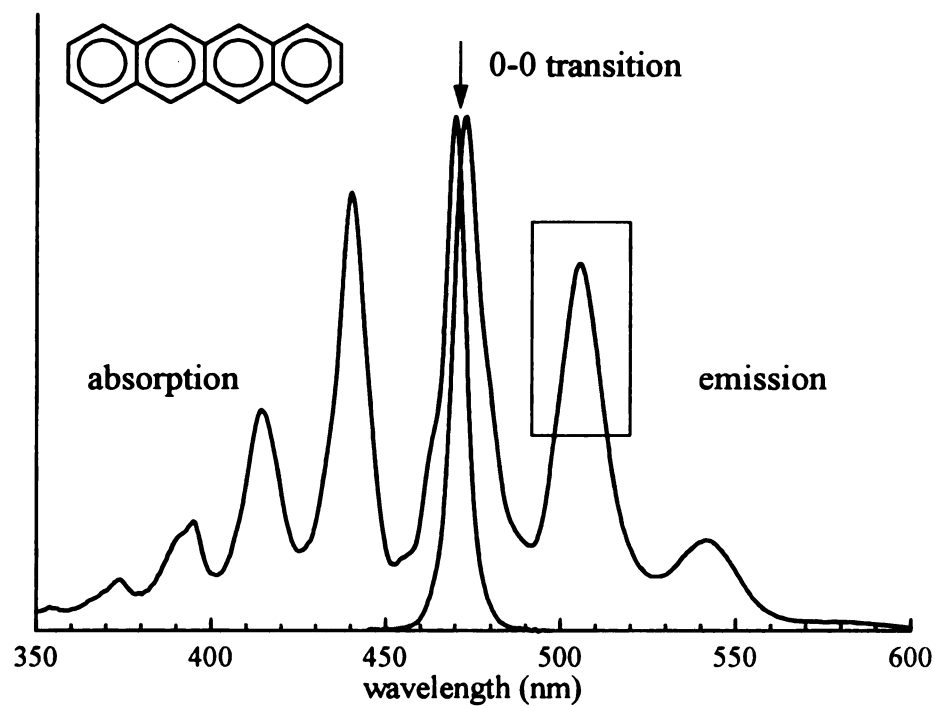


Figure V.1. Normalized absorption and emission spectra of tetracene in *n*-nonane. The arrow denotes the 0-0 transition ( $\lambda_{\text{pump}}$ ) and the boxed region indicates the spectral region containing the vibrational modes studied here ( $\lambda_{\text{probe}}$ ).

is  $\Delta v = 0$ . These experiments have indicated that the order of the polar donor-acceptor coupling is important in determining the length scale over which the relaxation event operates and also that solvent local organization exists in the proximity of the solute molecule. The purpose of the present investigation is to achieve an understanding of how the shape of the solute molecule alters the transfer of vibrational energy between molecules in solution. To achieve this understanding, we chose to examine three vibrational modes of tetracene in *n*-alkanes. We chose tetracene because its shape is significantly different than perylene. In addition, the linear optical response of this molecule is well understood,<sup>[3-6]</sup> and there is no spectroscopic evidence of significant vibronic coupling effects between singlet electronic manifolds.<sup>[7]</sup> We have examined three vibrational resonances in tetracene; two Raman-active fundamental modes (1462 cm<sup>-1</sup>, 1383 cm<sup>-1</sup>) that are degenerate with IR-active solvent acceptor modes and a third, Raman-active combination vibrational mode (1293 cm<sup>-1</sup>) that is degenerate with an IR-active resonance in tetracene (1294 cm<sup>-1</sup>). We have calculated the atomic displacements for these modes and show them in Figure V.2. We expected that the investigation of the two Raman-active fundamentals would yield information on the different environments probed by the two vibrational coordinates and that the combination mode could, potentially, provide insight into intramolecular energy transfer processes.

The absorption and emission spectra of tetracene in all of the *n*-alkane solvents are virtually identical to those shown in Figure V.1, with only minor spectral shifts arising from solute-solvent interactions. For all the T<sub>1</sub> measurements, the pump laser wavelength is set to the spectroscopic origin to avoid contributions to the data from excited state vibrational population relaxation.<sup>[1]</sup> The probe laser wavelength was varied across the

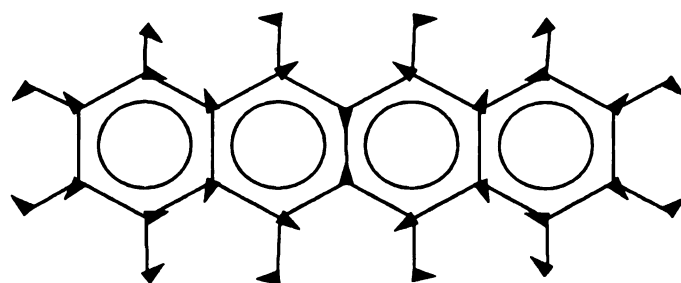
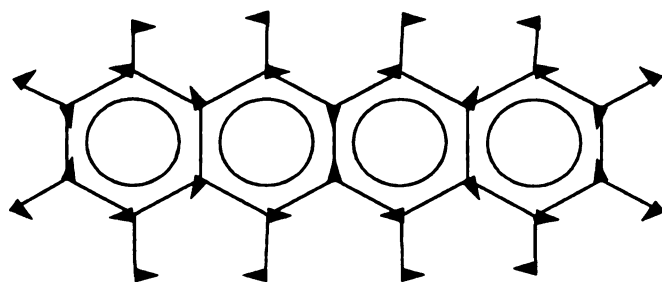
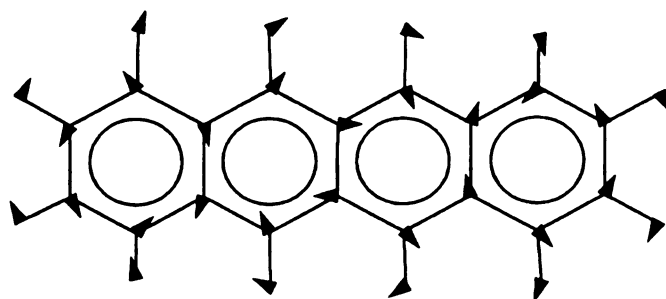
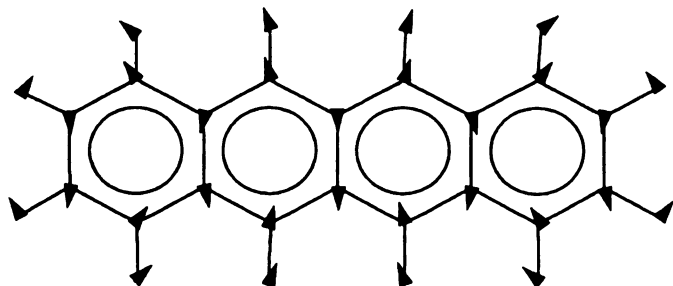
 $1462\text{cm}^{-1}$  (R) $1383\text{cm}^{-1}$  (R) $1293\text{cm}^{-1}$  (R) $1294\text{cm}^{-1}$  (IR)

Figure V.2. Schematic atomic displacements for the vibrational modes studied here. Frequencies and activities are indicated for each mode. The arrows are directional indicators only and are not meant to indicate the amplitudes of the displacements.

boxed region shown in Figure V.1 to access the 1462, 1383, and 1293  $\text{cm}^{-1}$  modes of tetracene. The  $T_1$  times we report here are the averages of at least two and usually four determinations. Each determination is, itself, the average of at least 10 (usually 20) individual time scans. As we had found for the  $T_1$  relaxation of perylene in the *n*-alkanes,<sup>[1]</sup> the experimental data exhibit both a solvent and vibrational mode dependence. For this reason, we consider the behavior of the modes individually before comparing the results of one mode to those of another.

The tetracene 1383  $\text{cm}^{-1}$  vibration should, in principle, provide a direct comparison to the perylene data because we are probing the same degenerate donor-acceptor relaxation effect in both experiments. We find that there is a measurable solvent dependence to the experimental data. Specifically,  $T_1$  is fast in *n*-pentane, *n*-hexane, and *n*-heptane, and there is a significant increase in  $T_1$  for this mode in *n*-octane. For the longer alkanes,  $T_1$  gradually decreases from its high of  $38 \pm 8$  ps in *n*-octane to  $<10$  ps in *n*-hexadecane (Figure V.3a and Table V.1). The observation of a discontinuous  $T_1$  dependence on the solvent aliphatic chain length is reminiscent of the behavior of perylene, but the details of the solvent dependence are significantly different. For the perylene 1375  $\text{cm}^{-1}$  mode, the fastest  $T_1$  times were reported for *n*-octane and *n*-nonane, exactly the opposite of the data we report here on tetracene. An obvious implication of these data is that the solvent environment formed around the tetracene molecule is significantly different than that formed around the perylene molecule. Because  $T_1$  does not vary regularly with solvent aliphatic chain length, however, these data indicate the presence of solvent local organization about the tetracene molecule. It is apparent that there is not enough information provided from these measurements to reveal the details of

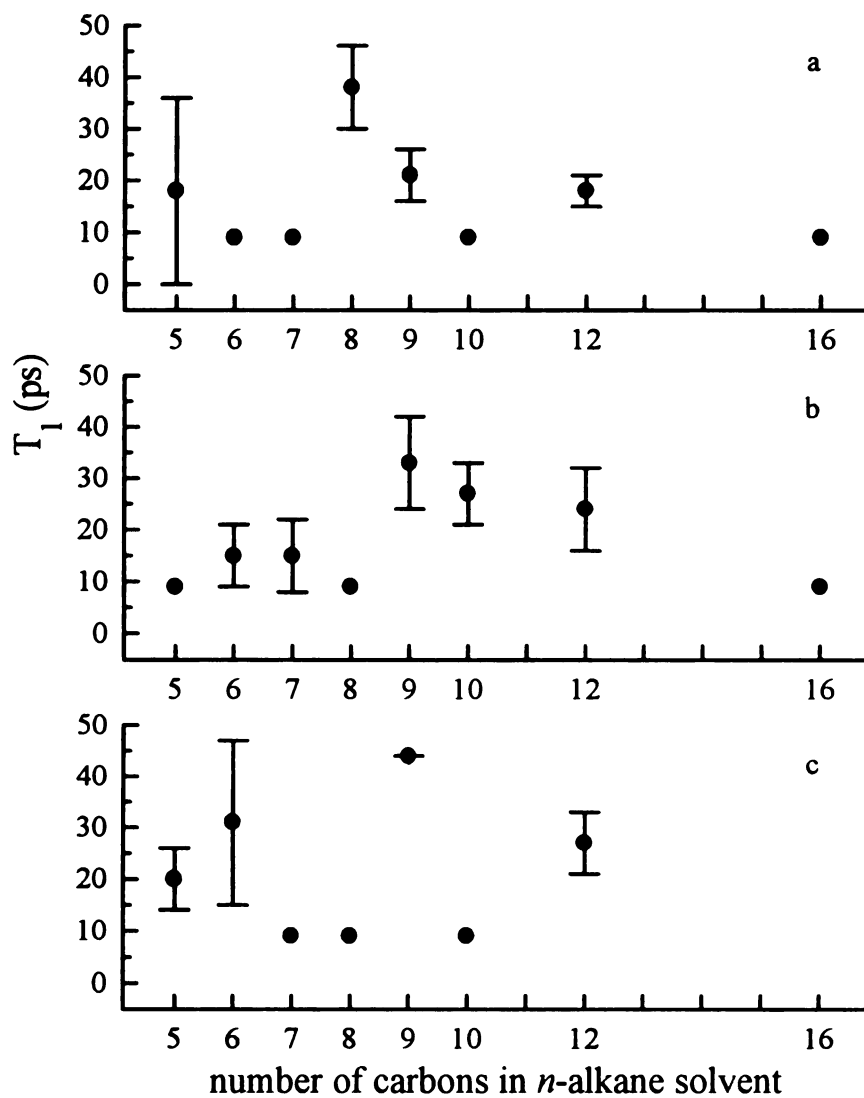


Figure V.3.  $T_1$  times of tetracene vibrations as a function of solvent aliphatic chain length. (a)  $1383\text{cm}^{-1}$  mode, (b)  $1293\text{cm}^{-1}$  mode, (c)  $1462\text{cm}^{-1}$  mode. For the  $1462\text{cm}^{-1}$  mode, the relaxation behavior in  $n$ -hexadecane is anomalous and is not included in the figure. See text for a discussion of this point.

solvent	vibrational mode (cm <sup>-1</sup> )	T <sub>1</sub> ± 1σ (ps)
<i>n</i> -pentane	1462	19 ± 6
	1383	18 ± 6
	1293	<10
<i>n</i> -hexane	1462	31 ± 16
	1383	<10
	1293	15 ± 6
<i>n</i> -heptane	1462	<10
	1383	<10
	1293	15 ± 7
<i>n</i> -octane	1462	<10
	1383	38 ± 8
	1293	<10
<i>n</i> -nonane	1462	44 ± 1
	1383	21 ± 5
	1293	33 ± 9
<i>n</i> -decane	1462	<10
	1383	<10
	1293	27 ± 6
<i>n</i> -dodecane	1462	27 ± 6
	1383	18 ± 3
	1293	24 ± 8
<i>n</i> -hexadecane	1462	58 ± 4 <sup>a</sup>
	1383	<10
	1293	<10

Table V.1. T<sub>1</sub> times of selected tetracene vibrations in *n*-alkanes. a) Sum of two exponential decays. See text for a discussion of these data.

organization of the solvent molecules around tetracene. We offer a speculative explanation only and do not claim to achieve a detailed understanding of solvent local organization. The fact that we observe the increase in  $T_1$  times at *n*-octane for this mode suggests that the shorter alkanes cannot span the length of the tetracene molecule, and therefore both terminal methyl groups, on which the solvent acceptor mode is significantly localized, are in close proximity to the vibrational coordinate. For the longer alkanes, where it is less likely that both methyl groups are in close proximity to the tetracene molecules, we observe longer  $T_1$  times. In order to be consistent with this hypothesis, the longer alkanes would have to “wrap around” tetracene, *i.e.*, exhibit a significant number of *gauche* bonds, to account for the decrease in  $T_1$  with increasing solvent length. We also note that the  $1383\text{ cm}^{-1}$  tetracene donor mode exhibits its dominant motion along the long molecular axis (Figure V.2), favoring coupling to solvent modes that are oriented similarly. Again, we provide this hypothesis only as a potential explanation that is consistent with the data.

The tetracene  $1293\text{ cm}^{-1}$  vibrational mode differs from the  $1383\text{ cm}^{-1}$  mode in that it is not a Raman-active fundamental mode. Rather, the  $1293\text{ cm}^{-1}$  mode is a combination resonance ( $307\text{ cm}^{-1} + 986\text{ cm}^{-1}$ ) that is in close energetic proximity to the IR-active  $1294\text{ cm}^{-1}$  mode. Amirav *et al.* have reported the low-temperature emission spectrum of isolated tetracene and indicate that both the  $307\text{ cm}^{-1}$  and  $986\text{ cm}^{-1}$  resonances are fundamental modes.<sup>[8]</sup> The combination mode they list at  $1314\text{ cm}^{-1}$  is not assigned specifically as a combination of these fundamentals but, to within their experimental uncertainty ( $\pm 10\text{ cm}^{-1}$ ), is in energetic agreement with this assignment. The intensity of the  $1314\text{ cm}^{-1}$  mode is similar to that of the  $1431$  and  $1483\text{ cm}^{-1}$  modes they report.<sup>[8]</sup>

Although it is not clear whether the  $1462\text{ cm}^{-1}$  mode we have studied corresponds to the  $1431\text{ cm}^{-1}$  or the  $1483\text{ cm}^{-1}$  mode in the isolated molecule, it is apparent that significant vibrational spectral shifts occur on solvation. The  $1293\text{ cm}^{-1}$  combination mode is not prominent in the off-resonance Raman spectrum of tetracene, but the Franck-Condon factors for combination modes can be enhanced significantly on resonance.<sup>[1]</sup> We have observed two different perylene combination modes that we enhanced significantly on resonance. We have observed two different perylene combination modes that are seen in low-temperature emission experiments<sup>[9,10]</sup> but are weak in spontaneous Raman measurements. The solvent dependence of  $T_1$  for the tetracene  $1293\text{ cm}^{-1}$  mode is presented in Figure V.3b. These data are similar to those shown in Figure V.3a for the  $1383\text{ cm}^{-1}$  mode, except that the abrupt increase in  $T_1$  occurs at *n*-nonane instead of *n*-octane. We believe that this mode-dependent  $T_1$  behavior results partly from the fact that we are probing two different vibrational normal coordinates, and therefore a different component of the solvent environment is accessed with the two modes. While we could attempt to relate the different  $T_1$  solvent dependence for these two modes solely to differences in their atomic displacements, we believe that an additional factor serves to cloud such an interpretation. The identity of the dominant solvent acceptor mode(s) may be different, because there is not a solvent acceptor mode at  $\sim 1300\text{ cm}^{-1}$ . Thus, the dominant relaxation, if direct and not through low frequency, anharmonically coupled modes, is likely to solvent resonances other than the  $1378\text{ cm}^{-1}$  mode. If the orientational distribution of the solvent molecules around the tetracene was random, which our  $T_1$  data demonstrate that it is not, then a coupling efficiency for each solvent mode could be estimated based solely on the donor-acceptor detuning. Because the solvent is organized

to some extent about the solute, however, it is not possible to accurately assess the dominant acceptor mode because of the undetermined average distance and orientation factors for each acceptor mode normal coordinate. The tetracene 1293  $\text{cm}^{-1}$  mode is essentially degenerate with the IR-active 1294  $\text{cm}^{-1}$  mode. If intramolecular coupling of these two modes were important, then we would expect the measured  $T_1$  times for the 1293  $\text{cm}^{-1}$  mode to be significantly faster than for the 1383  $\text{cm}^{-1}$  mode, due to the longer range coupling associated with dipole-dipole processes. We do not observe any such decrease in  $T_1$ , indicating that intramolecular coupling between these two modes is weak. This finding is consistent with the different parity of the two modes.

The tetracene 1462  $\text{cm}^{-1}$  vibrational mode solvent-dependent  $T_1$  behavior (Figure V.3c) does not yield a response as amenable to interpretation as that for either the 1293  $\text{cm}^{-1}$  or the 1383  $\text{cm}^{-1}$  modes. Perhaps one reason for the absence of a pattern in the solvent dependence is that fact that the relaxation of the  $S_1$  is more complicated for this experimental condition than it is for the other cases. The time scans for this vibrational mode yield responses described well by Equation II.4 and similar to those for the other modes in the solvents *n*-pentane through *n*-dodecane. In *n*-hexadecane, however, the time domain data are of a fundamentally different form (Figure V.4). Specifically, the time evolution of the tetracene 1462  $\text{cm}^{-1}$  mode in *n*-hexadecane stimulated response decays as a sum of two exponentials rather than the difference of two exponentials. We have encountered this decay functionality before in stimulated emission measurements of Coumarin 153 (Chapter VII.B).<sup>[11]</sup> There are, in general, two experimental conditions consistent with this decay functionality or our experiment. The first condition is that there is a competitive population decay channel for the excited electronic state, and the second

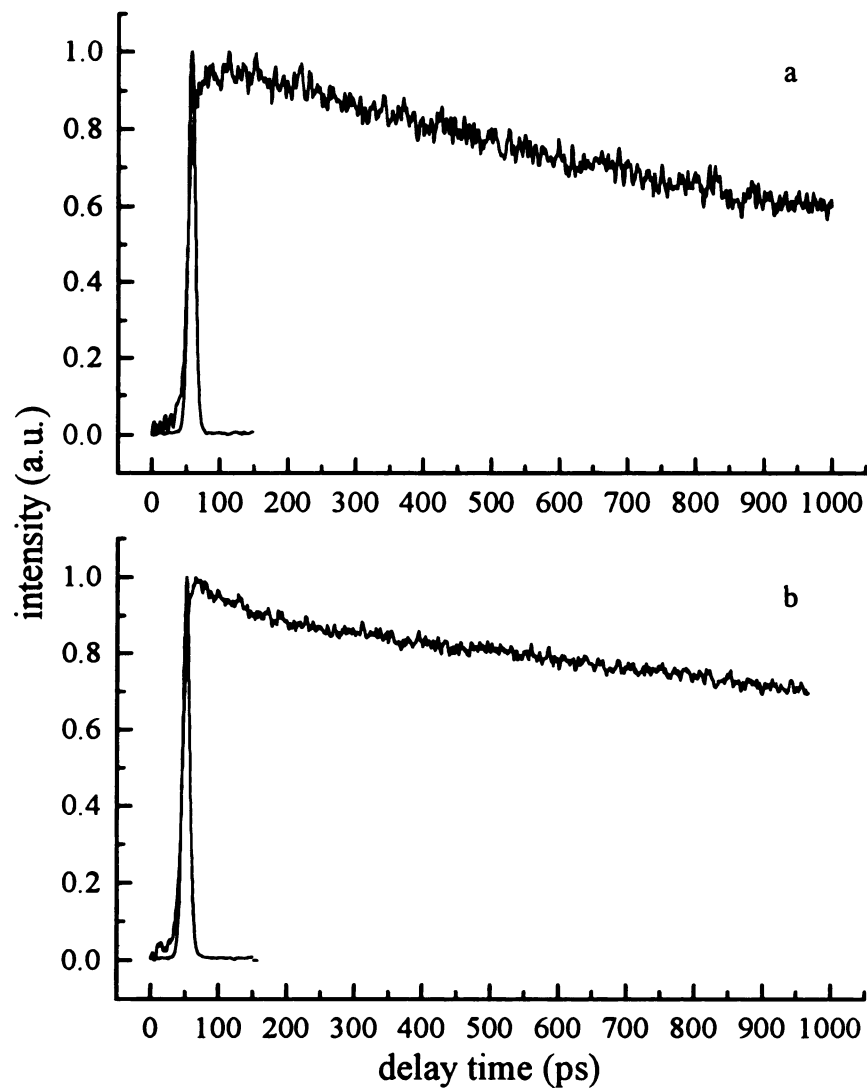


Figure V.4. Time scans for tetracene  $1462\text{cm}^{-1}$  mode in (a) *n*-dodecane and (b) *n*-hexadecane. For both measurements the probe laser electric field is oriented at  $54.7^\circ$  with respect to the pump laser electric field.

condition is that there exists a reversible isomerization where one of the conformers decays radiatively and the other is either nonradiative or decays radiatively in a spectral region not sensed by the experiment. The latter possibility is precluded because of the rigid structure of tetracene, indicating that we are accessing an additional population decay channel from the excited electronic state. For this condition, the expected form of the experimental signal is<sup>[11]</sup>:

$$\begin{aligned}
 S(t) = A(t) + B(t) = & \left[ \frac{k_{21}\lambda_4 - \lambda_3(\lambda_4 - k_{14} - k_{21})}{2k_{23}(\lambda_4 - k_{14} - k_{21})} \right] \exp(-\lambda_3 t) \\
 & + \left[ \frac{k_{21}\lambda_3 - \lambda_4(\lambda_3 - k_{14} - k_{21})}{2k_{23}(\lambda_3 - k_{14} - k_{21})} \right] \exp(-\lambda_4 t) \\
 \lambda_3 = & \left[ (k_{12} + k_{21} + k_{23} + k_{14}) - \left[ (k_{12} + k_{21} + k_{23} + k_{14})^2 - 4(k_{14}k_{21} + k_{14}k_{23} + k_{12}k_{23})^{1/2} \right] \right] \\
 \lambda_4 = & \left[ (k_{12} + k_{21} + k_{23} + k_{14}) + \left[ (k_{12} + k_{21} + k_{23} + k_{14})^2 - 4(k_{14}k_{21} + k_{14}k_{23} + k_{12}k_{23})^{1/2} \right] \right]
 \end{aligned}$$

[V.1]

where  $k_{14}$  is rate constant for the additional nonradiative decay channel (indicated by the dashed arrow in Figure II.2). It is important to note that this effect is solvent dependent and is not related to the photodegradation of tetracene. We understand this behavior in the context of solvent-dependent stabilization of a state in tetracene into which the energy from  $S_1$  can relax. The intersystem crossing behavior of tetracene and its analogs has been investigated before, and it is well established that there is a triplet state in close energetic proximity to the  $S_1$ .<sup>[12]</sup> Further, intersystem crossing has been demonstrated to be significant relaxation channel in tetracene;  $\Phi_{ISC} \sim 0.6$ .<sup>[13]</sup> The fluorescence quantum yield

of tetracene is  $\Phi_{\text{fl}} \sim 0.15$ ,<sup>[14]</sup> indicating that there are a variety of nonradiative relaxation pathways available to the  $S_1$ .<sup>[5,6]</sup> The fact that the efficiency of these nonradiative relaxation pathways depends on the identity of the immediate environment is potentially useful for the examination of interactions between tetracene and its surroundings, but a detailed understanding of this behavior remains to be developed. The fast component of the double exponential decay (Figure V.4b) can arise from either  $k_{23}$  or  $k_{14}$ . Because we have no independent means to determine whether  $k_{23}$  or  $k_{14}$  dominates the experimental response we see for the tetracene  $1462 \text{ cm}^{-1}$  mode in *n*-hexadecane, we do not include this data point in Figure V.3c.

We expected initially that the  $T_1$  relaxation behavior of tetracene in *n*-alkanes should be qualitatively similar to the behavior we reported previously for perylene in the same solvents. Our starting point in making this assumption was that both tetracene and perylene are of  $D_{2h}$  symmetry, and thus they possess centers of inversion. As outlined in Chapter IV, the interaction potential between a solute Raman-active mode and a solvent IR-active mode will scale  $r^{-8}$ . Because there is very little two-photon absorption associated with the  $S_1 \leftarrow S_0$  one photon-allowed transition in tetracene,<sup>[15]</sup> we believe that structural distortion of the chromophore by the surrounding solvent is insufficient to induce any significant IR activity in tetracene Raman-active modes. We expect the  $r^{-8}$  dependence of vibrational energy transfer to hold for tetracene. For this reason, and on the basis of the comparatively fast  $T_1$  times we see for tetracene compared to perylene, we assert that the difference in the  $T_1$  times seen for these two molecules is a consequence of different organization of the solvent molecules around the two probes. The observation that the  $T_1$  times for tetracene are, on aggregate, significantly faster than those for

perylene invites speculation. One possible reason for this effect is that tetracene samples a smaller distribution of solvent cage conformations than does perylene in the same solvent(s). Tetracene is significantly less soluble in the *n*-alkanes than is perylene, suggesting (but not proving) that a smaller number of solvent cage configurations exist for tetracene that are sufficiently stabilizing to overcome the intermolecular forces within the solid material. If this is the case, then only those solvent cage configurations where alignment of the molecules optimizes attractive interactions with the tetracene molecules will be allowed. We do not suggest that the solvent and solute are in closer proximity for tetracene than for perylene, but rather that the solvent and solute are better aligned with respect to one another for tetracene. This possible explanation is intuitively consistent with the different aspect ratios of the two molecules, but there is little direct evidence other than our  $T_1$  data to either support or refute this explanation. It is possible, in principle, that such alignment effects could be sensed by rotational diffusion measurements, but our earlier work on perylene indicates that quadrupole-dipole  $T_1$  relaxation does not display a significant correlation with reorientation dynamics.<sup>[1,12]</sup>

#### **V.D. Conclusions**

We have examined the population relaxation behavior of three tetracene vibrational resonances in the *n*-alkanes pentane through decane, dodecane, and hexadecane. We find evidence for local organization of the solvent molecules around the solute and that the portion of the local environment sensed in these experiments depends on the vibrational coordinate interrogated. We find that, for tetracene, where there are several possible (ill-understood) nonradiative relaxation channels from the  $S_1$ , the efficiency of these different

relaxation pathways depends on interactions between the solute and its immediate environment. In general, the  $T_1$  relaxation dynamics of tetracene in the *n*-alkanes are significantly faster than they are for perylene in these same solvents. We attribute this enhanced relaxation efficiency to better alignment, not closer proximity, between the solute donor vibrational coordinate and the solvent acceptor vibrational coordinate. This locally enhanced alignment is a consequence of the aspect ratio of tetracene and may be particularly obvious in this case because of the likely smaller number of solvent cages that can accommodate the presence of the tetracene molecule. We make this argument based on the comparatively low solubility of tetracene in *n*-alkanes and the experimental  $T_1$  data. We expect that these results will be directly applicable to the relaxation behavior of tetracene in two-dimensional molecular assemblies such as alkanethiolate / Au monolayers or zirconium phosphate multilayer structures, where short- and long-range organization is enforced more rigidly. These data also demonstrate the need for a comprehensive theoretical treatment of polar coupling processes in liquids.

## V.E. References

1. Jiang, Y.; Blanchard, G. J.; *J. Phys. Chem.*, **98**, 9417 (1994).
2. Jiang, Y.; Blanchard, G. J.; *J. Phys. Chem.*, **99**, 7904 (1995).
3. Birks, J. B. *Photophysics of Aromatic Molecules*; Wiley-Interscience: London, 1970.
4. Douris, R. G. *Ann. Chim.* **31**, 479 (1959).
5. Fleming, G. R.; Lewis, C.; Porter, G. *Chem. Phys. Lett.* **31**, 33 (1975).
6. Okajima, S.; Lim, E. C. *Chem. Phys. Lett.* **37**, 403 (1976).
7. Karpovich, D. S.; Blanchard, G. J. *J. Phys. Chem.* **99**, 3951 (1995).

8. Amirav, A.; Even, U; Jortner, J J. *Chem. Phys.* **75**, 3770 (1981).
9. Shpol'skii, E. V.; Personov, R. I. *Opt. Spectrosc.* **8**, 172 (1960).
10. Cyvin, S. J.; Cyvin, B. N.; Klaeboe, P. *Spectrosc. Lett.* **16**, 239 (1983).
11. Jiang, Y.; McCarthy, P.; Blanchard, G. J. *Chem. Phys.* **183**, 249 (1994).
12. Jiang, Y.; Blanchard, G. J. *J. Phys. Chem.* **98**, 6436 (1994).
13. Birks, J. B. *Photophysics of Aromatic Molecules*; Wiley-Interscience: London, 1970.
14. Douris, R. G. *Ann. Chim.* **31**, 479 (1959).
15. Razumova, T. K.; Starobogatov, I. O. *Opt. Spectrosc.* **58**, 145 (1985).

## **VI. CAN A CHEMICAL REACTION PROCEED ON A TIMESCALE RELEVANT TO VIBRATIONAL POPULATION RELAXATION? AN EXAMINATION OF 1-METHYLPERYLENE IN ALKENE SOLVENTS**

### **VI.A Abstract**

We have examined the relationship between vibrational population relaxation and photoreactivity for 1-methylperylene in a series of  $C_7H_{14}$  alkene solvents. Previous  $T_1$  studies on the  $1370\text{ cm}^{-1}$  mode of this probe molecule have demonstrated the central role of solvent local organization in mediating population relaxation. We examine here whether or not short range solvent organization in a chemically reactive system can influence vibrational population relaxation dynamics. The  $T_1$  times for the 1-methylperylene  $1370\text{ cm}^{-1}$  mode range between 10 ps and 50 ps in the alkenes studied here, and the  $\tau_{OR}$  times vary from 14 ps to 22 ps. 1-Methylperylene is photoreactive with the reaction proceeding in two steps. The first step is solvent non-specific, requires  $O_2$  and is enhanced by resonant  $S_1 \leftarrow S_0$  excitation. The second step of the reaction is highly solvent-specific and shares some portion of the coordinate space sampled by the  $T_1$  relaxation of the  $1370\text{ cm}^{-1}$  mode. Comparison of our  $T_1$  data for 1-methylperylene in alkenes to that in a non-reactive  $n$ -alkane indicates that vibrational relaxation proceeds too rapidly to be influenced significantly by the photochemical reaction.

## VI.B Introduction

The macroscopic properties of materials and solutions are determined, ultimately, by intermolecular interactions between the constituents of the system. The interactions between dissimilar molecules are particularly important because it is these interactions that are responsible for chemical reactions. Because so many reactions are carried out in solution, we have focused on understanding short range organization and interactions in this phase.

From past work on local organization and intermolecular interactions in solution, there have developed several broadly useful experimental approaches.<sup>[1-40]</sup> We use rotational diffusion<sup>[1-24]</sup> and vibrational population relaxation<sup>[41-52]</sup> measurements for these studies because of their complementary nature and exquisite sensitivity to the chromophore local environment. In our previous work, we have shown that the efficiency of energy transfer between dissimilar molecules depends on several system-specific factors such as donor-acceptor interactive distance,<sup>[53,54]</sup> acceptor density,<sup>[55]</sup> donor-acceptor resonance detuning<sup>[56]</sup> and the symmetries of the resonances involved. Vibrational population relaxation measurements<sup>[53,55,57-60]</sup> are more useful than electronic state energy transfer measurements for understanding local organization because of the magnitudes of the transition moments involved in each process. For electric dipole allowed electronic transitions, the critical transfer radius is typically on the order of 25 Å to 50 Å because of the large donor and acceptor transition moments.<sup>[61]</sup> Over this length scale, information on the surrounding medium is effectively averaged over all molecular orientations and thus there is little information on local organization of the solvent in the proximity of the solute contained in such data. For dipolar vibrational energy transfer measurements, the critical

transfer radius is typically  $\sim 10$  Å or less,<sup>[53]</sup> owing to the comparatively small cross-sections of vibrational transitions and their characteristically narrow linewidths. On this shorter length scale, a non-random orientational distribution of solvent molecules is sampled by the solute, with the distribution reflecting order within the system.

Our previous measurements of relaxation of the 1-methylperylene  $1370\text{ cm}^{-1}$  ring breathing mode have shown that the efficiency of relaxation for this mode depends sensitively on the molecular-scale organization of the solvent. The  $T_1$  times for 1-methylperylene we reported for a series of *n*-alkanes depended on the length of the solvent alkane in a discontinuous manner.<sup>[53]</sup> For these measurements, the solvent terminal methyl group rocking mode resonance at  $1378\text{ cm}^{-1}$  produces a degenerate donor-acceptor condition. Short *n*-alkanes ( $< \text{C}_8\text{H}_{18}$ ) yielded fast 1-methylperylene  $T_1$  times ( $\sim 10 - 20$  ps) with an abrupt increase in  $T_1$  to  $\sim 100$  ps for alkanes longer than  $\text{C}_9\text{H}_{20}$ . We interpreted these results in the context of the variation in average distance between the donor vibrational coordinate and the acceptor moieties as a function of solvent length. The  $T_1$  data, in concert with rotational diffusion measurements showing a solvent-dependent change of effective rotor shape, indicate that persistent solvent local organization plays a key role in determining population and orientational relaxation dynamics in the *n*-alkanes.

The existence of measurable solvent local organization is not unique to the *n*-alkanes. We have examined the  $T_1$  relaxation behavior of the 1-methylperylene  $1370\text{ cm}^{-1}$  mode in a series of  $\text{C}_7\text{H}_{16}$  branched alkane solvents, and found that increasing the solvent acceptor density (number of  $\text{CH}_3$  groups per solvent molecule) yields an increase in the  $T_1$  time.<sup>[55]</sup> These data correlate inversely with bulk solvent properties, such as boiling point, implicating the dominance of donor-acceptor intermolecular alignment over simple

acceptor density in mediating vibrational energy transfer.

Understanding local organization in solution is important not only in terms of relating molecular and bulk properties of a given system, but short range order and intermolecular alignment could, in principle, play a significant role in determining the pathway and efficiency of chemical reactions. Indeed, the notion of directional chemical attack is a fundamental premise on which much of our understanding of synthetic organic chemistry rests. Exploring the possibility that solvent local organization can play a mediating role in chemical reactivity is the focus of this paper. To relate the vibrational population relaxation and photochemical reaction behavior of 1-methylperylene in selected alkenes, we measured the  $T_1$  and rotational diffusion times of 1-methylperylene in a series of  $C_7H_{14}$  alkene solvents and *n*-heptane. Our  $T_1$  times for 1-methylperylene in a reactive solvent system indicate that, on the timescale of motional and population relaxation phenomena, the two-step photochemical reaction of the probe with alkenes does not alter the vibrational relaxation dynamics measurably.

## **VI.C Experimental**

### **VI.C.1 Time Resolved Stimulated Spectroscopy**

The pump-probe spectrometer used for our vibrational population and orientational relaxation measurements has been detailed in Chapter II. Both dye lasers were operated with Stilbene 420 laser dye (Exciton). The dye laser wavelengths, 432.4 nm (pump) and 459.6 nm (probe), correspond to the spectral overlap of the absorption and emission spectra and one resonance below that overlap, respectively.

## VI.C.2 Steady State Spectroscopies

The absorptive and emissive linear responses of 1-methylperylene in the alkenes were recorded with ~1 nm resolution with Hitachi U-4001 and F-4500 spectrometers, respectively. The linear response of 1-methylperylene in *cis*-2-heptene is shown in Figure VI.1. The absorption and emission spectra were identical for all solutions used in this work.

## VI.C.3 Photoreaction Product Studies

A Coherent Innova 90 Krypton laser operating in the violet (406 nm - 413 nm, all lines) was used to excite 1-methylperylene/alkene solutions. The average power output from this laser is ~260 mW (CW) in the violet region.

## VI.C.4 Chemicals and Sample Handling

1-Methylperylene was synthesized<sup>[62]</sup> and its structure confirmed by <sup>1</sup>H-NMR, mass spectrometry, and UV/visible spectroscopy. The alkenes 1-heptene, *cis*-2-heptene, *trans*-2-heptene, *cis*-3-heptene, and *trans*-3-heptene, and *n*-heptane were purchased at the highest available purity from Aldrich Chemical Co. and used as received. 1-Methylperylene solutions used for the dynamical measurements were ~10 μM. All measurements were made at 300 ± 0.2K using a temperature-controlled sample holder (brass block).

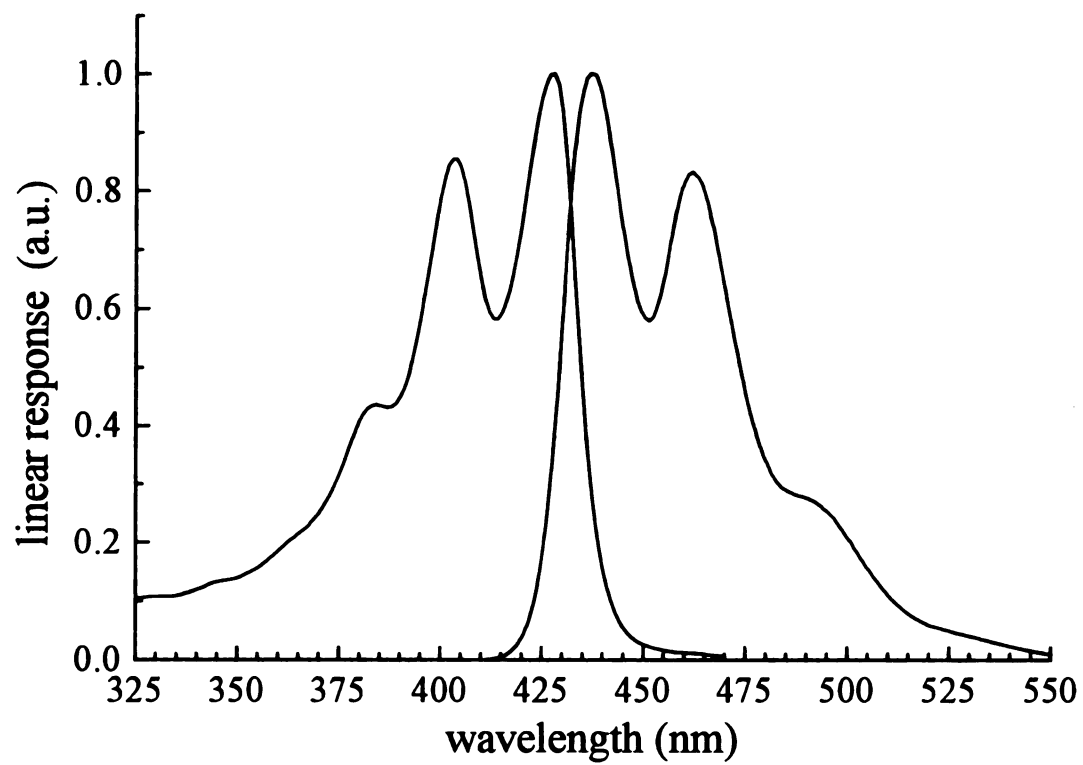


Figure VI.1. Absorption and emission spectra of 1-methylperylene in *cis*-2-heptene.

## VI.D Results and Discussion

We are interested in determining whether or not there is a relationship between the vibrational population relaxation and photoreaction coordinates of 1-methylperylene in selected alkenes. While this question may appear to have a trivial answer based on a simple comparison of the diffusion limited rate constant for such a reaction ( $k \sim 10^8 \text{ s}^{-1}$ ) and the rate constant for a typical vibrational population relaxation process ( $k \sim 10^{11} \text{ s}^{-1}$ ), it is not clear that such a simplification is appropriate for these experimental conditions. Our previous work on 1-methylperylene in alkanes has demonstrated persistent local organization of the solvent about the solute over a  $\sim 10 \text{ \AA}$  length scale. Thus it is possible that a photochemical reaction rate constant is not diffusion limited for this system and the influence of a chemical reaction on vibrational energy redistribution in the system may be measurable. In addition to the timescale issue, intramolecular coupling could, in principle, serve to make these processes irrelevant to one another. The photoreaction of interest here (*vide infra*) proceeds in the excited electronic state and it is fair to question the effect of a reaction on the  $S_1$  surface on the relaxation of a vibration in the  $S_0$  electronic manifold. For many conjugated organic systems, the electronic-vibrational coupling is strong (evidence the prominence of vibronic structure in the emission spectrum of 1-methylperylene) and for conjugated polymers this strong coupling gives rise to the phonon-mediated optical Stark effect.<sup>[63,64]</sup> In order to determine the influence of a photoreaction on vibrational population relaxation, it is necessary to understand the chemical reaction(s) that the 1-methylperylene probe molecule can undergo on excitation, the vibrational population relaxation rates for a mode that spans at least some portion of the photoreaction coordinate and a comparison of these data to that for systems where the

probe molecule does not react in a specific manner with the surrounding solvent. We consider these points individually.

Determining the vibrational population relaxation coordinate of 1-methylperylene is straightforward because the coordinate is defined by the normal mode from which the relaxation proceeds. There are a variety of possibilities for the relaxation of vibrational energy, such as collisional interactions with the surrounding solvent molecules, or initial intramolecular relaxation of the vibrational energy into low frequency solute modes followed by resonant intermolecular transfer to the solvent. While both of these mechanisms are dominant in certain systems, our work on the 1-methylperylene  $1370\text{ cm}^{-1}$  mode in alkanes, which possess a degenerate acceptor mode, has demonstrated that the dominant relaxation pathway is direct energy transfer from the  $1370\text{ cm}^{-1}$  1-methylperylene mode to the  $1378\text{ cm}^{-1}$  solvent terminal  $\text{CH}_3$  rocking acceptor mode. Thus the 1-methylperylene  $1370\text{ cm}^{-1}$  vibrational mode coordinate is representative of the vibrational population relaxation coordinate for these measurements. We have reported the atomic displacements for this mode previously<sup>[55]</sup> and, based on that report, it is clear that the vibrational relaxation coordinate relevant to these experiments lies in the same plane as the  $\pi$  system, *i.e.* the dominant atomic displacements for this mode are along the perimeter of the molecule. While this mode cannot be considered an “in-plane” vibration owing to the angle between the naphthalene moieties<sup>[65]</sup> in 1-methylperylene, we note that there is no significant bending character out of the  $\pi$  system for this mode.

We were able to monitor the progress of the photoreaction through changes in the absorption spectrum of the reactive system. The differences between the linear responses of the 1-methylperylene/alkane and 1-methylperylene/alkene systems are revealing in this

regard (Figure VI.2). For 1-methylperylene in *n*-heptane, the  $S_1 \leftarrow S_0$  transition decreases in intensity in proportion to the amount of chromophore that has reacted. The absorption spectrum of the reacting system possesses an isosbestic point with the 1-methylperylene absorption band, indicating a direct structural relationship between the reactant and the product characterized by the prominent absorption band between 300 nm and 360 nm. We show in Figure VI.3 the ratio of the reactant and product absorbances for the photoreaction of 1-methylperylene in *n*-heptane and in *cis*-2-heptene. These data demonstrate clearly the production of a single, stable product in the alkenes and the absence of a similar product in the alkanes. These data provide unambiguous proof for the existence of two reaction steps.

Establishment of the coordinate system for the photoreaction between 1-methylperylene and the alkenes requires that the reaction be known in detail. The first step in characterizing the reaction mechanism was to eliminate oxygen from the system through a series of freeze-pump-thaw cycles. In the absence of  $O_2$ , the photoreaction of 1-methylperylene characterized by a diminution of the 430 nm absorptive response did not proceed. Introduction of  $O_2$  to the same sample made the system become photo-reactive. Thus the first step in the 1-methylperylene photoreaction reported here is mediated by oxygen. We believe that the presence of  $O_2$  allows for the efficient abstraction of  $H\bullet$  from 1-methylperylene, most likely from the  $CH_3$  group. This step of the photoreaction is nominally solvent non-specific in the limit that the solubility of  $O_2$  is finite in all of the solvents considered. Once the radical intermediate is formed, several resonance structures may contribute to the description of this specie (Figure VI.4). The initial  $H\bullet$  abstraction and subsequent rearrangement yields a 7H-benz[*de*]anthracene chromophore with an

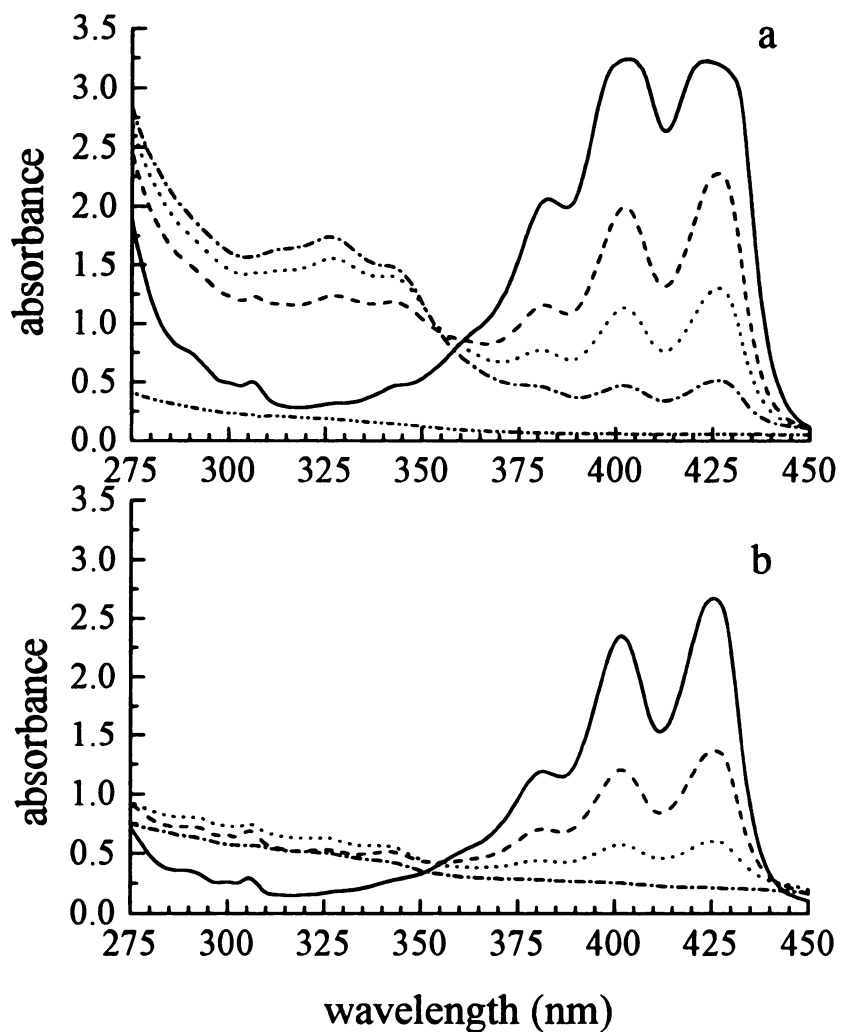


Figure VI.2. a) Absorption spectra of 1-methylperylene in *cis*-2-heptene at various stages of photoreaction: — 0 minutes, — 25 minutes, ... 36 minutes, --- 49 minutes, -·-·- 24 hours. b) Absorption spectra of 1-methylperylene in *n*-heptane at various stages of photoreaction: — 0 minutes, — 15 minutes, ... 30 minutes, --- 80 minutes.

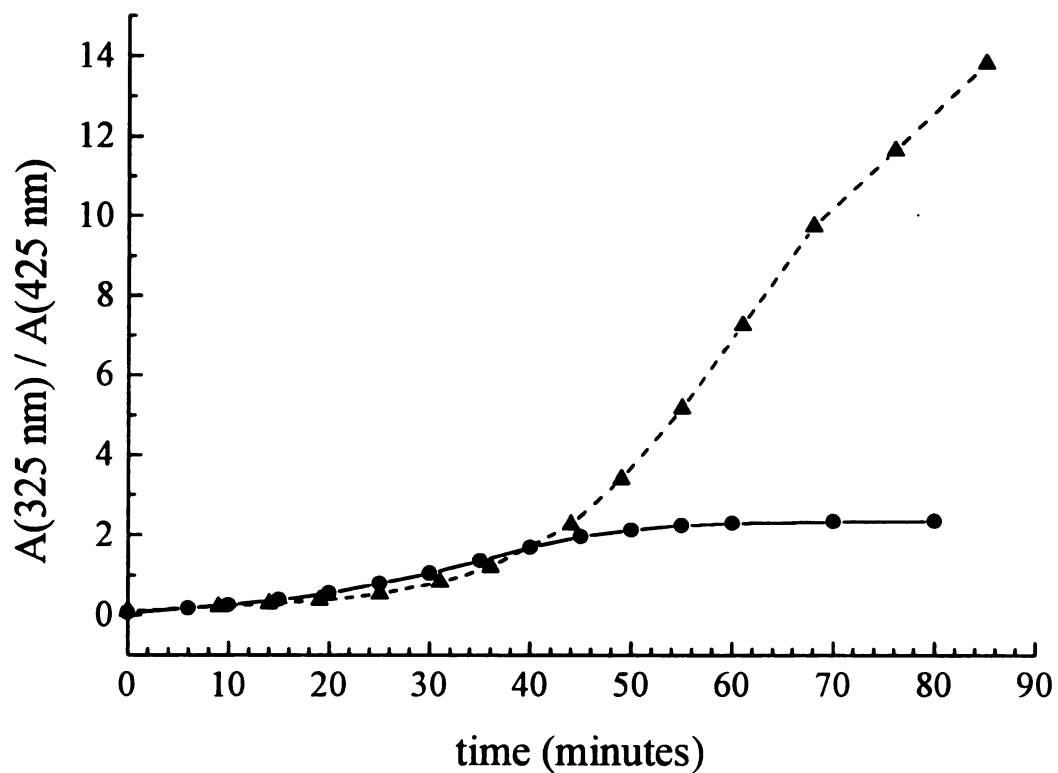


Figure VI.3. Solvent dependence of photoreaction products as manifested in the absorption response of the system: • *n*-heptane, ▲ *cis*-2-heptene. The absorption bands centered at 425 nm and 325 nm are representative of the 1-methylperylene and 7H-benz[*de*]anthracene chromophores, respectively.

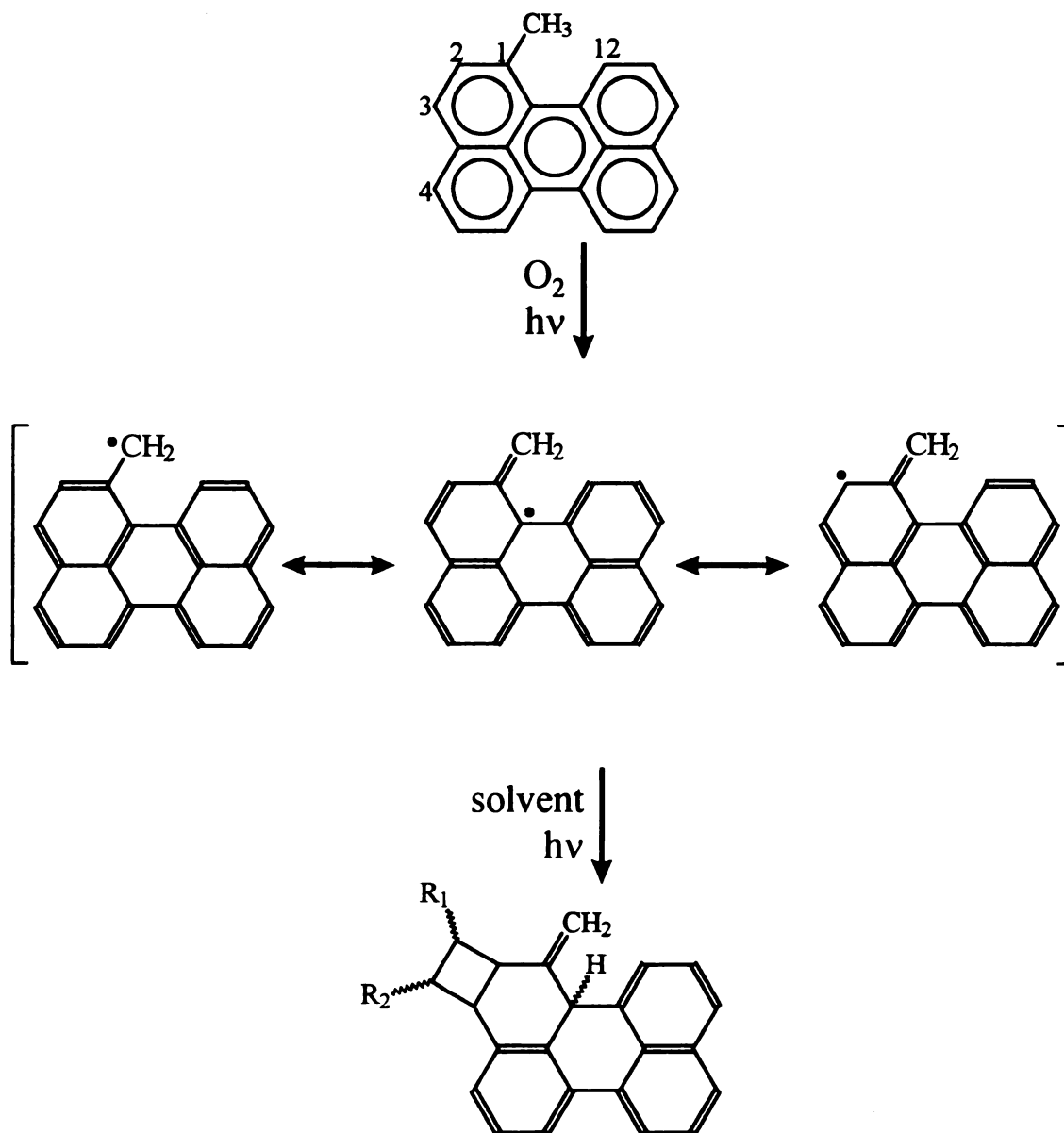


Figure VI.4. Reaction mechanism of 1-methylperylene with O<sub>2</sub> and alkenes, indicating resonance structures for the radical intermediate and site of alkene photo-addition.

additional, partially saturated ring fragment.  $^1\text{H}$  NMR data show that the reactive ring contains the terminal methyl group from the original 1-methylperylene substrate (Figure VI.5). The absorption spectrum of 7H-benz[*de*]anthracene has been reported previously<sup>[66]</sup> and it is characterized by the three prominent resonances between 300 nm and 360 nm that match the linear response of our photoproduct exactly. The second step in the reaction mechanism depends critically on solvent identity. For systems where there is no reactive solvent functionality, the reaction will terminate with the product distribution being determined by a number of possible radical intermediates that can yield intramolecular rearrangements and the presence of any other potentially reactive constituents (Figure VI.4). This is the case for alkane solvents, where there is no unsaturation with which the 1-methylperylene radical unsaturations can react. The  $T_1$  times reported for 1-methylperylene in the alkanes are representative of a population of probe molecules that undergo the  $\text{O}_2$  mediated  $\text{H}\bullet$  abstraction but do not undergo any subsequent single reaction with the solvent. In contrast, for 1-methylperylene in the alkenes, there is a cycloaddition reaction between the substituted 7H-benz[*de*]anthracene radical and the unsaturation in the alkene. The specific site of the Diels-Alder cycloaddition reaction is determined by orbital parity and the electron density distribution within the reactants<sup>[67]</sup>. Using the numbering scheme for 1-methylperylene (Figure VI.4), addition of the alkene across the *1* and *12* positions is unlikely due to steric hindrance caused by the torsional angle between the naphthalene moieties, the presence of the methyl(ene) group at the *1* position and the orbital parity constraints requiring this reaction to proceed from an excited substrate. Addition across the *1* and *2* positions is likewise unlikely based on steric constraints and molecular orbital parity requirements. A

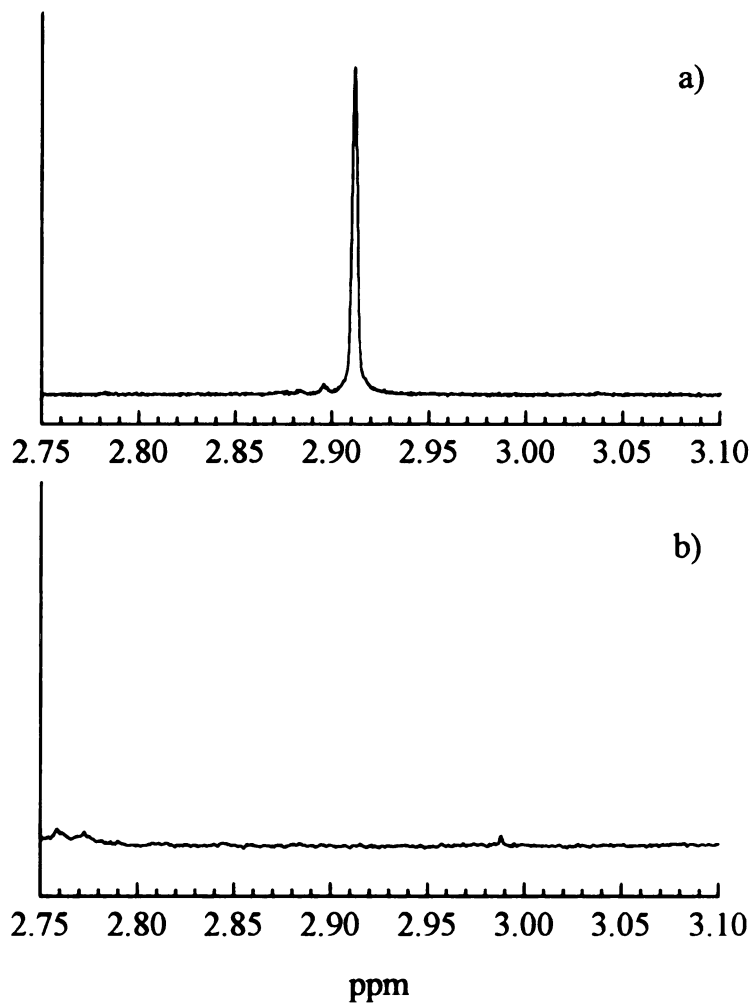


Figure VI.5. Changes in the  $^1\text{H-NMR}$  spectra of 1-methylperylene (a) before and (b) after the photoreaction. The peak at 2.91 ppm in (a) is the methyl group resonance of 1-methylperylene.

cycloaddition across the 3 and 4 positions would result in a [3 + 2] addition and is also unlikely. The most probable cycloaddition is a [2 + 2] reaction that occurs across the 2 and 3 positions. Reaction at this site satisfies the molecular orbital parity requirements<sup>[67]</sup> and, in addition, there is minimal steric hindrance at this site. We believe that the final product for the photoreaction between the substituted 7H-benz[*de*]anthracene moiety and the alkene solvents is a [2 + 2] cycloaddition across the 2 and 3 positions of the methylated ring residue.

The identity of the photoproduct requires that the approach of the alkene during the reaction is in the same plane as the 7H-benz[*de*]anthracene moiety with which it reacts. This plane is coincident with the 1-methylperylene 1370 cm<sup>-1</sup> vibrational mode coordinate, and thus the photoreaction can, if sufficiently fast, have a significant influence on the vibrational population relaxation dynamics of this mode. To address this point, we turn our attention to the relaxation dynamics of 1-methylperylene in the alkenes and compare these results to those for similar alkanes that we have reported previously.<sup>[53,55]</sup>

We have chosen the chemical system for this investigation carefully. There are several constraints that need to be considered in making such a choice. The first is, for vibrational population relaxation measurements, the order of the polar coupling process that mediates the transfer of vibrational energy between the 1-methylperylene donor and the alkene acceptor. Because neither 1-methylperylene nor any of the alkenes used here possesses a center of inversion, the coupling proceeds by dipole-dipole interactions.<sup>[68,69]</sup> A significant amount of work in this area has shown that, for the transitions involved, the critical transfer radius is on the order of 10 Å, a range that is sensed efficiently by molecular reorientation measurements. The second constraint that is important in these

measurements is the chemical identity of the acceptor vibrational mode. For the solvents used in this work, the  $1378\text{ cm}^{-1}$  solvent mode is the terminal  $\text{CH}_3$  group rocking mode, essentially degenerate with the donor mode. The extent of solvent branching determines the fractional density of acceptor modes present although, for the branched alkanes, simple solvent acceptor mode concentration did not account for the  $T_1$  times reported.<sup>[55]</sup> For the alkene solvents used in this work, all have similar chain length and similar acceptor moiety densities (Table VI.I). The data we report here can be compared directly to the data for 1-methylperylene in the  $\text{C}_7$  branched alkanes. We note that for the measurements we report here, the  $T_1$  and reorientation data are for the 1-methylperylene chromophore by virtue of the spectroscopic selectivity intrinsic to our pump-probe measurement schemes. The  $T_1$  times for the alkenes are, in fact, very similar to those we have reported for the alkanes previously. We do, however, note a substantially slower  $T_1$  time for 1-methylperylene in *trans*-3-heptene. These data indicate that the configuration of the solvent cage is such that the terminal methyl groups of the solvent are relatively isolated from the chromophore donor coordinate. Although it may be tempting to speculate on the intermolecular alignment(s) that give rise to the apparently anomalous  $T_1$  time for this system, it is clear that there is insufficient information at hand to make such an evaluation. As with the previous  $T_1$  measurements of 1-methylperylene in alkanes, there is a close correspondence between  $T_1$  and rotational diffusion time constants, demonstrating that relaxation is efficient and is mediated by the immediate environment of the probe molecule. More to the point for this work, however, is that the 1-methylperylene  $1370\text{ cm}^{-1}$  mode  $T_1$  times are so similar for both solvent families. These data demonstrate clearly that the second step in the photoreaction process does not play a significant role in

solvent	$T_1 \pm 1\sigma$ (ps)	$\tau_{OR} \pm 1\sigma$ (ps)	$R(0) \pm 1\sigma$ (ps)	acceptor density
1-heptene	$11 \pm 5$	$14 \pm 1$	$0.32 \pm 0.02$	1 / 7
<i>cis</i> -2-heptene	$12 \pm 5$	$15 \pm 2$	$0.26 \pm 0.05$	2 / 7
<i>trans</i> -2-heptene	<10	$18 \pm 1$	$0.26 \pm 0.02$	2 / 7
<i>cis</i> -3-heptene	$15 \pm 3$	$21 \pm 2$	$0.09 \pm 0.01$	2 / 7
<i>trans</i> -3-heptene	$50 \pm 10$	$18 \pm 1$	$0.22 \pm 0.02$	2 / 7
<i>n</i> -heptane	$18 \pm 2$	$15 \pm 1$	$0.24 \pm 0.04$	2 / 7

Table VI.1. Vibrational relaxation, rotational diffusion, and acceptor density for 1-methylperylene  $1370\text{cm}^{-1}$  mode in the alkene solvents. \*Jiang, Y.; Blanchard, G. J.; *J. Phys. Chem.*, **99**, 7904 (1995).

determining the vibrational relaxation behavior of the solute. The first reaction, the O<sub>2</sub>-mediated formation of the probe radical, may play some role in determining the T<sub>1</sub> times we measure for these two systems based on the similar times for all solvents examined. It is also possible to argue that the similarity of the T<sub>1</sub> times for the alkanes and the alkenes results from the strength of the dipolar coupling process and the presence of similar acceptor vibrational modes in both systems. Indeed, it has not been demonstrated that there is any persistent complex between the 1-methylperylene probe and dissolved O<sub>2</sub>, and thus, at best the initial reaction step is likely diffusion limited. If this is the case then there is a significant temporal mismatch of the timescales over which the relaxation and reaction processes proceed and the absence of any influence of the T<sub>1</sub> times for this system is thus not a surprising result, even in the case limit of persistent organization of the alkene solvent about the probe molecule.

## **VI.E Conclusions**

We have examined the vibrational population relaxation dynamics of 1-methylperylene in a family of C<sub>7</sub>H<sub>14</sub> alkenes. These chemical systems are photoreactive with the probe molecule, and we have demonstrated that the reaction proceeds in two steps; the first step is mediated by the presence of O<sub>2</sub>, and the second step is determined by the identity of the solvent. Our previous T<sub>1</sub> measurements of 1-methylperylene in non-photoreactive solvents have demonstrated the existence and importance of local organization of the solvent about the solute.<sup>[24,53-60]</sup> Thus for the second step of the photoreaction we observe in the alkenes, it is likely that there is significant intermolecular alignment. The T<sub>1</sub> data for the 1-methylperylene 1370 cm<sup>-1</sup> mode in the alkenes are very

similar to those for alkanes. Comparison of the 1-methylperylene  $1370\text{ cm}^{-1}$  mode coordinate to the expected reaction coordinate of the cycloaddition with the alkene suggests that there is significant overlap between the two. The absence of an influence of photoreactivity must thus be due to the temporal mismatch between the  $T_1$  time and the likely diffusion limited rate constant for the  $O_2$ -mediated first step in the photoreaction. The next step in this work is to determine experimentally the role of  $O_2$  in mediating  $T_1$  times for this 1-methylperylene mode in the same solvents. A significant lesson from this work is, however, that vibrational excitation with energies significantly greater than  $k_B T$  is unlikely, except under exceptional circumstances, to have much influence on the course of rate of a chemical reaction.

## VI.F. References

1. Sanders, M. J.; Wirth, M. J.; *Chem. Phys. Lett.*, **101**, 361 (1983).
2. Gudgin-Templeton, E. F.; Quitevis, E. L.; Kenney-Wallace, G. A.; *J. Phys. Chem.*, **89**, 3238 (1985).
3. Von Jena, A.; Lessing, H. E.; *Chem. Phys.*, **40**, 245 (1979).
4. Von Jena, A.; Lessing, H. E.; *Ber. Bunsen-Ges. Phys. Chem.*, **83**, 181 (1979).
5. Von Jena, A.; Lessing, H. E.; *Chem. Phys. Lett.*, **78**, 187 (1981).
6. Eisenthal, K. B.; *Acc. Chem. Res.*, **8**, 118 (1975).
7. Fleming, G. R.; Morris, J. M.; Robinson, G. W.; *Chem. Phys.*, **17**, 91 (1976).
8. Shank, C. V.; Ippen, E. P.; *Appl. Phys. Lett.*, **26**, 62 (1975).
9. Millar, D. P.; Shah, R.; Zewail, A. H.; *Chem. Phys. Lett.*, **66**, 435 (1979).
10. Gudgin-Templeton, E. F.; Kenney-Wallace, G. A.; *J. Phys. Chem.*, **90**, 2896 (1986).

11. Blanchard, G. J.; Wirth, M. J.; *J. Phys. Chem.*, **90**, 2521 (1986).
12. Blanchard, G. J.; *J. Chem. Phys.*, **87**, 6802 (1987).
13. Blanchard, G. J.; Cihal, C. A.; *J. Phys. Chem.*, **92**, 5950 (1988).
14. Blanchard, G. J.; *J. Phys. Chem.*, **92**, 6303 (1988).
15. Blanchard, G. J.; *J. Phys. Chem.*, **93**, 4315 (1989).
16. Blanchard, G. J.; *Anal. Chem.*, **61**, 2394 (1989).
17. Alavi, D. S.; Hartman, R. S.; Waldeck, D. H.; *J. Phys. Chem.*, **95**, 6770 (1991).
18. Hartman, R. S.; Alavi, D. S.; Waldeck, D. H.; *J. Phys. Chem.*, **95**, 7872 (1991).
19. Hu., C. M.; Zwanzig, R.; *J. Chem. Phys.*, **60**, 4354 (1974).
20. Youngren, G. K.; Acrivos, A.; *J. Chem. Phys.*, **63**, 3846 (1975).
21. Zwanzig, R.; Harrison, A. K.; *J. Chem. Phys.*, **83**, 5861 (1985).
22. Ben-Amotz, D.; Scott, T. W.; *J. Chem. Phys.*, **87**, 3739 (1987).
23. Ben-Amotz, D.; Drake, J. M.; *J. Chem. Phys.*, **89**, 1019 (1988).
24. Jiang, Y.; Blanchard, G. J.; *J. Phys. Chem.*, **98**, 6436 (1994).
25. Gochanour, C. R.; Andersen, H. C.; Fayer, M. D.; *J. Chem. Phys.*, **70**, 4254 (1979).
26. Anfinrud, P. A.; Hart, D. E.; Hedstrom, J. F.; Struve, W. S.; *J. Phys. Chem.*, **90**, 2374 (1986).
27. Anfinrud, P. A.; Struve, W. S.; *J. Chem. Phys.*, **87**, 4256 (1987).
28. Causgrove, T. P.; Bellefeuille, S. M.; Struve, W. S.; *J. Phys. Chem.*, **92**, 6945 (1988).
29. Causgrove, T. P.; Yang, S.; Struve, W. S.; *J. Phys. Chem.*, **93**, 6844 (1989).
30. Declémy, A.; Rullière, C.; Kottis, Ph.; *Chem. Phys. Lett.*, **133**, 448 (1987).
31. Castner, E. W.; Maroncelli, M.; Fleming, G. R.; *J. Chem. Phys.*, **86**, 1090 (1987).
32. Mokhtari, A.; Chesnoy, J.; Laubereau, A.; *Chem. Phys. Lett.*, **155**, 593 (1989).

33. Wagener, A.; Richert, R.; *Chem. Phys. Lett.*, **176**, 329 (1991).
34. Nagarajan, V.; Brearly, A. M.; Kang, T. J.; Barbara, P. F.; *J. Chem. Phys.*, **86**, 3183 (1987).
35. Maroncelli, M.; Fleming, G. R.; *J. Chem. Phys.*, **86**, 6221 (1987).
36. Simon, J. D.; *Acc. Chem. Res.*, **21**, 128 (1988).
37. Barbara, P. F.; Jarzeba, W.; *Adv. Photochem.*, **15**, 1 (1990).
38. Maroncelli, M.; Fee, R. S.; Chapman, C. F.; Fleming, G. R.; *J. Phys. Chem.*, **95**, 1012 (1991).
39. Jarzeba, W.; Walker, G. C.; Johnson, A. E.; Barbara, P. F.; *Chem. Phys.*, **152**, 57 (1991).
40. Horng, M. L.; Gardecki, J. A.; Papazyan, A.; Maroncelli, M.; *J. Phys. Chem.*, **99**, 17311 (1995).
41. Elsaesser, T.; Kaiser, W.; *Annu. Rev. Phys. Chem.*, **42**, 83 (1991).
42. Lingle, R., Jr.; Xu, X.; Yu, S. C.; Zhu, H.; Hopkins, J. B.; *J. Chem. Phys.*, **93**, 5667 (1990).
43. Anfinrud, P. A.; Han, C.; Lian, T.; Hochstrasser, R. M.; *J. Phys. Chem.*, **94**, 1180 (1990).
44. Heilweil, E. J.; Casassa, M. P.; Cavanagh, R. R.; Stephenson, J. C.; *Ann. Rev. Phys. Chem.*, **40**, 143 (1989).
45. Heilweil, E. J.; Cavanagh, R. R.; Stephenson, J. C.; *Chem. Phys. Lett.*, **134**, 181 (1987).
46. Heilweil, E. J.; Cavanagh, R. R.; Stephenson, J. C.; *J. Chem. Phys.*, **89**, 230 (1989).
47. Heilweil, E. J.; Casassa, M. P.; Cavanagh, R. R.; Stephenson, J. C.; *J. Chem. Phys.*, **85**, 5004 (1986).
48. Chang, T. C.; Dlott, D. D.; *Chem. Phys. Lett.*, **147**, 18 (1988).
49. Hill, J. R.; Dlott, D. D.; *J. Chem. Phys.*, **89**, 830 (1988).
50. Hill, J. R.; Dlott, D. D.; *J. Chem. Phys.*, **89**, 842 (1988).

51. Chang, T. C.; Dlott, D. D.; *J. Chem. Phys.*, **90**, 3590 (1989).
52. Kim, H.; Dlott, D. D.; *J. Chem. Phys.*, **94**, 8203 (1991).
53. Jiang, Y.; Blanchard, G. J.; *J. Phys. Chem.*, **99**, 7904 (1995).
54. McCarthy, P. K.; Blanchard, G. J.; *J. Phys. Chem.*, **99**, 17748, (1995).
55. McCarthy, P. K.; Blanchard, G. J.; *J. Phys. Chem.*, **100**, 5182, (1996).
56. McCarthy, P. K.; Blanchard, G. J.; *J. Phys. Chem.*, **100**, 14592, (1996).
57. Hambir, S. A.; Jiang, Y.; Blanchard, G. J.; *J. Chem. Phys.*, **98**, 6075 (1993).
58. Jiang, Y.; Blanchard, G. J.; *J. Phys. Chem.*, **98**, 9411 (1994).
59. Jiang, Y.; Blanchard, G. J.; *J. Phys. Chem.*, **98**, 9417 (1994).
60. Heitz, M. P.; Horne, J. C.; Blanchard, G. J.; Bright, F. V.; *Appl. Spec.*, in press.
61. Yardley, J. T.; "Introduction to Molecular Energy Transfer", Academic Press, New York, 1980.
62. Zieger, H. E.; Laski, E. M.; *Tetrahedron Lett.* **32**, 3801 (1966).
63. Blanchard, G. J.; Heritage, J. P.; Von Lehmen, A. C.; Kelly, M. K.; Baker, G. L.; Etemad, S.; *Phys. Rev. Lett.*, **63**, 887 (1989).
64. Blanchard, G. J.; Heritage, J. P.; *J. Chem. Phys.*, **93**, 4377 (1990).
65. Grimme, S.; Lohmannsroben, H.-G.; *J. Phys. Chem.*, **96**, 7005 (1992).
66. Dannenberg, H.; Kessler, H.-J.; *Justus Liebig Ann. Chem.*, **606**, 184 (1957).
67. Wade, L. G., Jr.; Organic Chemistry, Prentice-Hall, 1987, p. 593 ff.
68. Gray, C. G.; Gubbins, K. E.; Theory of Molecular Fluids: Volume 1: Fundamentals, Clarendon Press, Oxford 1984.
69. Rigby, M.; Smith, E. B.; Wakeham, W. A.; Maitland, G. C.; "The Forces Between Molecules", Clarendon Press, Oxford 1986.

## VII.A. AN AM1 STUDY OF THE ELECTRONIC STRUCTURE OF COUMARINS

### VII.A.1 Abstract

We report our calculations on a series of coumarin molecules. Using semi-empirical methods with an AM1 parameterization, we have calculated the ground state, first excited triplet state and first excited singlet state energies and dipole moments as well as their dependence on the geometries of different labile side groups. We find that for all of the coumarins there are excited triplet states in close energetic proximity to the excited singlet states, and the relative ordering of these states depends on the substituents attached to the coumarin chromophore.

### VII.A.2 Introduction

The coumarins are a family of molecules that have been studied extensively because of their application as laser dyes and their substantial state-dependent variation in static dipole moment.<sup>[1]</sup> Indeed, this latter property gives rise to characteristically large Stokes shifts, sometimes on the order of 100 nm. These large static Stokes shifts, in combination with their broad and featureless linear responses in solution, have attracted attention to the coumarins as probe molecules for the examination of ultrafast solvation effects.<sup>[2-8]</sup> Several of these experimental investigations have found that, subsequent to

excitation with a short laser pulse, the coumarin fluorescence spectrum evolves in time from an initially blue-shifted feature to the static emission profile, and the time over which this spectral evolution occurs can be correlated with various solvent properties, such as Debye longitudinal relaxation time,  $\tau_L$ . The mechanism put forth for the observed spectral evolution is that excitation of the coumarin molecule creates instantaneously a species with a substantially larger dipole moment than was present before the excitation, and the solvent surrounding this newly formed dipole moment must reorganize to accommodate to its presence.<sup>[2-4,6]</sup> Because this reorganization is not instantaneous, the excited coumarin derivative finds itself initially in a non-equilibrated environment, and its excited electronic state is thus higher in energy than at times long after excitation. The reorganization of the local solvent environment is thought to mediate the relaxation of the coumarin excited state to its steady state geometry and energy.

Several investigators have raised questions regarding the origin of the spectral relaxation properties observed for the coumarins, based on both theoretical considerations<sup>[9]</sup> and experimental evidence.<sup>[8]</sup> The mechanism postulated for the transient spectral relaxation assumes implicitly that intramolecular processes in the coumarins, such as vibrational relaxation and intersystem crossing, are unimportant, at least on the timescale of the solvent reorganization. Given these assumptions, the measured response arises solely from intermolecular processes and the emission band is treated as a *single* spectral feature. If the absorption and emission bands of the coumarins can truly be treated as individual features, *i.e.* if they are homogeneously broadened, then at least vibrational population relaxation within the coumarins can be ignored. The featureless fluorescence band of most coumarin derivatives is on the order of  $3000\text{ cm}^{-1}$  wide, and

their fluorescence lifetimes are typically  $\sim 5$  ns, yielding a time-bandwidth product,  $\Delta\nu\Delta t \approx 4.5 \times 10^5$ . The transform limited time-bandwidth product expected for a homogeneous line is 0.22,<sup>[10]</sup> and therefore the emission response of coumarin derivatives exhibits substantial inhomogeneous broadening. Thus, we need to consider the possible contribution of intramolecular relaxation processes to the transient spectral shifts measured experimentally.

We examined the transient spontaneous emission response of coumarin 153 recently, and found experimental evidence for multiple electronic states within its emission manifold (see Chapter VII.B).<sup>[8]</sup> In order to elucidate the identity of these electronic states, we performed a series of semi-empirical calculations, and the results indicated the presence of several electronic states within the experimental bandwidth of the coumarin 153 spontaneous emission profile. We present in this paper a series of semi-empirical calculations on coumarin and several coumarin derivatives. The purpose of these calculations is to determine the extent to which this family of molecules exhibits multiple excited electronic states in close proximity to one another, and how conformational effects for coumarins with labile side groups affect the ordering and energetic separation of these excited states. We find that, for all the coumarin derivatives we have studied, there are several electronic states in close proximity to the  $S_1$ , and the ordering of these states depends sensitively on the identity and conformation of substituent groups.

### VII.A.3 Calculations

Austin Model 1 (AM1) semi-empirical molecular orbital calculations were performed on the molecules shown in Figure VII.A.1 using Hyperchem software. The

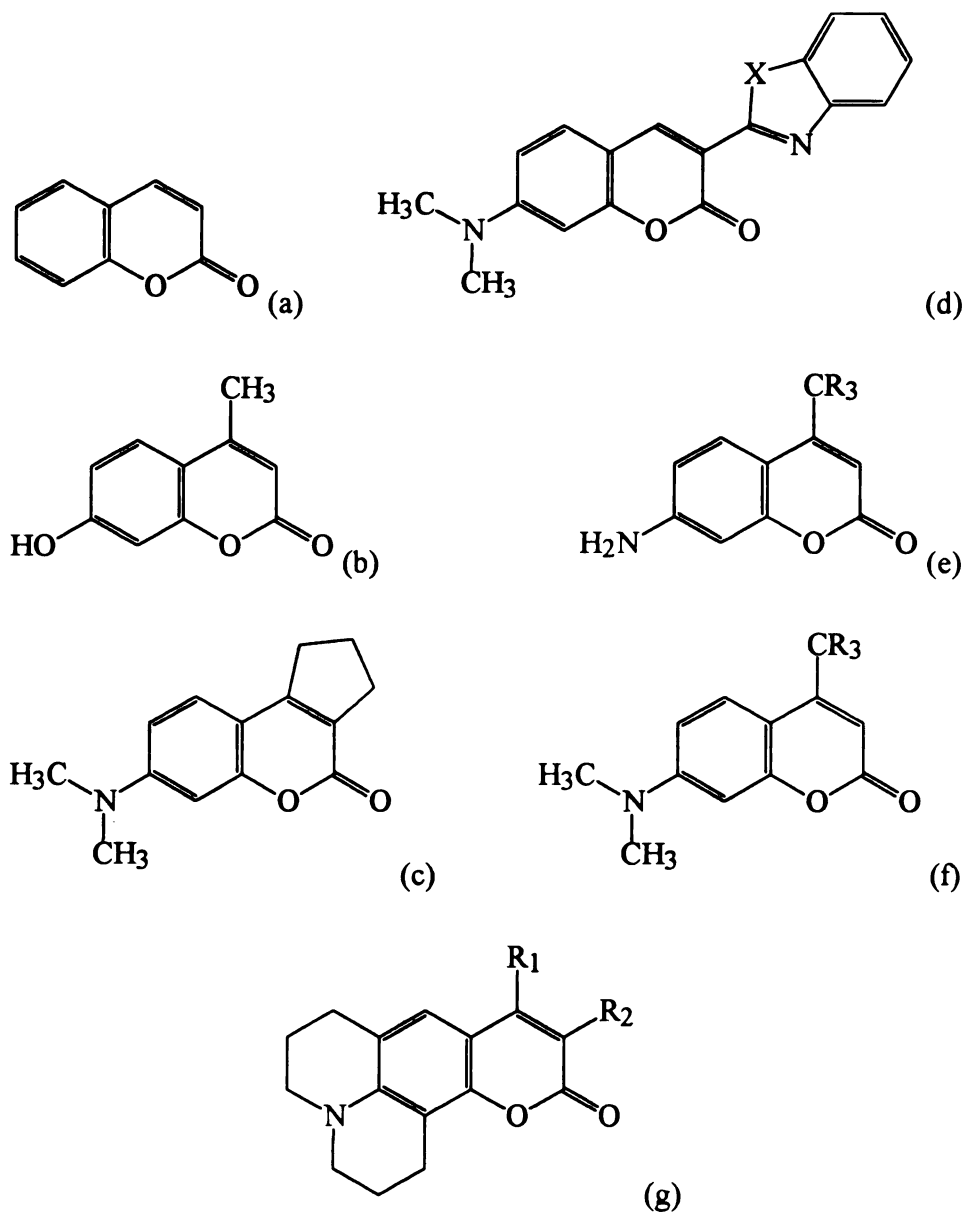


Figure VII.A.1. Structures of the coumarin molecules for which AM1 calculations were performed. Only one resonance structure is shown for each molecule: (a) coumarin, (b) coumarin 4, (c) coumarin 138, (d) X = S for coumarin 6, X = NCH<sub>3</sub> for coumarin 30, (e) R = H for coumarin 120, R = F for coumarin 151, (f) R = H for coumarin 102, R<sub>1</sub> = CF<sub>3</sub> for coumarin 152, (g) R<sub>1</sub> = CH<sub>3</sub> and R<sub>2</sub> = H for coumarin 102, R<sub>1</sub> = CF<sub>3</sub> and R<sub>2</sub> = H for coumarin 153, R<sub>1</sub> = H and R<sub>2</sub> = COCH<sub>3</sub> for coumarin 334, R<sub>1</sub> = H and R<sub>2</sub> = CN for coumarin 337, R<sub>1</sub> = H and R<sub>2</sub> = COOH for coumarin 343.

AM1 semi-empirical method<sup>[11-13]</sup> is a modification of MNDO,<sup>[14,15]</sup> offering more accurate parameterizations for polar systems and transition states. For our calculations, the geometry of a given molecule was first optimized at the empirical level using an MM+ molecular mechanics routine,<sup>[16]</sup> followed by unrestricted geometric optimization at the semi-empirical level using an SCF calculation. For several of the coumarins there was found to be more than one stable conformation, and for these species we continued optimization until the lowest energy conformation was found. Electronic energy calculations were performed on the geometrically SCF-optimized molecule for the  $S_0$ ,  $S_1$  and  $T_1$  electronic states. For all electronic energy calculations, the ground state ( $S_0$ ) optimized geometry was used and the RHF closed shell calculations were performed using configuration interaction with 100 microstates. The use of this many microstates in the CI calculation provides a fair representation of correlation effects in the coumarins. We found that electronic transition energies were slightly smaller ( $\sim 5$  kcal/mol) for CI calculations than for SCF calculations, as is expected for the inclusion of correlation effects. We chose to use the AM1 parameterization for our calculations because it is known to be optimized for polar systems. For the coumarins shown in Figure VII.A.1f, dimethylamino end groups were used in place of diethylamino end groups for computational simplicity. This substitution yielded no changes in electronic state energies or dipole moments.

In addition to calculation of the electronic state energies of the geometrically optimized coumarin derivatives, we calculated the geometry-dependence of the ground state, first excited singlet state and first triplet state energies for two labile coumarins. For coumarin 1, the dimethylamino group was rotated about its bond to the coumarin ring

system and for coumarin 6 the benzthiazolyl group was rotated about its bond to the coumarin ring system. The electronic state energies reported for these calculations were likewise obtained using the AM1 parameterization with configuration interaction.

#### VII.A.4. Results And Discussion

Our purpose in performing these calculations was to elucidate the generality of the state ordering and proximity that we observed experimentally for coumarin 153 (see Chapter VII.B).<sup>[8]</sup> Related questions that we investigated were the effect of chemical substitution on the transition energies and state ordering for the coumarins, and the extent to which we expect conformational freedom in labile coumarins to affect their optical response. We present the results of our semi-empirical calculations for the geometrically optimized coumarins in Table VII.A.1.

The data in Table VII.A.1 contain several qualitative trends, at least some of which may be compared to experimental data in the literature. The first trend is that the energy of the  $S_0 \rightarrow S_1$  transition decreases with increasing substitution to the coumarin chromophore, in qualitative agreement with experimental data.<sup>[17]</sup> We show in Figure VII.A.2 the correlation between experimental liquid phase absorption maxima and calculated transition energies. This correlation is not strictly valid because we are comparing  $S_0^{v=0} \rightarrow S_1^{v=0}$  calculations to  $S_0^{v=0} \leftrightarrow S_1^{v=n}$  experimental data, where  $n$  is largely unidentified. Despite this mismatch, we do expect a correlation because of the similarity of the  $S_1$  surface for all of the coumarins. The modest deviations from a direct correlation reflect subtle substituent-dependent variations in the Franck-Condon factors for the experimental absorption data as well as unaccounted-for solvent polarity effects. In

molecule	$\Delta H_f$ (kcal/mol)	energy relative to $S_0$ ( $\text{cm}^{-1}$ )						$\mu(S_0)$ (D)	$\mu(T_1)$ (D)	$\mu(S_1)$ (D)
		$T_2$	$S_1$	$T_3$	$S_2$	$\mu(S_0)$ (D)	$\mu(T_1)$ (D)			
coumarin	-37.31	27189	30866	31479	33754	4.82	5.09	6.21		
coumarin 4	-90.58	26918	29999	31241	31431	4.14	3.66	5.32		
coumarin 138	-37.15	25443	27354	29269	29352	5.97	6.90	8.45		
coumarin 6	+37.28	24486	25106	26884	30381	7.00	9.62	8.60		
coumarin 30	+57.88	26712	26872	28295	33904	8.06	8.96	7.82		
coumarin 120	-47.87	26315	28796	29896	30991	6.03	6.29	8.19		
coumarin 151	-190.68	25083	26702	28546	30187	6.04	8.38	11.27		
coumarin 1	-35.90	25913	27865	29830	30253	6.35	7.78	9.81		
coumarin 152	-179.45	25094	25848	28190	30317	6.32	10.08	13.11		
coumarin 102	-54.63	24731	26749	28914	28659	6.43	8.14	10.09		
coumarin 153	-197.61	24049	24675	27081	28168	6.68	10.86	13.64		
coumarin 334	-84.33	25135	25422	27505	27340	7.39	10.19	12.77		
coumarin 337	-13.18	24804	25040	27229	27183	9.68	12.26	15.11		
coumarin 343	-133.56	25139	25206	27396	27436	10.41	13.47	15.70		

Table VII.A.1. Calculated properties of several coumarins.  $\Delta H_f$  is the heat of formation and the quantities  $\mu$  and the calculated dipole moments for the states indicated. Units are D, (1D =  $3.336 \times 10^{-30}$  C·m).

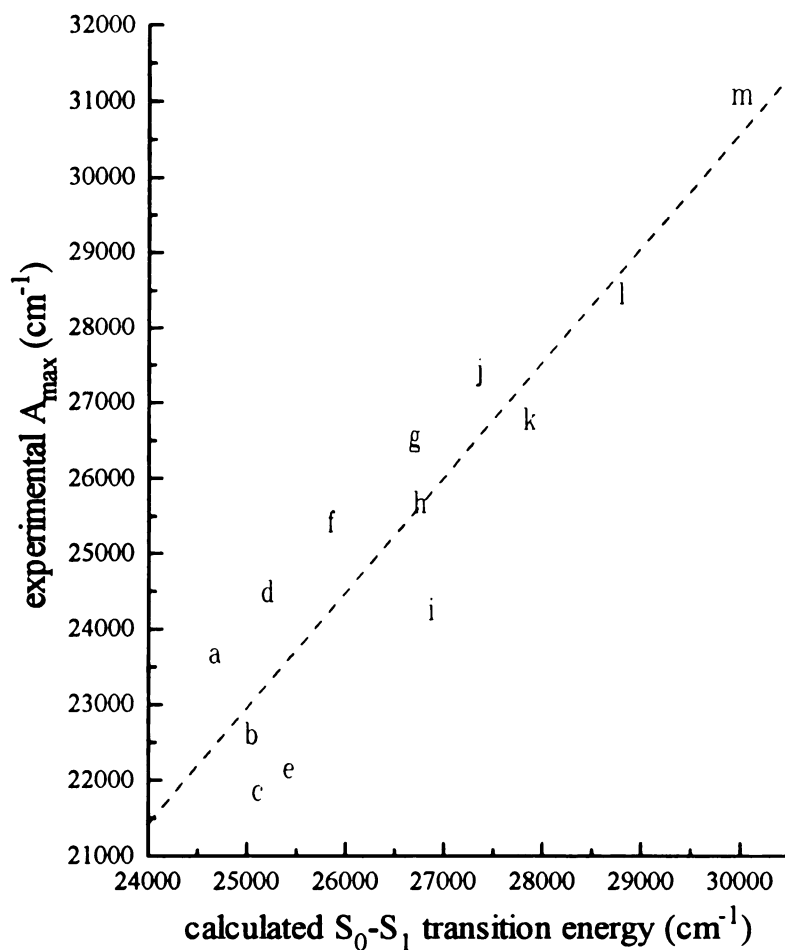


Figure VII.A.2. Comparison of experimental absorption maxima (Optical Products, Publication JJ-169, Eastman Kodak Co., pp. 12-36.) to the calculated 0-0 transition energies for the coumarins shown in Figure VII.A.1: a = coumarin 153; b = coumarin 337; c = coumarin 6; d = coumarin 343; e = coumarin 334; f = coumarin 152; g = coumarin 102; h = coumarin 151; i = coumarin 30; j = coumarin 138; k = coumarin 1; l = coumarin 120; m = coumarin 4.

addition to a qualitative correlation, we note that our calculated results for  $S_0 \rightarrow S_1$  transition energies are in good agreement with experimental gas phase origin measurements for the few coumarins for which the origin has been measured<sup>[18]</sup> (Table VII.A.2). Based on these correlations with experimental data, we believe that our calculations reflect the electronic properties of the coumarins accurately. Our calculations show that there are several electronic states in close proximity to the  $S_1$ ; the  $T_2$ ,  $S_2$  and  $T_3$  states. While this generalization holds for all of the coumarins, we observe that the chemical identity of the substituents to the coumarin chromophore can alter the relative ordering of the states. It may be tempting to view changes in state ordering as significant in and of themselves, but it is clear from a careful examination of the data in Table 1 that these variations arise from *slight* changes in energies for states that lie in very close energetic proximity to one another.

In addition to calculating the singlet transition energies, we have calculated the triplet-triplet transition energies, and indicate certain of these in Table VII.A.3. We have listed the energies for transitions between  $T_1$  and  $T_2$  through  $T_5$ , and these transitions lie in the energy range of  $\sim 8000 \text{ cm}^{-1}$  to  $\sim 13000 \text{ cm}^{-1}$ . Transitions between the  $T_1$  state and higher lying triplet states fall in a band between  $\sim 20000 \text{ cm}^{-1}$  and  $27000 \text{ cm}^{-1}$ , and these transitions may play a significant role in the transient optical response of coumarins.<sup>[19-21]</sup> Experimental data has shown that triplet-triplet absorption can play an important role in the photophysics and lasing efficiency of these coumarin derivatives, but the spectra show these resonances to be broad and relatively featureless. It is therefore not possible to make a direct comparison between our calculated results and individual T-T resonances observed experimentally.

molecule	experimental 0-0 (cm <sup>-1</sup> )	calculated energy	
		planar amino group (cm <sup>-1</sup> )	twisted amino group (cm <sup>-1</sup> )
coumarin 151	28060	26702	29502
coumarin 152	26687	25848	29169
coumarin 153	25196	24675	N/A

Table VII.A.2. Comparison of experimental and calculated 0-0 transition energies. The planar amino group heading refers to a calculation where the amino group dihedral angle with respect to the coumarin ring system was optimized and  $\sim 0^\circ$ . The twisted amino group refers to calculations where a stable conformation of the amino group was at  $\sim 90^\circ$  with respect to the coumarin ring system. Experimental data were taken from N. P. Ernsting, M. Asimov, F. P. Scharfer, *Chem. Phys. Lett.*, **91**, 231, (1982)..

molecule	$\Delta E(S_0-T_1)$ ( $\text{cm}^{-1}$ )	transition energy for $T_1-T_n$ ( $\text{cm}^{-1}$ )			
		$T_2$	$T_3$	$T_4$	$T_5$
coumarin	21085	5432	6595	14168	15434
coumarin 4	20214	8358	8852	9895	13606
coumarin 138	17630	8164	9477	12221	14010
coumarin 6	16518	7997	10224	11400	20137
coumarin 30	17116	9442	10410	11295	18948
coumarin 120	19166	7643	8574	10471	12679
coumarin 151	17265	8255	9851	11924	12920
coumarin 1	18674	7601	8195	10560	12920
coumarin 152	16909	8094	9909	11809	12865
coumarin 102	18119	7262	8013	9409	12223
coumarin 153	16170	8224	9672	11637	12354
coumarin 334	16909	8432	9702	10932	12304
coumarin 337	16499	7969	9429	10933	12274
coumarin 343	16581	8589	9950	11263	12262

Table VII.A.3. Calculated triplet-triplet absorption energies, and the energetic displacement of the  $T_1$  state from the  $S_0$  ground state.

Some polar organic molecules, most notably the oxazines, exhibit significant shifts in electronic charge at their heteroatom sites on excitation, giving rise to state-dependent dynamical properties.<sup>[22-27]</sup> The coumarins, however, do not exhibit this same characteristic. We present in Table VII.A.4 and Figure VII.A.3 our calculated results for  $S_0$  and  $S_1$  coumarin 1. The majority of the state-dependent charge shifts occur within the ring structure, and there is little state-dependence to the charges on either the heterocyclic oxygen or keto oxygen. We note that, on excitation, the dimethylamino nitrogen of coumarin 1 becomes more positive by  $\sim 0.11e$ , but there appears to be no significant negative charge accumulation at the keto oxygen. These results for coumarin 1 are representative of those for the other derivatives we report here. It may therefore be misleading to consider the excited states of the coumarins as zwitterionic, as is typically indicated in the literature.<sup>[1]</sup> The majority of the change in dipole moment seen on excitation is calculated to occur as a consequence of charge redistribution within the coumarin ring structure and along the N-C axis. The dipole moment change on excitation occurs primarily along the 2-6-19-20 molecular axis, (Figure VII.A.3) and involves very little contribution from either of the oxygens.

Some of the utility of these calculations lies in their ability to predict the state-dependent change in dipole moment accurately. We show in Table VII.A.1 our calculated ground state ( $S_0$ ), excited triplet state ( $T_1$ ) and excited singlet state ( $S_1$ ) dipole moments. The dipole moments for the coumarins have, in general, not been measured, and therefore a direct comparison of our calculated results to experimental data is not possible. The dipole moment for  $S_0$  coumarin has, however, been reported,  $\mu = 4.62 \text{ D}$ ,<sup>[28]</sup> and we calculate the dipole moment for  $S_0$  coumarin to be  $4.82 \text{ D}$ . Maroncelli and Fleming have

Atom No. (Fig. VII.A.3)	S <sub>0</sub> charge	S <sub>1</sub> charge	Δ(charge) (S <sub>1</sub> -S <sub>0</sub> )
1	-0.196	-0.180	+0.016
2	+0.045	-0.034	-0.079
3	-0.217	-0.118	+0.099
4	-0.235	-0.152	+0.083
5	+0.138	+0.114	-0.024
6	-0.187	-0.008	+0.179
7	-0.043	-0.183	-0.140
8	-0.251	-0.329	-0.078
9	+0.334	+0.308	-0.026
10	-0.298	-0.326	-0.028
11	-0.073	-0.092	-0.019
12	-0.070	-0.092	-0.022
13	+0.135	+0.142	+0.007
14	+0.166	+0.161	-0.005
15	+0.087	+0.093	+0.006
16	+0.069	+0.089	+0.020
17	+0.084	+0.093	+0.009
18	+0.075	+0.091	+0.016
19	+0.153	+0.008	-0.145
20	-0.284	-0.169	+0.115
21	-0.195	-0.168	+0.027
22	+0.097	+0.087	-0.010
23	+0.097	+0.087	-0.010
24	+0.097	+0.086	-0.011
25	+0.093	+0.133	+0.040
26	+0.160	+0.155	-0.005
27	+0.093	+0.108	+0.015
28	+0.083	+0.096	+0.013

Table VII.A.4. Calculated atomic charges, expressed as decimal fractions of an electron charge, for coumarin 1. The atom numbers corresponding to this table appear in Figure VII.A.3.

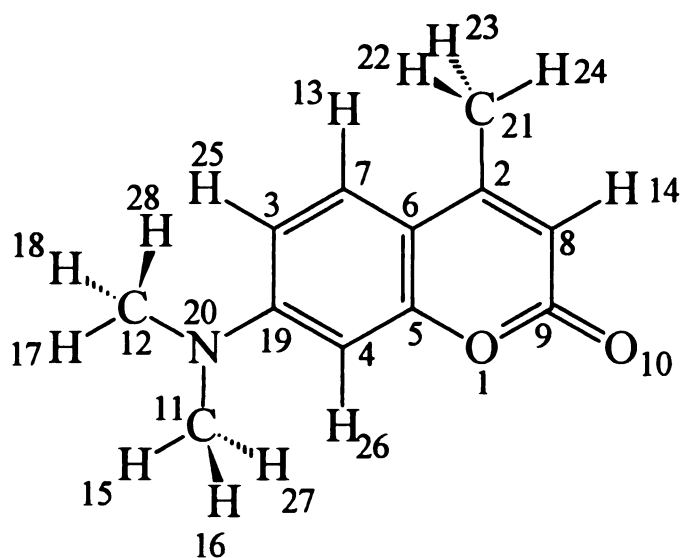


Figure VII.A.3. Structure and atom number assignment for coumarin 1. Partial charges are given for each atom for the  $S_0$  and  $S_1$  states in Table VII.A.4.

reported a calculated dipole moment of 4.58 D for coumarin using an MNDO parameterization,<sup>[2]</sup> but we have chosen to use the AM1 Hamiltonian because of its better parameterization for polar and excited state systems. The dominant trends in our calculated results are that the  $S_1$  dipole moment is typically 50-100% larger than that of the corresponding ground state species and the  $T_1$  dipole moment is usually intermediate between those of  $S_0$  and  $S_1$ . There are some significant exceptions to this trend, especially with the more highly substituted coumarins, and we believe these exceptions to arise from partial cancellation of the coumarin moiety dipole moment by that of the labile substituent. The coumarins with fluorinated substituents exhibit the largest changes in dipole moment on excitation, presumably because of the strong electron-withdrawing character of the trifluoromethyl group at the 2-position. The addition of substituents at the 8-position (Figure VII.A.3) of the coumarin chromophore can have a profound effect on the dipolar properties of the molecule. Coumarin 337 and 343, for example, have comparatively large ground and excited state dipole moments because of the presence of the cyano and carboxylic acid groups, respectively. For coumarins 6 and 30, where the 8-substituent is substantially larger, the state-dependent change in dipole moment becomes much smaller, likely due to partial cancellation of the dipole moments from the two ring structures. Interpretation of the results for coumarins 6 and 30 may be more complicated than that for many of the other coumarins because the benzthiazolyl and benzimidazolyl sidegroups on coumarins 6 and 30 distort the coumarin ring structure to a slightly non-planar geometry.

We focus now on the effect of conformation on the calculated electronic properties of the coumarins. Indeed, the rotational freedom of substituents to the coumarin ring structure has been invoked as a possible explanation for the complicated and solvent

polarity-dependent electronic response of several coumarin derivatives. In the course of our calculations we noted that the transition energies depend on the dihedral angle between the dimethylamino group and the coumarin ring system for molecules where the amino group was not "rigidized", and also on the dihedral angle made by groups attached to the coumarin ring system at the 8-position. To explore the dependence of the calculated transition energies on the rotational conformation of the substituents, we have used two representative coumarin derivatives, coumarin 1 and coumarin 6. We find that the potential energy surfaces for rotation of either group vary with electronic state and also according to which group is rotated.

We show in Figure VII.A.4 our calculation of the state energy as a function of dimethylamino group rotation for the  $S_0$ ,  $T_1$  and  $S_1$  states of coumarin 1. There is a significant barrier to rotation of the dimethylamino group in all of the states calculated, but the barrier is higher in the  $S_1$  and the  $T_1$  than the  $S_0$ . These calculated barrier heights are almost certainly not quantitative; our recent comparison of calculation to experiment for the ground and excited state barrier heights of DODCI shows that the AM1 parameterization overestimates the barrier heights, but that the trends predicted by the calculation are correct.<sup>[29]</sup> Thus we do not intend this calculation of coumarin 1 to be quantitative, but rather to indicate that the excited singlet and triplet state barriers to amino group rotation in the coumarins are larger than that for the ground state. The observation of a barrier for all of the electronic states calculated indicates the contribution of the amino group orbitals to the  $\pi$  and  $\pi^*$  molecular orbitals of the chromophore. The results for rotation of the benzthiazolyl group at the 8-position of coumarin 6 present a sharply different picture, shown in Figure VII.A.5. These calculations indicate an  $S_0$  and

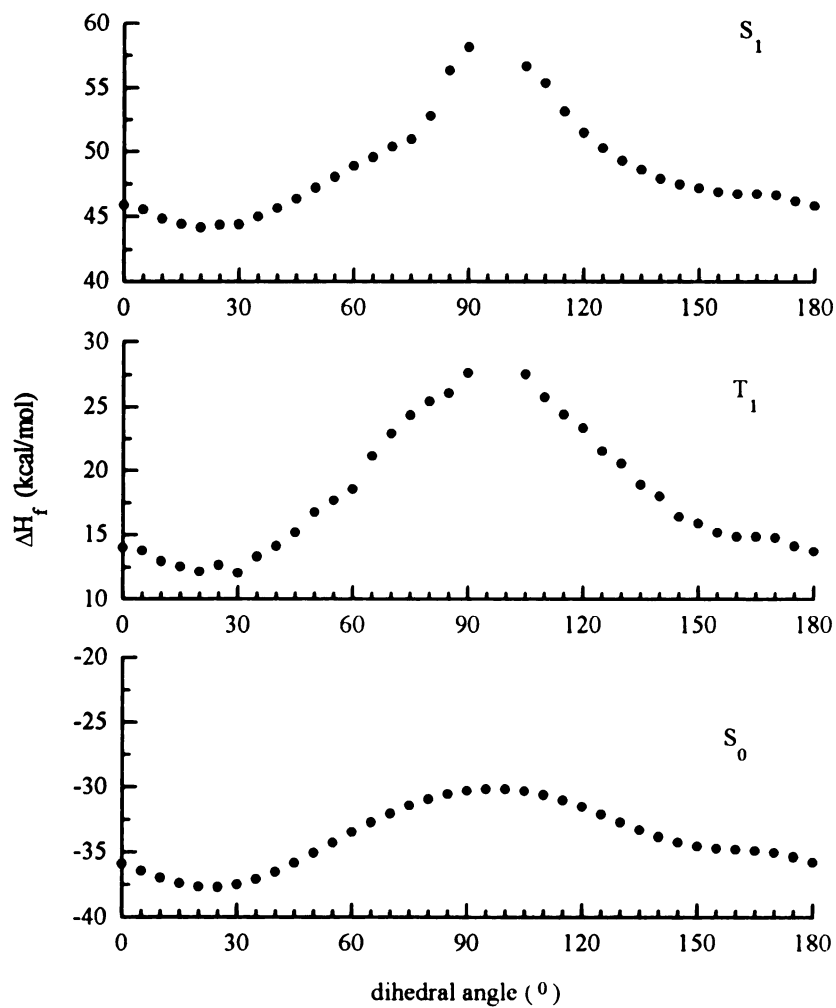


Figure VII.A.4. Calculated energy dependence of the dimethylamino group rotation for the  $S_0$ ,  $T_1$ , and  $S_1$  states of coumarin 1. The dihedral angle is the angle made by the amino group with respect to the coumarin chromophore. Missing points indicate a failure of the calculated structure to converge at the given dihedral angle.

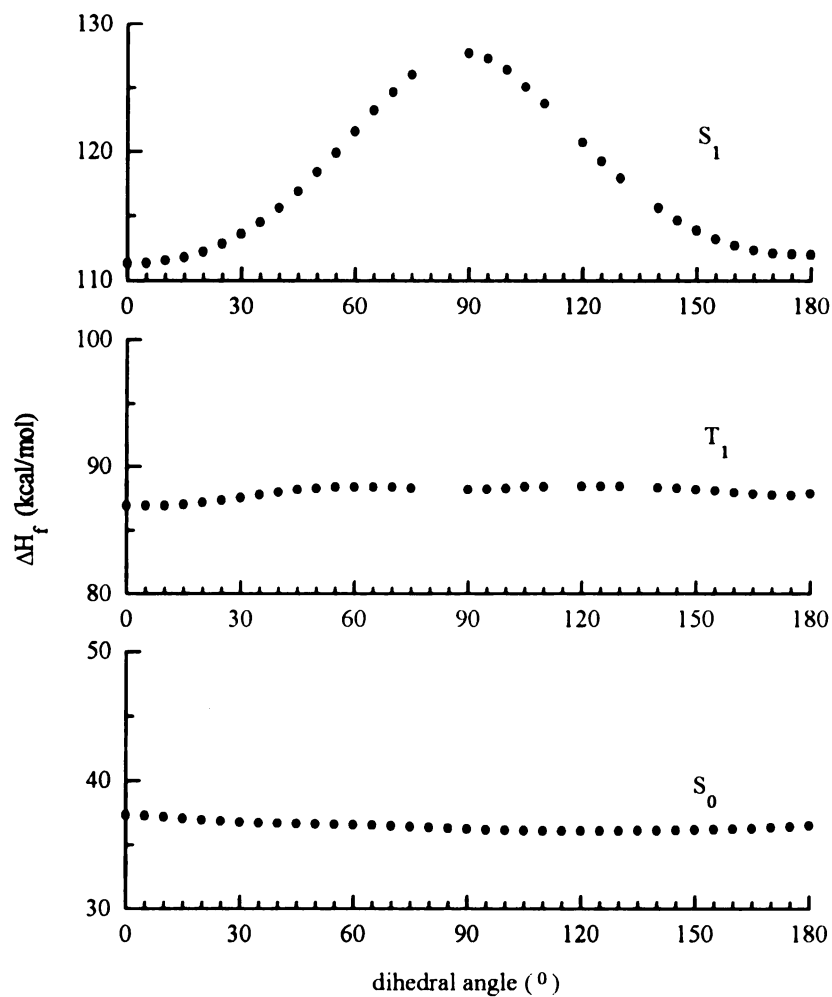


Figure VII.A.5. Calculated energy dependence of the benzothiazolyl group rotation for the S<sub>0</sub>, T<sub>1</sub>, and S<sub>1</sub> states of coumarin 6. The dihedral angle is the angle made by the benzothiazolyl group with respect to the coumarin chromophore. Missing points indicate a failure of the calculated conformation to converge at the given dihedral angle.

$T_1$  rotation barrier of  $\leq 1$  kcal/mol, indicating that the benzthiazole moiety does not contribute significantly to the ground or first triplet electronic states of coumarin 6. In the  $S_1$  state, however, there is a substantial barrier to rotation, calculated to be  $>15$  kcal/mol. We interpret this to indicate an increase in double bond character at the bond joining the benzthiazole and the coumarin sub-units. Modification of the amino group substituents can affect the energies of both the ground and excited electronic states of coumarin derivatives while substitution at the 8-position will affect only the  $S_1$  isomerization surface significantly.

#### **VII.A.5. Conclusions**

Our calculations reveal several interesting properties of the coumarins, some of which have been established previously through experimentation. The state dependence of the coumarin dipole moment varies with the identity and location of substituents on the coumarin ring system, but with few exceptions,  $\mu^* \sim 1.5-2\mu$ . We have also calculated isomerization barriers for two coumarins, one for rotation of a dimethylamino group at the 19-position and one for rotation of a benzthiazolyl group at the 8-position. Rotation of the dimethylamino group affects the ground state and the excited singlet and triplet states of the molecule. Rotation of the group at the 8-position affects the first excited singlet state strongly while having little influence on the ground singlet state or the first triplet state. This result offers an opportunity to predict the optical response of the chromophore as a function of chemical substitution and steric hindrance. The data presented in Table VII.A.1 demonstrate the complexity associated with the optical response of the coumarins. Because of the multitude of electronic states in close energetic proximity to

S<sub>1</sub>, and the known propensity of coumarins to intersystem cross to their triplet manifold,<sup>[19-21]</sup> it appears that the coumarins as a class are less than ideal for probing transient photophysical and dynamical processes.

## VII.A.6. References

1. Drexhage, K. H.; in *Topics in Applied Physics, Vol 1, Dye Lasers*, ed. F. P. Schafer, (Springer, Berlin, 1973.).
2. Maroncelli, M.; Fleming, G. R.; *J. Chem. Phys.*, **86**, 6221 (1987).
3. Barbara, P. F.; Jarzeba, W.; *Adv. Photochem*, **15**, 1 (1990).
4. Jarzeba, W.; Walker, G. C.; Johnson, A. E.; Barbara, P. F.; *Chem. Phys.*, **152**, 57 (1991).
5. Fee, R. S.; Milson, J. A.; Maroncelli, M.; *J. Phys. Chem.*, **95**, 5170 (1991).
6. Maroncelli, M.; Macinnis, J.; Fleming, G. R.; *Science*, **243**, 1674 (1989).
7. Moog, R. S.; Bankert, D. L.; Maroncelli, M.; *J. Phys. Chem.*, **97**, 1496 (1993).
8. Jiang, Y.; McCarthy, P. K.; Blanchard, G. J.; *Chem. Phys.*, **183**, 249 (1994).
9. Agmom, N.; *J. Phys. Chem.*, **94**, 2959 (1990).
10. Sala, K. L.; Kenney-Wallace, G. A.; Hall, G. E.; *IEEE J. Quant. Electron.*, **QE-16**, 990 (1980).
11. Dewar, M. J. S.; Zoebisch, E. G.; Healy, E. F.; Stewart, J. J. P.; *J. Am. Chem. Soc.*, **107**, 3902 (1985).
12. Dewar, M. J. S.; Dieter, K. M.; *J. Am. Chem. Soc.*, **108**, 8075 (1986).
13. Stewart, J. J. P.; *J. Comp. Aided Molec. Design*, **4**, 1 (1990).
14. Dewar, M. J. S.; Thiel, W.; *J. Am. Chem. Soc.*, **99**, 4899 (1977).
15. Dewar, M. J. S.; Thiel, W.; *J. Am. Chem. Soc.*, **99**, 4907 (1977).
16. Allinger, N. L.; *J. Am. Chem. Soc.*, **99**, 8127 (1977).

17. Optical Products, *Publication JJ-169*, Eastman Kodak Co., pp. 14-36.
18. Ernsting, N. P.; Asimov, M.; Scharfer, F. P.; *Chem. Phys. Letters*, **91**, 231 (1982).
19. Dempster, D. N.; Morrow, T.; Quinn, M. F.; *J. Photochem.*, **2**, 329 (1973).
20. Pavlopoulos, T. G.; Golich, D. J.; *J. Appl. Phys.*, **64**, 521 (1988).
21. Priyadarsini, K. I.; Naik, D. B.; Moorthy, P. N.; *Chem. Phys. Letters*, **148**, 572 (1988).
22. Blanchard, G. J.; *Chem. Phys.*, **138**, 365 (1989).
23. Blanchard, G. J.; *J. Phys. Chem.*, **95**, 5293 (1991).
24. Blanchard, G. J.; *Anal. Chem.*, **61**, 2394 (1989).
25. Blanchard, G. J.; *J. Phys. Chem.*, **93**, 4315 (1989).
26. Blanchard, G. J.; *J. Phys. Chem.*, **92**, 6303 (1988).
27. Blanchard, G. J.; Cihal, C. A.; *J. Phys. Chem.*, **92**, 5950 (1988).
28. Griffiths, V. S.; Westmore, J. B.; *J. Chem. Soc.*, 4941 (1963).
29. Awad, M. M.; McCarthy, P. K.; Blanchard, G. J.; *J. Phys. Chem.*, **98**, 1454 (1994).

## **VII.B. THE ROLE OF MULTIPLE ELECTRONIC STATES IN THE DISSIPATIVE ENERGY DYNAMICS OF COUMARIN 153**

### **VII.B.1. Abstract**

We have examined the transient spectral relaxation properties of coumarin 153 in three polar solvents using ultrafast spontaneous emission spectroscopy. The time evolution of the coumarin 153 spontaneous emission spectrum exhibits an excitation energy-dependence, demonstrating that the spectral dynamics of this molecule are determined primarily by intramolecular population relaxation processes. Semi-empirical molecular orbital calculations of the electronic states of coumarin 153 predict the presence of two closely spaced singlet states as well as several triplet states, consistent with our experimental data. Our data and calculations demonstrate collectively that coumarins are, in general, not ideal molecular probes of solvation dynamics because of their complex electronic structure and intramolecular energy dissipation characteristics.

### **VII.B.2. Introduction**

The study of molecular interactions in the liquid phase has produced a substantial body of knowledge relating to transient solvation processes. The primary motivation for research in this area is that the vast majority of synthetic chemistry as well as a substantial amount of chemical processing is performed in solution. Controlling and optimizing any

chemical reaction or process requires a fundamental understanding of the molecular interactions that determine the dynamics and energetics of the process. Both gas phase and solid systems are more amenable to experimental study than liquids because dynamics in these phases are typically slower than in solution and intermolecular interactions can often be treated statistically. In the gas phase, intermolecular interactions are less frequent than in the liquid phase and also tend to be dominated less by polar, shorter range forces. Dynamical and dissipative processes in the solid state are better understood than those in the liquid state because of the fixed spatial relationships amongst the molecules comprising a solid system. The difficulty in understanding liquid phase dynamical processes lies in the strength and time scale of the intermolecular interactions responsible for both solvation and macroscopic system properties.

A variety experimental means have been used to infer information about intermolecular processes in the liquid phase, and short optical pulses have proven to be one of the most effective tools for these experiments.<sup>[1]</sup> Four experimental observables have been used extensively in ultrafast spectroscopic examinations of liquid phase dynamics because of their mutually complementary nature. These are reorientation dynamics,<sup>[2-14]</sup> transient electronic spectral shifts,<sup>[15-22]</sup> vibrational relaxation (dephasing and population decay)<sup>[23-36]</sup> and vibrational spectroscopy of transient species.<sup>[37-39]</sup> A common thread in the measurement of these phenomena is the use of a probe molecule to interrogate some property of its local solvent environment. The volume of the probe molecule, typically  $200 \text{ \AA}^3$  -  $500 \text{ \AA}^3$ , is often substantially larger than that of the individual solvent molecules surrounding it, and thus the optical response of the probe is influenced by and averaged over a large number of interactions between itself and the surrounding

solvent.

The choice of a probe molecule is often determined by its ability to exhibit some spectroscopic property well suited to the experimental question at hand, such as absorption and/or emission frequency, the magnitude of its static Stokes shift, or the presence of strong and well characterized vibrational resonances. The identity of the probe molecule can have a profound effect on the information obtained from the experiment. This is especially obvious for rotational diffusion experiments, where a large body of information on many chemical systems exists in the literature. The orientational relaxation time of many probe molecules in polar solvents has been modeled by the Debye-Stokes-Einstein expression,<sup>[2-14]</sup> where the probe reorientation time is related to its hydrodynamic volume,  $V$ , and the viscosity of the solvent,  $\eta$ ,

$$\tau_{or} = \frac{\eta V}{kT} \cdot f \cdot s \quad \text{[VII.B.1]}$$

The terms  $f$  and  $s$  are included to compensate for the solvent-solute boundary condition and solute shape, respectively.<sup>[40,41]</sup> There is no explicit contribution from specific intermolecular interactions in this model, and one might expect to obtain the same result, corrected for molecular volume, for any probe molecule. This prediction is clearly not consistent a large body of experimental evidence.<sup>[2-14]</sup> Some probe molecules exhibit state-dependent reorientation dynamics,<sup>[10-14]</sup> and others, while not exhibiting this state-dependence, deviate significantly from the Debye-Stokes-Einstein prediction for reasons that are often unclear. Results from population dynamics measurements, such as vibrational mode-specific and solvent-dependent vibrational population relaxation,<sup>[36]</sup> also serve to underscore the important role that the molecular identity of both the solvent and

the solute play in determining the course of transient relaxation processes in liquids.

Some of the most significant experiments aimed at understanding polar solvation processes have focused on probe molecules that exhibit a transient emission spectral red-shift subsequent to ultrafast optical excitation.<sup>[15-22]</sup> Results from this body of work have been interpreted to indicate that a solvent system accommodates to an instantaneous dipolar perturbation at a rate limited approximately by its longitudinal relaxation time,  $\tau_L$ , a quantity related to the reorientation of the individual solvent molecules, and the zero and infinite frequency bulk dielectric responses of the solvent,

$$\tau_L = \frac{\epsilon_0}{\epsilon_\infty} \tau_D \quad \text{[VII.B.2]}$$

$\tau_D$  is the Debye relaxation time of the solvent. Deviations from this correlation have been observed, and they are generally considered to be related to the intrinsically molecular nature of solvation. Transient spectral shifts have been observed for several probe molecules, with the coumarins being the group examined most extensively.<sup>[16-19]</sup> The central assumptions made in interpreting transient spectral shift measurements are that the shifting emission band is a single, uniform feature and that vibronic structure within the band does not contribute to the observed response. Implicit in these assumptions is the absence of any contribution from probe molecule-specific intramolecular relaxation processes. These assumptions are necessarily suspect for complex organic molecules,<sup>[42]</sup> but are difficult to either verify or disprove, owing to the spectroscopic complexity of the probe molecules and the extremely short-lived nature of the relevant transient effect. In this paper we evaluate the validity of these assumptions and discuss how the results we have obtained using ultrafast spontaneous emission spectroscopy are related to the

transient spectral shifts reported previously for the coumarins. We find that the spectral dynamics of coumarin 153 are not representative of spectral shifts, but rather are population relaxations between multiple excited electronic states.

### **VII.B.3. Background**

#### **VII.B.3.A. Spectroscopy of the Coumarins**

The spectroscopy of the coumarins has been the subject of many investigations because this family of molecules is used widely for dye laser operation between ~430 nm and ~560 nm.<sup>[43]</sup> There are two classes of coumarins; those with amino end groups free to rotate and those with rigidized amino end groups, as depicted in Figure VII.A.1.<sup>[44,45]</sup> The coumarins with a free amino end group exhibit pronounced solvent polarity-dependent absorption and emission responses, including emission from multiple bands, because a twisted intramolecular charge transfer (TICT) excited state involving the rotated amino group can be stabilized efficiently in polar solvents. The rigidized coumarins typically do not exhibit multiple resolvable emission features because their end amino group does not possess the rotational freedom required to stabilize a charge. All coumarins do, however, exhibit solvent polarity-dependent fluorescence quantum efficiencies. For coumarin 153,  $\phi_f$  ranges from 0.93 in ethyl acetate to 0.12 in water.<sup>[45]</sup> Efficient and solvent-dependent non-radiative relaxation pathways can play an important role in the dissipative dynamics of this class of molecules.

In addition to what is thought to be a prominent  $S_1 \leftarrow S_0$  transition, the coumarins

also exhibit moderately strong  $T_n \leftarrow T_1$  absorption in the same spectral region as emission from the  $S_1$ .<sup>[46]</sup> The cross-sections for T-T transitions in the coumarins are often within a factor of 5 of those for the  $S_1 \leftarrow S_0$  transition, and the efficiency with which  $T_1$  is populated increases markedly with excitation to higher excited singlet states.<sup>[47]</sup> Several coumarins have been shown to exhibit strong  $S_n \leftarrow S_1$  absorption under high intensity excitation at 266 nm and 355 nm.<sup>[47,48]</sup> The electronic spectroscopy of the coumarins is complex, with multiple transitions possibly contributing to the observed linear and nonlinear optical responses. The empirical observation of broad and featureless absorption and emission profiles for the coumarins should not be taken as an indication that their spectroscopic response is necessarily dominated by transitions between only two electronic manifolds.

### VII.B.3.B. Transient Stokes Shift Spectroscopies

There have been several means used to measure transient spectral dynamics in coumarins and other polar organic molecules. Time-correlated single photon counting over different wavelength regions of the probe molecule fluorescence band, followed by reconstruction of the data in the frequency domain to yield emission spectra at a series of delay times, has been used for chemical systems where spectral relaxations occur over tens of picoseconds.<sup>[19,20]</sup> The detection bandwidth of time-correlated single photon counting experiments is dictated by the efficiency of fluorescence collection and for most measurements on coumarins has been on the order of 15 nm.<sup>[19,20]</sup> Fluorescence up-conversion has also been used to detect transient spectral dynamics.<sup>[49,50]</sup> Fluorescence up-conversion is significantly more complex experimentally than time-correlated single

photon counting, but this level of complexity is required to time-resolve extremely fast relaxations. Up-conversion experiments employ very short laser pulses both for time resolution and for the high peak power required for efficient nonlinear frequency mixing. The bandwidth of the up-converted signal can also be large, depending on the time duration of the pulses, the phase matching properties of the sum frequency generation (SFG) crystal and the bandwidth selected by the monochromator between the SFG crystal and the photomultiplier detector. The monochromator bandwidth is typically set to  $\sim 1$  nm,<sup>[49]</sup> but for very short pulses, the spectral width of both the excitation pulse and the molecular fluorescence determine collectively the uncertainty in the frequency components used to generate the sum frequency signal. If the probe molecule exhibits substructure in the emission band, it is possible that such structure would be substantially narrower than the detection bandwidth of either type of detection system, and would therefore be partially resolved at best. Neither of these detection techniques are particularly well-suited to the elucidation of complex substructure within an emission manifold. In fact, a recent examination of LDS-750 in the butanols using transient stimulated emission spectroscopy,<sup>[51]</sup> a technique with a substantially narrower detection bandwidth, has revealed substructure not resolved with the spontaneous techniques.<sup>[20]</sup>

The transient spectral response of coumarin 153 is the focus of this paper. We have chosen to examine coumarin 153 for two reasons. First, a substantial body of information exists in the literature relating to both the static and dynamic optical response of coumarin 153, and second, coumarin 153 possesses a rigidized amino end group (Figure VII.A.1) so that any molecular geometry-dependence to the optical response is obviated. The excitation energy-dependence of the transient spontaneous emission

response shows that the spectral relaxation dynamics of coumarin 153 are not consistent with those of a single shifting feature, but that multiple states are involved in a population relaxation “cascade”.

#### **VII.B.4. Experimental**

##### **VII.B.4.A. Time-Domain Spectroscopy**

The time correlated single photon counting spectrometer we used in these studies has been described elsewhere.<sup>[52]</sup> Briefly, the light source for this spectrometer is a frequency doubled CW mode-locked Nd<sup>3+</sup>:YAG laser (Quantronix 416) that is used to pump synchronously a cavity dumped dye laser (Coherent 702). The dye laser was operated at 750 nm (LDS751, Exciton) and 820 nm (LDS821, Exciton). The pulses are output from this laser at a repetition rate of 4 MHz and produce an autocorrelation trace of ~5 ps FWHM. Typical average output power of this laser is 60 mW. The output of this dye laser is frequency doubled to produce excitation wavelengths of 375 nm and 410 nm. Excitation of the sample at 427 nm is accomplished using laser output from the system described in Chapter II (also set to produce output at 4 MHz repetition rate for the spontaneous emission measurements). Fluorescence is collected from the excited sample over all polarization angles to ensure the absence of a rotational diffusion contribution to the measured decay times. The collected light is polarization-scrambled and is imaged on the entrance slit of a subtractive double monochromator (American Holographic DB10-S). Detection of the fluorescence is accomplished using a cooled two-plate microchannel plate PMT (Hamamatsu R2809U-07), the output of which is sent directly to a constant fraction

discriminator (Tennelec TC454) and then to signal processing electronics. The instrument response function of this detection system is 25 ps FWHM.

#### **VII.B.4.B. Static Spectroscopies**

The linear absorption spectra of all solutions were measured using a Beckman DU-64 spectrophotometer operating with  $\sim 1$  nm resolution. Fluorescence spectra were recorded with  $\sim 1$  nm resolution using a Perkin-Elmer model LS-5 fluorescence spectrophotometer. Data output from these instruments were digitized and input into a computer using a digitizing tablet and associated software (Jandel Scientific). We show the absorption and spontaneous emission spectra of coumarin 153 in 1-butanol in Figure VII.B.1. The infrared spectrum of solid coumarin 153 was recorded on a Nicolet series 740 FTIR using a DTGS detector at  $\sim 8$   $\text{cm}^{-1}$  resolution. Spontaneous Raman scattering spectra of coumarin 153 were obtained using 568.2 nm  $\text{Kr}^+$  excitation from a Coherent Innova 90-K laser. The Raman samples were contained in melting point capillary tubes. The Raman detection equipment consisted of a SPEX 1877 Triplemate spectrograph with a SPEX 1459 Illuminator, with 600 and 1200 groove/mm gratings mounted in the filter and spectrograph stages, respectively. The detector was an EG&G Princeton Applied Research Model 1421 intensified diode array with a Model 1463 controller. The spectra were the result of the summation of 10 exposures of 2 sec each.

#### **VII.B.4.C. Chemicals And Sample Handling**

Coumarin 153 was obtained from Exciton Chemical Co. and was used without further purification. Solvents 1-butanol, N,N-dimethyl formamide (DMF) and dimethyl

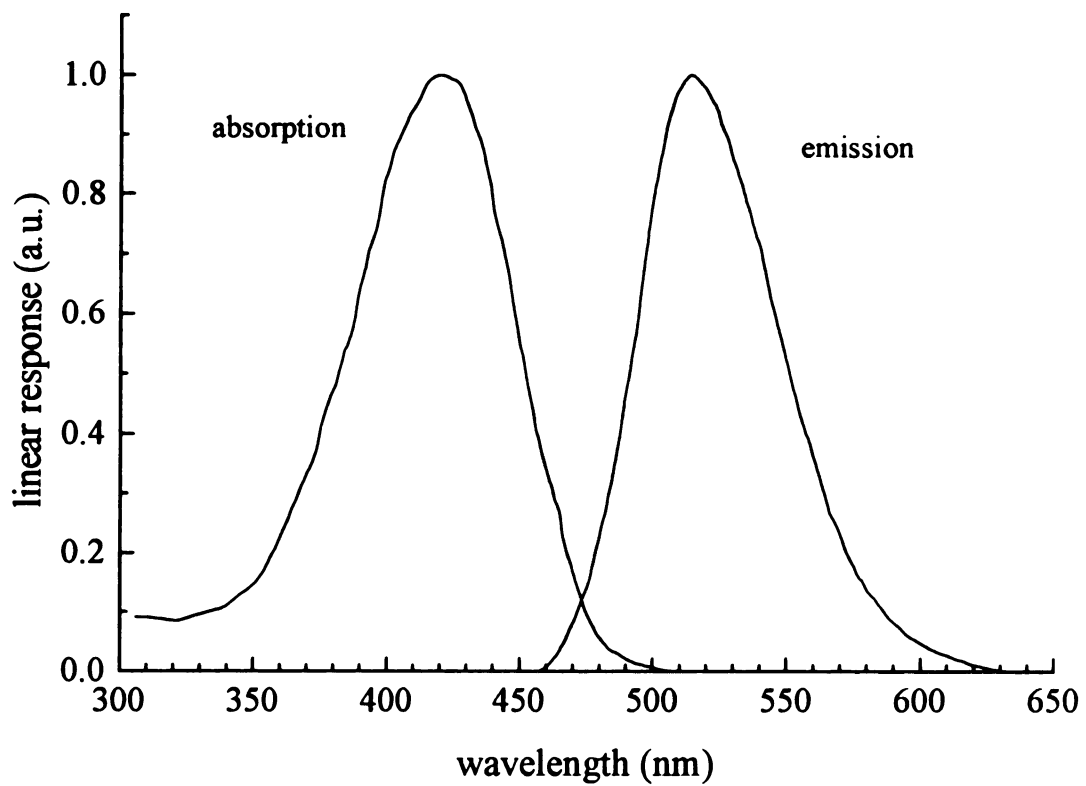


Figure VII.B.1. Absorption and spontaneous emission spectra of coumarin 153 in 1-butanol. Both spectra have been normalized to appear as the same intensity.

sulfoxide (DMSO) were purchased from Aldrich Chemical Company and used as received. For the transient spontaneous emission experiments, the coumarin 153 solutions ( $\sim 15 \mu\text{M}$ ) were contained in a 3 mm path length quartz cuvette with two blacked sides to eliminate “ghost” signals arising from reflections of the exciting light within the cell.

#### **VII.B.4.D. Calculations**

Molecular orbital calculations were performed using the Hyperchem release 3.0 software package. The geometric structure of ground state coumarin 153 was optimized at the semi-empirical level using the AM1 Hamiltonian, and no geometric restrictions were set on the molecular structure. The electronic energies and dipole moments we report here were calculated using configuration interaction with 400 configurations for the ground state ( $S_0$ ), the first excited singlet state ( $S_1$ ), and the first triplet state ( $T_1$ ) of coumarin 153. While there are several stable conformations of the amino end group and its associated tethers, the limited conformational freedom available to the tethered amino group affects the calculated electronic energies and dipole moments of the molecule negligibly. We have covered the computed results for coumarin 153 and some other coumarins in Chapter VII.A.

#### **VII.B.5. Results And Discussion**

Previous reports on the transient room temperature spectral dynamics of coumarin 153 in polar solvents have suggested that the fluorescence spectrum of this molecule red-shifts uniformly in time - *as a single feature* - from its initial position in close energetic proximity to the absorption band immediately following excitation, to its steady state

position.<sup>[16,19]</sup> Following initial reports, there has ensued a discussion in the literature as to the origin of several curious features exhibited by the transient spontaneous emission spectrum of coumarin 153 and a closely related fluorophore, coumarin 102. Agmon<sup>[42]</sup> presented an explanation for the transient spectral shifts that differs from that put forth by Maroncelli and Fleming. Agmon's interpretation is based on the observation that the integrated intensity of the emission band decays non-exponentially in time. Such a total intensity decay, he argues, can be explained by the presence of multiple subfeatures within the emission envelope. This is an entirely plausible explanation, because many of the early experimental studies of the coumarins detected the shifts of the emission band using instrumental bandwidths on the order of 15 nm, and under such experimental conditions, the resolution of multiple spectral features would be difficult at best. For rigidized systems, like coumarin 153, the formation on a TICT state is precluded, but other reasons for the existence of substructure within the emission band are possible (*vide infra*). Maroncelli *et al.*<sup>[53]</sup> have countered Agmon's interpretation with the assertion that nonexponential intensity decay is a general and expected result based on the  $\nu^3$  dependence of the spontaneous emission transition cross-section. Therefore, any emission band with a significant spectral width is expected to exhibit nonexponential population decay. Their experimental data for coumarin 102 in 1-propanol over a range of temperatures indicate that this mechanism is consistent with the observed non-exponentiality. Because of the plausibility of both Agmon's and Maroncelli's interpretation and the potential importance of conclusions drawn from such experiments, we have undertaken an examination of coumarin 153, reporting how our spontaneous emission time resolved spectroscopic results, to help elucidate the operative mechanism(s) for the

observed transient spectral response from this class of molecules.

If the spectral dynamics measured for the coumarins arise from emission along a *single* excited state surface, as postulated,<sup>[19]</sup> then the same response should be observed regardless of where on that excited state surface the excitation is initially placed. In other words, if the spectral dynamics observed for the coumarins are accounted for by the shifting of a single band, then the observed shift should display no excitation energy dependence. We have tested this hypothesis by measuring the transient spontaneous emission spectral response of coumarin 153 in 1-butanol, DMSO and DMF at three excitation wavelengths; 375 nm (blue side of the absorption band), 410 nm (near the absorption maximum) and 427 nm (red side of the absorption band). We present these data in Figures VII.B.2-VII.B.4. These data were processed by normalization of individual time scans to the static spontaneous emission profile at times long after excitation (9 ns). Prior to normalization, the time scans were checked and shifted if necessary to ensure that the zero time point, determined from the response functions taken just prior to each scan, occurred at the same relative position on all time scans. The spontaneous emission data we report here were recorded using a 10 nm detection bandwidth at 10 nm intervals. We compared these data with sets taken using 2 nm and 20 nm detection bandwidths, and all data were identical to within the experimental uncertainty. The data reported in Figures VII.B.2-VII.B.4 represent the average of three individual data sets for each excitation wavelength and each solvent. Figures VII.B.2-VII.B.4 show experimental data points and are not derived from mathematical fits to the data. There are several interesting features contained in these data. First, we observe the apparent shift seen by others for coumarin 153 in 1-butanol, but the shifts are not seen for

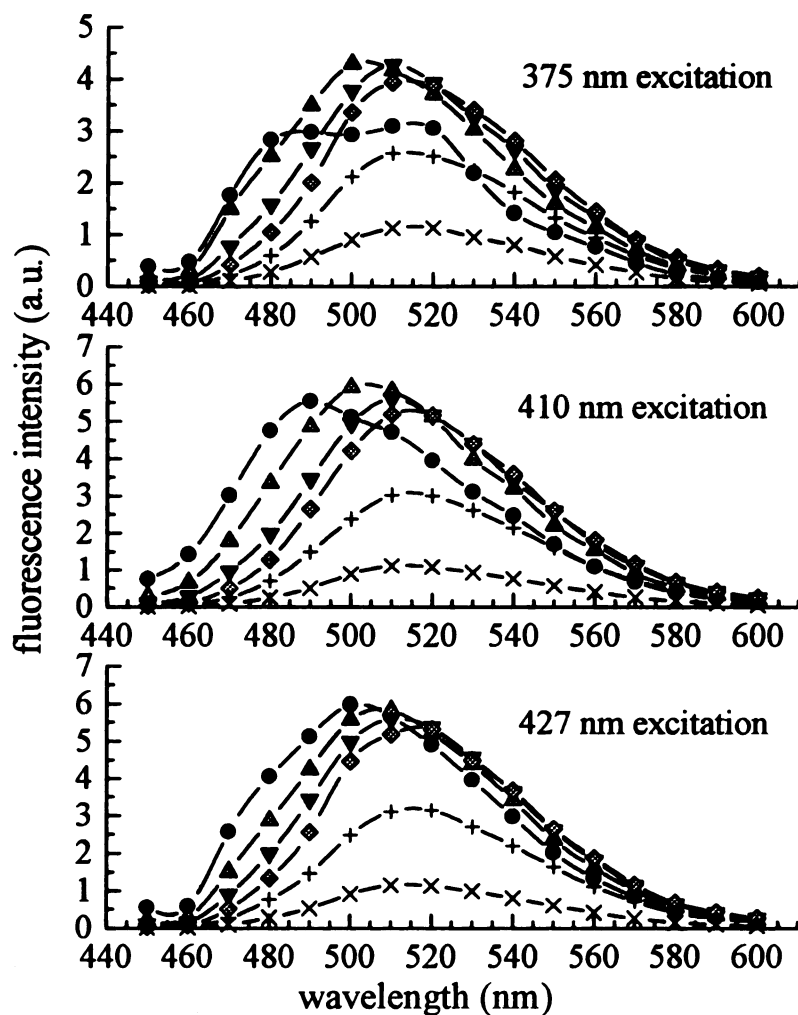


Figure VII.B.2. Time resolved spontaneous emission spectra of coumarin 153 in 1-butanol. Spectra were reconstructed from individual time scans. See text for a discussion of the data processing. The times after excitation are: (●) 30 ps, (▲) 90 ps, (▼) 210 ps, (◆) 500 ps, (+) 3000 ps, (×) 8000 ps. Excitation wavelengths are indicated for each family of spectra.

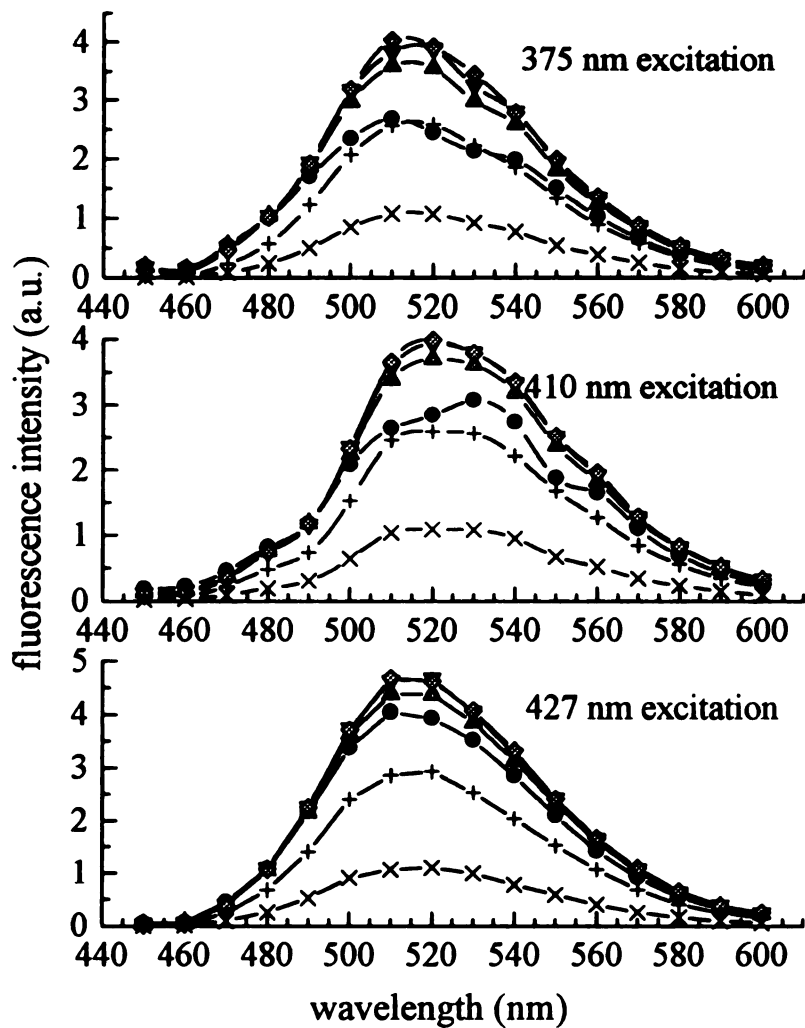


Figure VII.B.3. Time resolved spontaneous emission spectra of coumarin 153 in DMSO. Spectra were reconstructed from individual time scans. See text for a discussion of the data processing. The times after excitation are: (●) 30 ps, (▲) 90 ps, (▼) 210 ps, (◆) 500 ps, (+) 3000 ps, (×) 8000 ps. Excitation wavelengths are indicated for each family of spectra.

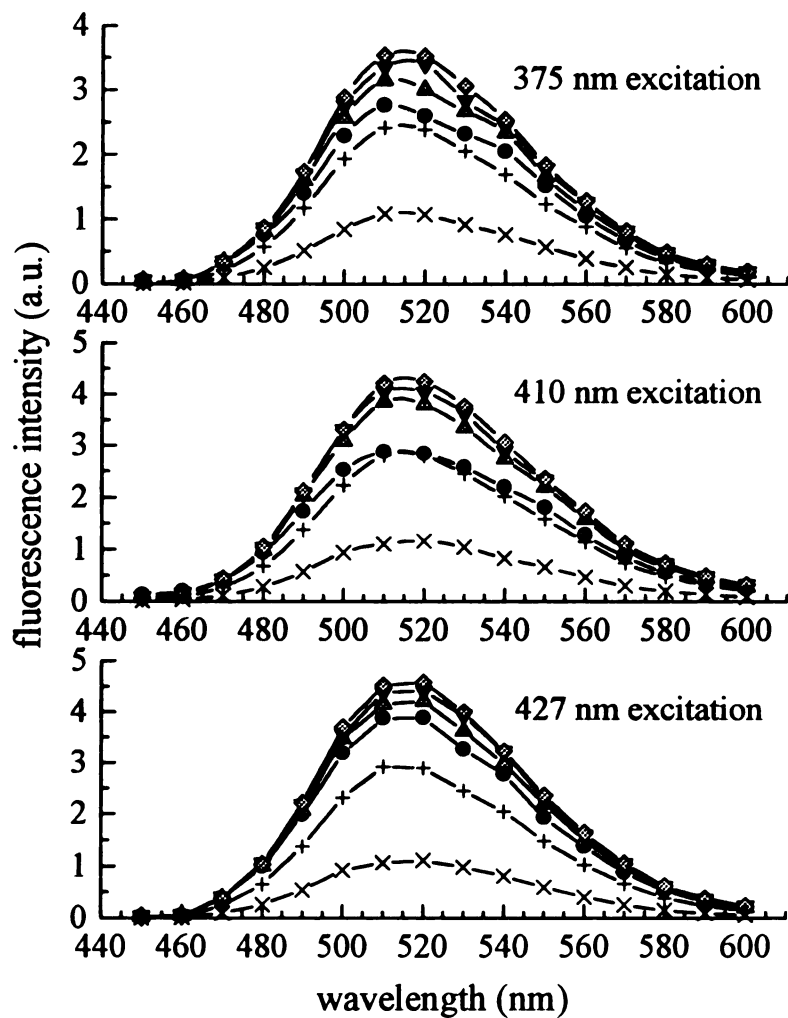


Figure VII.B.4. Time resolved spontaneous emission spectra of coumarin 153 in DMF. Spectra were reconstructed from individual time scans. See text for a discussion of the data processing. The times after excitation are: (●) 30 ps, (▲) 90 ps, (▼) 210 ps, (◆) 500 ps, (+) 3000 ps, (×) 8000 ps. Excitation wavelengths are indicated for each family of spectra.

DMSO and DMF. This is consistent with the spectral dynamics of coumarin 153 occurring on a femtosecond-to-picosecond timescale in these polar aprotic solvents, much faster than our instrumental time resolution. In addition to the spectral dynamics, our data provide evidence for substructure in the emission band, with the initial distribution of population amongst these sub-features depending on the excitation wavelength. The spectral dynamics observed for coumarin 153 occur on the high energy side of the emission band. Examination of the spontaneous emission time profile at a single emission wavelength shows clearly that the spectral dynamics depend critically on the excitation energy. These data, presented in Figures VII.B.5- VII.B.7, demonstrate that the spectral dynamics seen for coumarin 153 are not accounted for simply by the transient relaxation of a population along a single excited state surface. These data provide insight into the states involved in the relaxation process, and we will return to a discussion of this point following the presentation of our stimulated emission data.

The spontaneous emission spectra do not provide the only indications that multiple electronic states contribute to the optical response of coumarin 153 in polar solvents; reorientation dynamics measurements corroborate this assertion<sup>[54]</sup>. The rotational diffusion behavior of some polar molecules depends on the electronic state of the reorienting molecule,<sup>[10-14]</sup> and a different report from the Blanchard group has found this to be the case for coumarin 153 in 1-butanol. In that work, the reorientation times of coumarin 153 in 1-butanol, DMF and DMSO for excitation at 410 nm and 427 nm were measured. For both sets of measurements the experimental signal was obtained by stimulating emission at 500 nm, and we show these results in Table VII.B.1. For DMF and DMSO, the reorientation times are independent of the excitation wavelength, but for

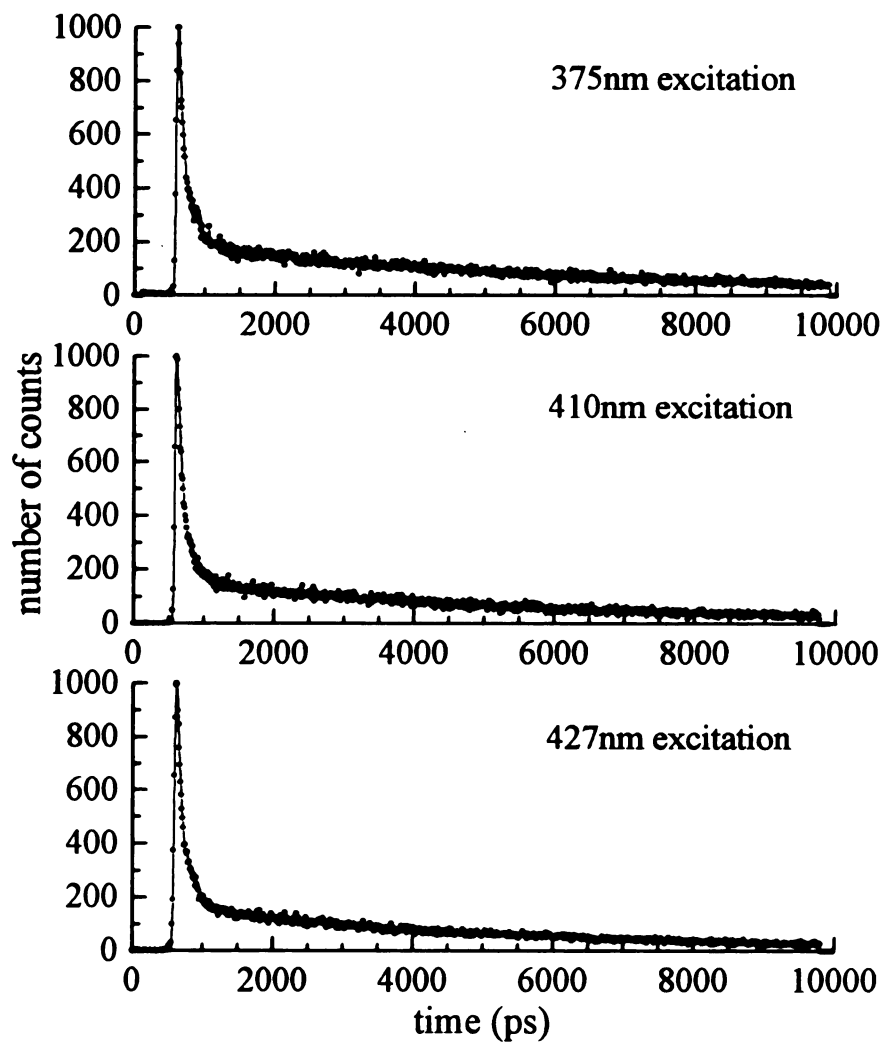


Figure VII.B.5. Spontaneous emission time scans of coumarin 153 in 1-butanol detected at 470 nm. The three excitation wavelengths are indicated beside the time scans.

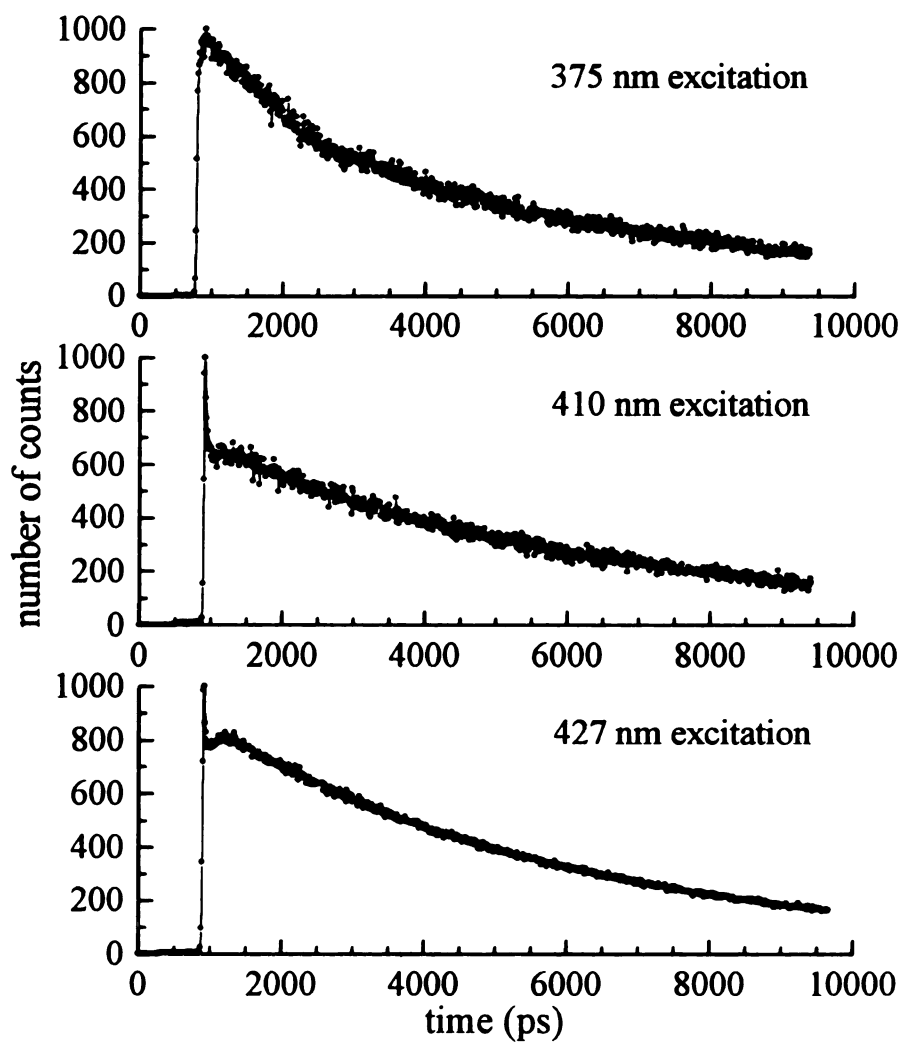


Figure VII.B.6. Spontaneous emission time scans of coumarin 153 in DMSO detected at 470 nm. the three excitation wavelengths are indicated beside the time scans. Note the build-up in intensity subsequent to decay of the fast response for excitation at 427 nm.

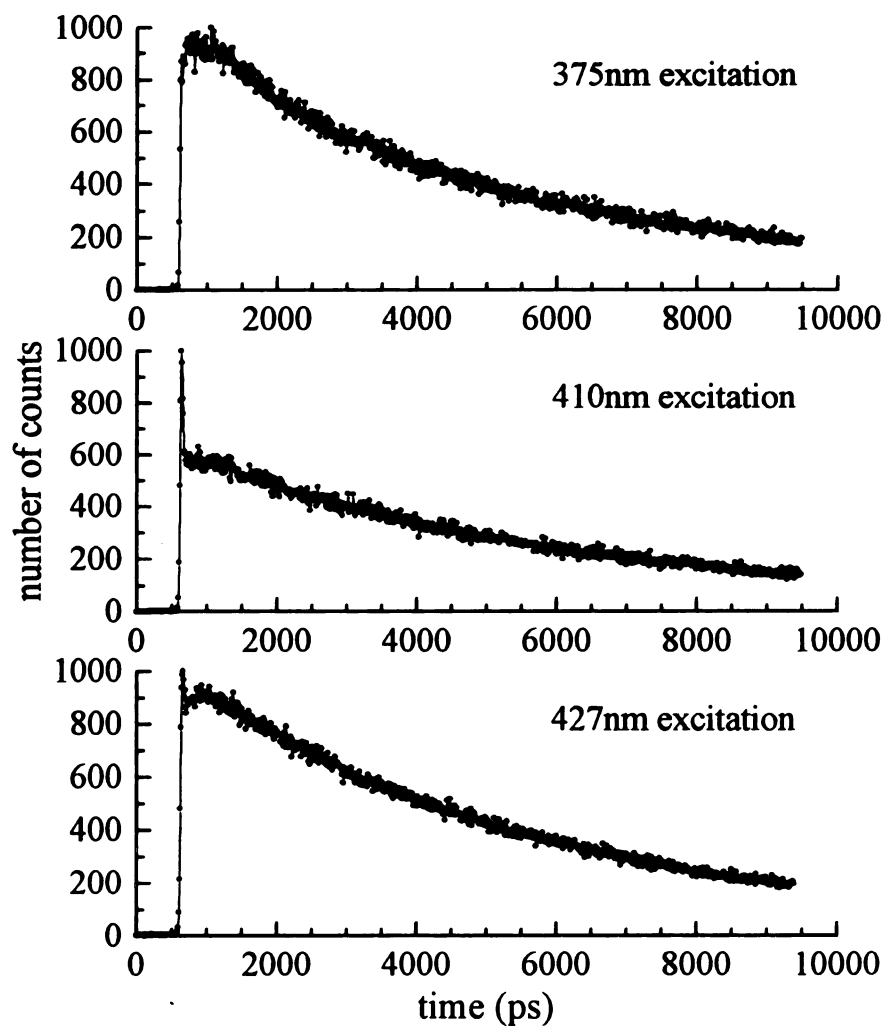


Figure VII.B.7. Spontaneous emission time scans of coumarin 153 in DMF detected at 470 nm. the three excitation wavelengths are indicated beside the time scans. Note the build-up in intensity subsequent to decay of the fast response for excitation at 427 nm.

solvent	410nm excitation		427nm excitation	
	R(0)	$\tau_{OR}$ (ps)	R(0)	$\tau_{OR}$ (ps)
1-butanol	$0.22 \pm 0.01$	$108 \pm 4$	$0.22 \pm 0.01$	$134 \pm 4$
DMF	$0.31 \pm 0.01$	$47 \pm 2$	$0.30 \pm 0.01$	$45 \pm 2$
DMSO	$0.33 \pm 0.01$	$104 \pm 7$	$0.30 \pm 0.06$	$93 \pm 9$

Table VII.B.1. Reorientation times of coumarin 153 at two excitation wavelengths. Jiang, Y.; McCarthy, P. K.; Blanchard, G. J.; *Chem. Phys.*, **183**, 249 (1994).

1-butanol, the reorientation of coumarin 153 excited at 427 nm is slower than for excitation at 410 nm. We believe the reason for this effect is that the state accessed by 427 nm excitation is more amenable to hydrogen bonding interactions with the solvent than the state accessed by 410 nm excitation. Formation of a complex between the solvent and the excited coumarin 153 probably also occurs with the polar aprotic solvents, but the average lifetime for such a complex is expected to be substantially shorter than for a hydrogen bonding liquid. Our data are consistent with the recent observation of excitation energy-dependent reorientation dynamics for coumarin 102 in a mixed hydrogen-bonding solvent system.<sup>[55]</sup> The formation of complexes between coumarin 102 and numbers of solvent molecules was given as the explanation of the observed excitation energy dependence, although the presence of multiple excited electronic states was not considered in their interpretation of the data.

Coumarin 153 has been reported before to produce multiple exponential anisotropy decays at low temperature in polar solvents, and the reasons for this behavior were not clear.<sup>[19]</sup> It is possible that the effective rotor shape of the coumarin is that of a prolate ellipsoid, and such a rotor shape could give rise to multiple exponential decays in the anisotropy.<sup>[9]</sup> At room temperature, however, only single exponential anisotropy decays have been observed for coumarin 153. Previous reports of coumarin 153 reorientation in 1-butanol at room temperature indicate  $\tau_{OR} \sim 250$  ps,<sup>[19]</sup> and  $\tau_{OR}$  times between 108 ps and 134 ps were measured more recently<sup>[54]</sup>. In all reports,  $R(0) = 0.22$ , indicating the relative orientation of the excited and observed transition dipole moments are consistent between the two sets of measurements, and thus the reorientation times for the two reports are directly comparable. We have not yet investigated the reorientation

dynamics of coumarin 153 in sufficient detail to resolve the reason(s) for this discrepancy.

The reorientation data provide further evidence for the existence of two excited electronic states in close energetic proximity. We now turn our attention to the identities of these electronic states. Stimulated emission data<sup>[54]</sup> indicate that the electronic state accessed by 410 nm excitation is not populated significantly by 427 nm excitation, although at 427 nm there is  $\sim 2000\text{ cm}^{-1}$  of excess energy in the excited state(s) manifold. The linear absorption and emission spectra do not provide an indication of multiple features in polar solvents, and published gas phase and supersonic jet spectra of coumarin 153 do not access a spectral region with sufficient excess spectroscopic energy to provide a meaningful comparison with our data.<sup>[56]</sup> Despite this limitation the spontaneous emission data we report here indicate the presence of at least two excited electronic states. We have used semi-empirical molecular orbital calculations to address the identity of these states. Semi-empirical calculations have been used before to augment experimental data on transient spectral shifts in coumarins<sup>[19]</sup> and substituted amino-3-methyl-1,4-benzoxazine 2-one compounds,<sup>[21]</sup> and state-dependent reorientation dynamics of oxazines and thiazines in polar solvents.<sup>[10-14,57]</sup> Such calculations have provided a rationale for the interpretation of the experimental data in each case. For the coumarin<sup>[19]</sup> and modified benzoxazine<sup>[20]</sup> spectral shift data, a substantial change in dipole moment on excitation was correlated with the observed shifts. For oxazine reorientation,<sup>[10-14]</sup> an excited singlet state redistribution of electron density into a non-bonding heterocyclic nitrogen orbital was calculated and related to the observed state-dependent change in reorientation time.<sup>[57]</sup> Recent advances in computational chemistry at the semi-empirical level, including the development of AM1, a parameterization optimized for the calculation of polar systems,

<sup>[58-60]</sup> and the ability to accommodate a large number of configurations in configuration interaction calculations, has allowed moderately high level calculations to be performed on molecules as large as coumarin 153. We show the results of our calculations in Figure VII.B.8. No geometries were restricted in these calculations. We found that slight conformational changes in the amino nitrogen tethers did not affect the calculated energies or dipole moments significantly. The inclusion of configuration interaction did, however, produce significant changes in the calculated energies of the populated and neighboring excited states, as expected. For CI calculations on coumarin 153 using 400 microstates, the triplet states  $T_3$  and  $T_4$  and the singlet state  $S_2$  are all within several hundred  $\text{cm}^{-1}$  of  $S_1$ . These calculations assume an isolated coumarin 153 molecule in a vacuum, so it is not reasonable to expect quantitative agreement our experimental results. None-the-less, we expect the qualitative predictions made by these calculations to be valid. The calculated  $S_1 \leftarrow S_0$  transition energy is  $26429 \text{ cm}^{-1}$ , and the gas phase origin for coumarin 153 has been measured at  $\sim 25196 \text{ cm}^{-1}$ ,<sup>[56]</sup> indicating that the AM1 parameterization is substantially better suited to the calculation of coumarin excited states than the MNDO parameterization, which predicted this same transition to occur at  $30,700 \text{ cm}^{-1}$ .<sup>[19]</sup> The presence of triplet states  $T_3$  and  $T_4$  in close proximity to singlet states  $S_1$  and  $S_2$  is consistent with our experimental spontaneous emission, stimulated emission and reorientation data. The spontaneous emission time scans shown in Figures VII.B.5-VII.B.7 provide insight into the roles of these multiple electronic states.

The data shown in Figures VII.B.6 and VII.B.7 for coumarin 153 in DMSO and DMF excited at 427 nm show that subsequent to a fast ( $<20 \text{ ps}$ ) relaxation, there is a build-up in emission intensity ( $\tau \sim 200 \text{ ps}$ ) followed by a slower ( $\sim 5.5 \text{ ns}$ ) intensity decay

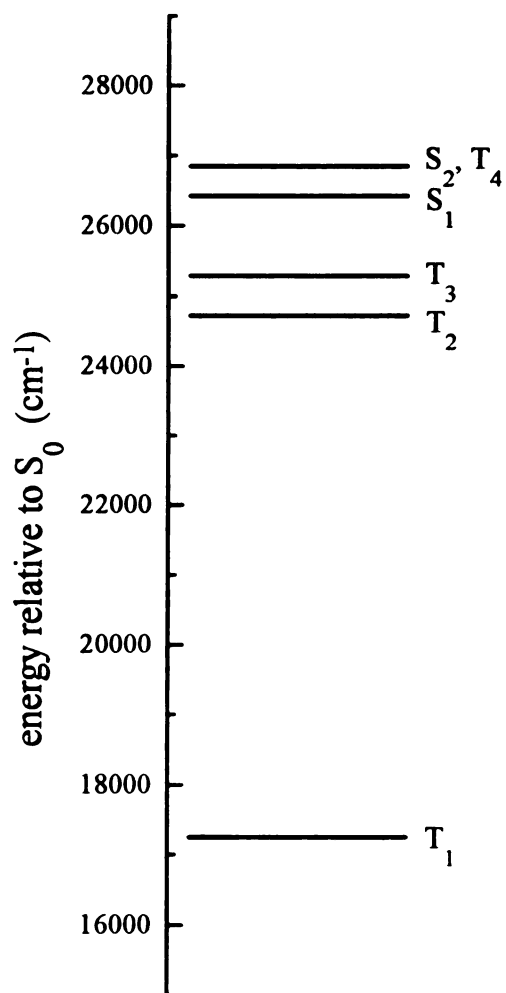
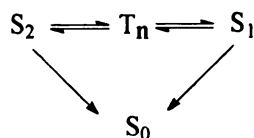


Figure VII.B.8. Energy levels calculated for excited electronic states of coumarin 153. The configuration interaction energies depend on the excitation calculated, but the relative ordering remains the same. Details of this calculation are reported in the text.  $\mu(S_0)$  is calculated to be 5.2D,  $\mu(S_1) = 11.0\text{D}$  and  $\mu(S_2) = 8.4\text{D}$ .

(see Table VII.B.2). The presence of the build-up in these data cannot be explained if only two radiative electronic states are responsible for the spontaneous optical response. If only two radiative states were involved in the optical response, then the population decay of the system must be monotonic, *i.e.* there is no means by which population can be stored and later re-released in a system with only two electronic states. A build-up in the spontaneous emission time profile necessarily implies the storage of some fraction of the population in a non-radiative state. Further, the non-radiative state must be able to exchange population with both of the radiative states for a build-up to occur. The stimulated emission data show that there are two excited singlet electronic states in close energetic proximity, and semi-empirical calculations indicate that there are several triplet states close in energy to the  $S_1$  and  $S_2$  states.

There are likely a variety of energy level schemes consistent with our data. We show in Figure VII.B.9 a schematic of one series of potential energy surfaces consistent with our data and calculations. The kinetic model consistent with population exchange between these surfaces is;



For excitation at 427 nm, both  $S_1$  and  $S_2$  are populated initially, with the excitation into  $S_2$  decaying rapidly ( $< 20$  ps in DMF and DMSO, 75 ps for 1-butanol) into either an excited triplet states or directly to  $S_1$  via an activated curve crossing. Because both  $S_1$  and  $S_2$  can decay radiatively, the presence of the build-up in the data indicates that the dominant population transfer from  $S_2$  to  $S_1$  proceeds through the triplet state, likely  $T_4$ , based on the

solvent	$\lambda_{exc}$ (nm)	fast decay (ps)	build-up (ps)	slow decay (ps)
1-butanol	375	74±4	N/A	5650±420
	410	73±5	N/A	4780±350
	427	92±6	N/A	4880±70
DMF	375	N/A	N/A	(1) 1080±110 (2) 5990±220
	410	11±5	N/A	5670±160
	427	<20	203±52	5250±30
DMSO	375	N/A	N/A	(1) 682±18 (2) 5550±60
	410	19±9	N/A	5520±170
	427	< 20	194±83	5200±50

**Table VII.B.2.** Decay and build-up time constants for spontaneous emission data. These times were determined from the data presented in Figures VII.B.5-VII.B.7. N/A indicates that a build-up was not detected or resolvable.

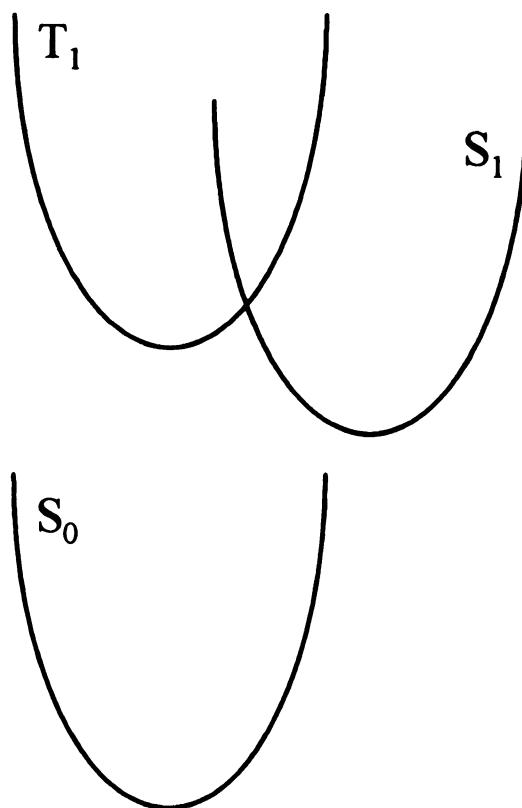


Figure VII.B.9. Schematic of energy surfaces consistent with the spontaneous and stimulated emission data reported here.

calculation results presented in Figure VII.B.8. Excitation at 410 nm accesses both  $S_2$  and  $S_1$ , but with enough excess energy<sup>[54]</sup> that population relaxation between  $S_2$  and  $S_1$  is essentially a barrierless process, and thus a build-up is not resolved in these data. Excitation at 375 nm accesses predominantly the  $S_1$  surface, presumably owing to favorable Franck-Condon factors, and thus no fast response is observed because  $S_2$  remains essentially unpopulated. We observe a two-component slow decay for excitation at 375 nm, and believe that the  $\sim 1$  ns decay represents the reversible relaxation pathway from  $S_1$  to  $T_n$  and  $S_2$ . Our data on coumarin 153 in 1-butanol are consistent with this model. The barriers to intersystem crossing and internal conversion are modified by 1-butanol to produce a longer  $S_2$  radiative lifetime than is seen for DMSO or DMF.

Reconciliation of these data with the shifts reported in the literature is an important consideration. As our data show, excitation near the maximum of the absorption band yields apparently monotonic population decays, and these data are consistent with published reports on the coumarins.<sup>[16,19]</sup> Within the framework of the model presented in Figure VII.B.9, where the radiative responses of  $S_2$  and  $S_1$  are unresolved due to extensive spectral overlap, we believe that the solvation of  $S_1$  and  $S_2$  are fundamentally different because of the different charge distributions in each state. The semi-empirical calculations for coumarin 153 indicate that the static dipole moment for  $S_1$  is 11 D, and for  $S_2$  we calculate  $\mu = 8.4$  D. The state-dependent polarity exhibited by coumarin 153 is corroborated by rotational diffusion measurements in 1-butanol (Table VII.B.1). The solvation of  $S_1$  and  $S_2$  will stabilize these states differently and thus cause the coupling amongst the states to be strongly solvent dependent. The fact that the strengths of these couplings are observed to correlate with solvent longitudinal relaxation times is

interesting, but the fundamental reasons for this correlation are not clear. Predicting such a correlation would require detailed knowledge of the  $S_1$ ,  $S_2$ ,  $T_3$  and  $T_4$  surfaces as well as an understanding of the local dielectric field imposed by the immediate solvent environment. It is known, however, that the identity of the solvent does affect the fluorescence quantum yield of coumarin 153, indicating that the relative efficiencies of radiative and nonradiative relaxation channels are affected by local dielectric effects. Our data are consistent with previous reports, but do not reveal the reasons for the observed correlation with solvent longitudinal relaxation time. It is fair to question whether or not coumarin 153 is anomalous because of the presence of some specific functionality, such as its  $CF_3$  group. Our calculations on a series of substituted coumarins indicate that the presence of the  $CF_3$  group in coumarin 153 does not alter the proximity of other electronic states to the  $S_1$ , but rather this result is general for the coumarins.<sup>[61]</sup>

## VII.B.6. Conclusions

We have reported the ultrafast spontaneous spectroscopic response of coumarin 153 in three polar solvents at room temperature. We find that these responses exhibit an excitation energy dependence. The excitation energy dependence of the spontaneous emission response provides direct evidence that the spectral dynamics of coumarin 153 are not accounted for by the shifting of a single spectral feature. The spontaneous emission data demonstrate that population exchange between the two radiative states is mediated by a mutual coupling to a nonradiative state. These findings are corroborated by reorientation measurements<sup>[54]</sup> and semi-empirical molecular orbital calculations. Our data reveal collectively the *absence* of a spectral shift in the coumarins and the *presence* of

multiple electronic states in close proximity to the  $S_1$ . We suggest that complex, rapid and solvent-dependent population relaxation processes contribute significantly to the transient optical response of the coumarins. More work is clearly required to understand the origin of these transient optical effects in coumarins and the role that intramolecular population relaxations play in addition to any intermolecular solvation processes.

### VII.B.7. References

1. Fleming, G. R.; Chemical Applications of Ultrafast Spectroscopy, Oxford University Press, London, (1986), and references therein.
2. Fleming, G. F.; Knight, A. E. W.; Morris, J. M.; Robbins, R. J.; Robinson, G. W.; *Chem. Phys. Letters*, **49**, 1 (1977).
3. Von Jena, A.; Lessing, H. E.; *Chem. Phys.*, **40**, 245 (1979).
4. Ben-Amotz, D.; Scott, T. W.; *J. Chem. Phys.*, **87**, 3739 (1987).
5. Ben-Amotz, D.; Drake, J. M.; *J. Chem. Phys.*, **89**, 1019 (1988).
6. Alavi, D. S.; Waldeck, D. H.; *J. Phys. Chem.*, **95**, 2828 (1991).
7. Alavi, D. S.; Hartman, R. S.; Waldeck, D. H.; *J. Chem. Phys.*, **94**, 4509 (1991).
8. Alavi, D. S.; Waldeck, D. H.; *J. Chem. Phys.*, **94**, 6196 (1991).
9. Blanchard, G. J.; *J. Chem. Phys.*, **87**, 6802 (1987).
10. Blanchard, G. J.; Cihal, C. A.; *J. Phys. Chem.*, **92**, 5950 (1988).
11. Blanchard, G. J.; *J. Phys. Chem.*, **92**, 6303 (1988).
12. Blanchard, G. J.; *J. Phys. Chem.*, **93**, 4315 (1989).
13. Blanchard, G. J.; *Anal. Chem.*, **61**, 2394 (1989).
14. Blanchard, G. J.; *J. Phys. Chem.*, **95**, 5293 (1991).

15. Barbara, P. F.; Jarzeba, W.; *Adv. Photochem.*, **15**, 1 (1990).
16. Jarzeba, W.; Walker, G. C.; Johnson, A. E.; Barbara, P. F.; *Chem. Phys.*, **152**, 57 (1991).
17. Simon, J. D.; *Acc. Chem. Res.*, **21**, 128 (1988).
18. Fee, R. S.; Milson, J. A.; Maroncelli, M.; *J. Phys. Chem.*, **95**, 5170 (1991).
19. Maroncelli, M.; Fleming, G. R.; *J. Chem. Phys.*, **86**, 6221 (1987).
20. Castner, E. W.; Maroncelli, M.; Fleming, G. R.; *J. Chem. Phys.*, **86**, 1090 (1987).
21. Declémy, A.; Rullière, C.; Kottis, Ph.; *Chem. Phys. Letters*, **133**, 448 (1987).
22. Maroncelli, M.; Macinnis, J.; Fleming, G. R.; *Science*, **243**, 1674 (1989).
23. Brito Cruz, C. H.; Fork, R. L.; Knox, W. H.; Shank, C. V.; *Chem. Phys. Letters*, **132**, 341 (1986).
24. Bardeen, C. J.; Shank, C. V.; *Chem. Phys. Letters*, **203**, 535 (1993).
25. Casassa, M. P.; Heilweil, E. J.; Stephenson, J. C.; Cavanagh, R. R.; *J. Chem. Phys.*, **84**, 2361 (1986).
26. Heilweil, E. J.; Casassa, M. P.; Cavanagh, R. R.; Stephenson, J. C.; *J. Chem. Phys.*, **85**, 5004 (1986).
27. Heilweil, E. J.; Cavanagh, R. R.; Stephenson, J. C.; *Chem. Phys. Letters*, **134**, 181 (1987).
28. Heilweil, E. J.; Cavanagh, R. R.; Stephenson, J. C.; *J. Chem. Phys.*, **89**, 230 (1988).
29. Lingle, Jr., R.; Xu, X.; Yu, S. C.; Zhi, H.; Hopkins, J. B.; *J. Chem. Phys.*, **93**, 5667 (1990).
30. Lingle, Jr., R.; Xu, X.; Yu, S. C.; Chang, Y. J.; Hopkins, J. B.; *J. Chem. Phys.*, **92**, 4629 (1990).
31. Yu, S. C.; Xu, X.; Lingle, Jr., R.; Hopkins, J. B.; *J. Am. Chem. Soc.*, **112**, 3668 (1990).
32. Xu, X.; Lingle, Jr. R.; Yu, S. C.; Chang, J.; Hopkins, J. B.; *J. Chem. Phys.*, **92**, 2106

- (1990).
33. Hopkins, J. B.; Rentzepis, P. M.; *Chem. Phys. Letters*, **142**, 503 (1987).
  34. Anfinrud, P.; Han, C.; Hansen, P. A.; Moore, J. N.; Hochstrasser, R. M.; Ultrafast Phenomena VI, Yajima, T.; Yoshihara, K.; Harns, G. B.; and Shionoyz, S.; Eds., Springer, Berlin, 1990, 442-446.
  35. Anfinrud, P. A.; Han, C.; Lian, T.; Hochstrasser, R. M.; *J. Phys. Chem.*, **94**, 1180 (1990).
  36. Hambir, S. A.; Jiang, Y.; Blanchard, G. J.; *J. Chem. Phys.*, **98**, 6075 (1993).
  37. Gustafson, T. L.; Roberts, D. M.; Chernoff, D. A.; *J. Chem. Phys.*, **79** 1559 (1983).
  38. Gustafson, T. L.; Roberts, D. M.; Chernoff, D. A.; *J. Chem. Phys.*, **81**, 3438 (1984).
  39. Gustafson, T. L.; Chernoff, D. A.; Palmer, J. F.; Roberts, D. M.; in Time Resolved Vibrational Spectroscopy, G. H. Atkinson, Ed. Gordon and Breach, New York, 1987, 265-285.
  40. Hu, C. M.; Zwanzig, R.; *J. Chem. Phys.*, **60**, 4353 (1974).
  41. Youngren, G. K.; Acrivos, A.; *J. Chem. Phys.*, **63**, 3846 (1975).
  42. Agmon, N.; *J. Phys. Chem.*, **94**, 2959 (1990).
  43. Drexhage, K. H.; in Topics in Applied Physics, Vol. 1, Dye Lasers, Ed. by F. P. Schäfer, Springer, Berlin (1973).
  44. Jones II, G.; Jackson, W. R.; Halpern, A. M.; *Chem. Phys. Letters*, **72**, 391 (1980).
  45. Jones II, G.; Jackson, W. R.; Choi, C. Y.; Bergmark, W. R.; *J. Phys. Chem.*, **89**, 294 (1985).
  46. Pavlopoulos, T. G.; Golich, D. J.; *J. Appl. Phys.*, **64**, 521 (1988).
  47. Sahyun, M. R. V.; Sharma, D. K.; *Chem. Phys. Letters*, **189**, 571 (1992).
  48. Speiser, S.; Shakkour, N.; *Appl. Phys. B*, **38**, 191 (1985).
  49. Kahlow, M. A.; Jarzeba, W.; DeBruil, T. P.; Barbara, P. F.; *Rev. Sci. Instrum.*, **59**, 1098 (1988).

50. Walker, G. C.; Jarzeba, W.; Kang, T. J.; Johnson, A. E.; Barbara, P. F.; *J. Opt. Soc. Am. B*, **7**, 1521 (1990).
51. Blanchard, G. J.; *J. Chem. Phys.*, **95**, 6317 (1991).
52. DeWitt, L.; Blanchard, G. J.; LeGoff, E.; Benz, M. E.; Liao, J. H.; Kanatzidis, M. G.; *J. Am. Chem. Soc.*, **115**, 12158 (1993).
53. Maroncelli, M.; Fee, R. S.; Chapman, C. F.; Fleming, G. R.; *J. Phys. Chem.*, **95** 1012, (1991).
54. Jiang, Y.; McCarthy, P. K.; Blanchard, G. J.; *Chem. Phys.*, **183**, 249 (1994).
55. Moog, R. S.; Bankert, D. L.; Maroncelli, M.; *J. Phys. Chem.*, **97**, 1496 (1993).
56. Ernsting, N. P.; Asimov, M.; Schafer, F. P.; *Chem. Phys. Letters*, **91**, 231 (1982).
57. Blanchard, G. J.; *Chem. Phys.*, **138**, 365 (1989).
58. Dewar, M. J. S.; Zoebisch, E. G.; Healy, E. F.; Stewart, J. J. P.; *J. Am. Chem. Soc.*, **107**, 3902 (1985).
59. Dewar, M. J. S.; Dieter, K. M.; *J. Am. Chem. Soc.*, **108**, 8075 (1986).
60. Stewart, J. J. P.; *J. Comp. Aided Mol. Design*, **4**, 1 (1990).
61. McCarthy, P. K.; Blanchard, G. J.; *J. Phys. Chem.*, **97**, 12205 (1993).

## **VIII. PHOTOISOMERIZATION OF CYANINES. A COMPARATIVE STUDY OF OXYGEN AND SULFUR CONTAINING SPECIES**

### **VIII.A. Abstract**

We have compared the photoisomerization properties of two cyanine analogs, 3,3'-diethyloxadicarbocyanine iodide (DODCI) and 3,3'-diethylthiadicarbocyanine iodide (DTDCI). These two molecules are structurally similar, differing only in the presence of oxygen or sulfur at two heteroatom sites. Measurement of the radiative and nonradiative population relaxation kinetics of these molecules reveals a difference in their equilibrium geometries despite their outward similarities. We relate this difference to the steric constraints imposed by the oxygen and sulfur heteroatoms and to the occurrence of an excited state barrier predicted by semi-empirical calculations of the ground and excited state isomerization surfaces for these molecules.

### **VIII.B. Introduction**

The cyanines are a class of molecules used for a wide range of applications related to their ability to change shape upon absorption of light.<sup>[1]</sup> Cyanines have been used for many years for the photosensitization of silver halide particles in the photoimaging industry<sup>[2]</sup> and have more recently found application as mode-locking dyes in passively mode-locked lasers. Each of these applications depends to some extent on the details of

the photoisomerization for the particular cyanine used. Understanding the chemical and structural dependence of cyanine isomerization surfaces is a necessary step in gaining predictive control over these processes.

Cyanine photoisomerization has been studied extensively,<sup>[3-11]</sup> but remains understood to only a limited extent. The questions central to understanding photoisomerization of the cyanines are the identities of their ground state equilibrium geometries in solution and the identification of the isomerization coordinate. We will examine the structure and isomerization coordinate of two outwardly similar cyanines through measurement of their radiative and nonradiative population relaxation kinetics. Since these photolabile molecules have found use primarily in polar and/or viscous environments, we have chosen to study their behavior in the liquid phase, using 1-propanol and ethylene glycol as solvents. Both of these liquids exhibit extensive hydrogen bonding, but differ significantly in their bulk viscosities (~2 cP vs. ~20 cP). The viscosity difference between these two liquids is important in elucidating which energy relaxation pathways involve intramolecular motion and which step in a multi-step relaxation process is rate limiting. We have also performed semi-empirical molecular orbital calculations to understand the ground and excited state energy surfaces along which these molecules isomerize. Our calculated results are in excellent agreement with Rulliere's model for cyanine isomerization.<sup>[3]</sup> For the rotation of one polar cyanine end group moiety, these calculations predict a sharp excited state barrier. We believe the origin of this barrier is a "sudden polarization" effect,<sup>[12-15]</sup> and the presence of this unexpected excited state barrier provides an explanation for the anomalous relaxation kinetics of 3,3'-diethylthiadicarbocyanine iodide (DTDCI), the sulfur containing analog of DODCI.

### VIII.C. Experimental Results

We have studied the population relaxation kinetics of 3,3'-diethyloxadicarbocyanine iodide (DODCI, Figure VIII.1a) and 3,3'-diethylthiadicarbocyanine iodide (DTDCI, Figure VIII.1b) in 1-propanol and ethylene glycol, and have modeled the ground and excited state isomerization surfaces of these molecules using semi-empirical computational methods. The population relaxation dynamics of excited state ( $S_1$ ) processes were studied using stimulated emission. While the information content of the stimulated emission response is much higher than that of the corresponding spontaneous emission response,<sup>[16,17]</sup> the fundamental electronic relaxation processes that determine the stimulated emission response are the same as those for spontaneous emission. Recovery of the ground state population of DODCI and DTDCI was monitored through absorption band depletion recovery. Both of these techniques were performed with several picosecond time resolution.

The laser spectrometer used to acquire these data has been described before,<sup>[18]</sup> and we provide only the essential details here. The output of a mode-locked  $Ar^+$  laser operating at 514.5 nm (100 ps pulses, 82 MHz repetition rate) is used to excite synchronously two dye lasers. Each dye laser produces pulses of  $\sim 5$  ps duration, and the cross-correlation between output from the dye lasers is typically 10 ps FWHM. The pulses of one dye laser excite (pump) the sample and the pulses from the other dye laser interrogate (probe) the status of the excitation. The relative time registration between the two pulse trains is controlled mechanically. The wavelength of the pump laser is set to coincide with the absorption band of the particular cyanine under examination ( $\lambda_{\text{pump}} = 595$  nm for DODCI and  $\lambda_{\text{pump}} = 650$  nm for DTDCI). The wavelength of the probe laser

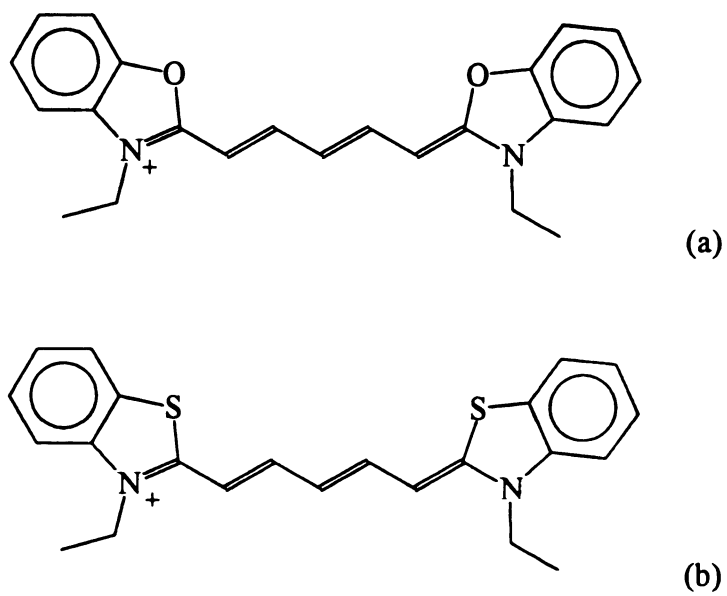


Figure VIII.1. (a) Structure of 3, 3'-diethyloxadecarboyanine iodide (DODCI). (b) Structure of 3, 3'-diethylthiadecarboyanine iodide (DTDCI). For each molecular the iodide counter ion has been omitted and only one resonance structure is shown.

determines the phenomenon under investigation. For stimulated emission measurements, the probe laser is set to lie within the spontaneous emission envelope at a wavelength not overlapped with the absorption band ( $\lambda_{\text{probe}} = 660$  nm for DODCI and  $\lambda_{\text{probe}} = 690$  nm for DTDCI). These wavelengths were chosen to also minimize overlap with cyanine vibrational resonances, but vibrational relaxation effects were observed at short times (<100 ps) for certain of our measurements.<sup>[17]</sup> For ground state depletion measurements, the probe laser wavelength coincides with the absorption band of the sample, in a region not overlapped with the spontaneous emission band ( $\lambda_{\text{probe}} = 590$  nm for DODCI and  $\lambda_{\text{probe}} = 640$  nm for DTDCI). For all measurements, the polarization of the probe laser pulse is set to  $54.7^\circ$  with respect to that of the pump laser pulse to eliminate contributions to the signal from rotational diffusion. The stimulated emission and ground state recovery signals are detected using a radio frequency modulation technique capable of shot noise limited sensitivity.<sup>[19-21]</sup>

The cyanines (DODCI and DTDCI) and the solvents were obtained from Aldrich Chemical Co. as their highest purity grade and were used without further purification. The temperature of the samples was controlled at  $300 \pm 0.1$  K and flowed through a 1 mm path length flow cell to minimize thermal contributions to the signal.

The isomerization surfaces for both the ground state ( $S_0$ ) and the first excited singlet state ( $S_1$ ) of DODCI and DTDCI were calculated using Hyperchem software. All calculations were performed at the semi-empirical level (AM1)<sup>[22-24]</sup> and configuration interaction (100 microstates) was used.

## **VIII.D. Results And Discussion**

The reason for continued scientific interest in the cyanines lies in the difficulties associated with understanding the details of their photoisomerization. The radiative relaxation pathways of DODCI have been studied extensively and, on the basis of these studies, its photoisomerization properties are thought to be well understood.<sup>[3,7,9]</sup> DODCI will serve as a benchmark in our work. Some of the measurements we report here for DODCI, however, are new findings that are consistent with the accepted model for its photoisomerization. Understanding the photoisomerization of DODCI does not provide an adequate explanation of this process for all cyanines. Changes in polyene chain length and heteroatom identity can modify the optical and vibrational response<sup>[25]</sup> and, possibly the photoisomerization surfaces of cyanines. We focus here on the effect of heteroatom substitution for dicarbocyanines. In contrast to DODCI, the photoisomerization of DTDCI has received little experimental or theoretical attention. We demonstrate here, using both experimental data and semi-empirical calculations, that despite the outward similarities of DODCI and DTDCI, their photoisomerization properties are markedly different.

### **VIII.D.1. DODCI**

Rulliere developed a model for the ground and excited state isomerization surfaces of DODCI,<sup>[3]</sup> and a schematic representation of this model is presented in Figure VIII.2. The population relaxation kinetics of this system can be modeled easily.

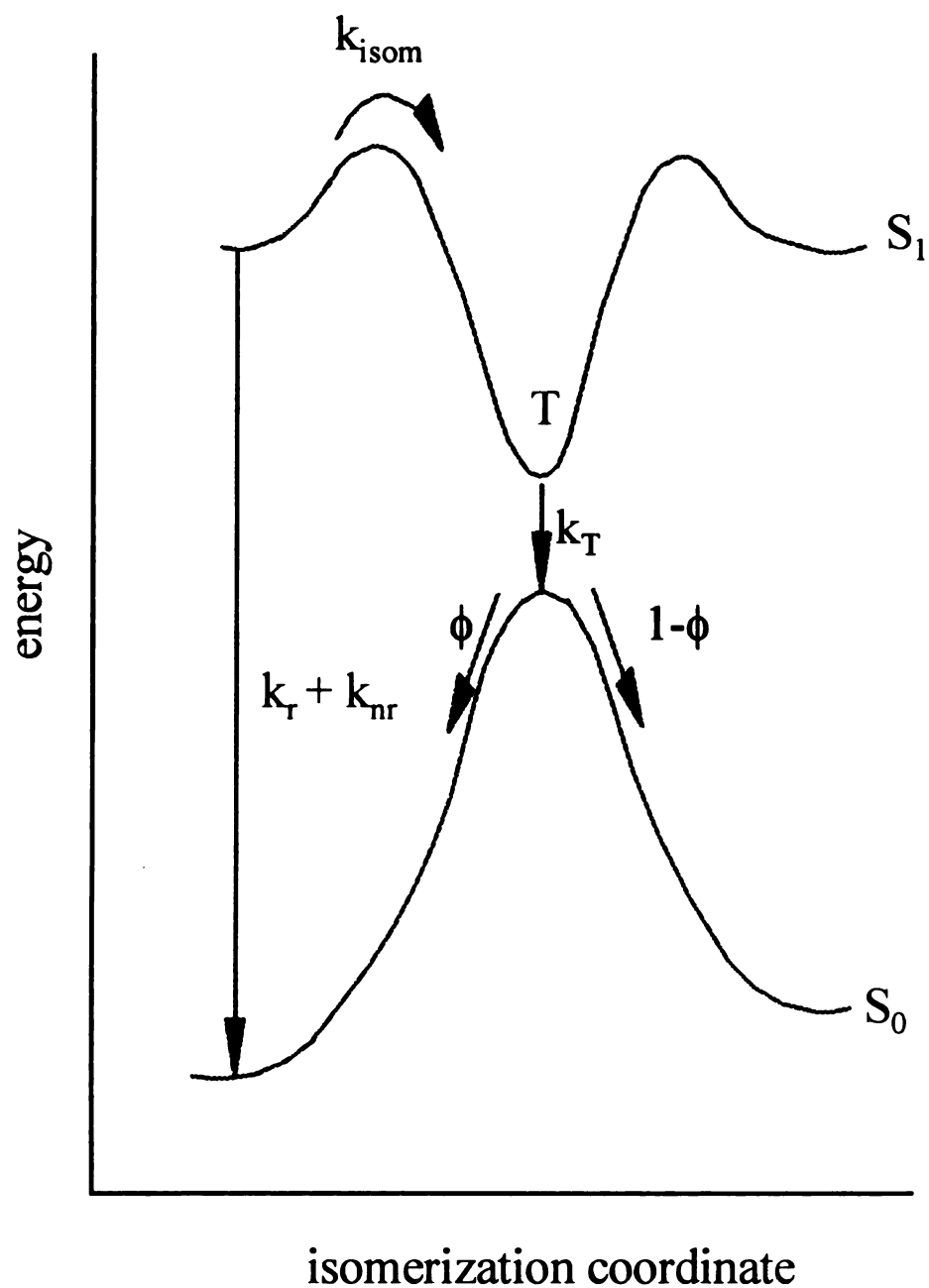


Figure VIII.2. Schematic of the dependence of isomerization surface energy for  $S_0$  and  $S_1$ . The model was developed initially by Rulliere (Rulliere, C.; *Chem. Phys. Letters*, **43**, 303 (1976)). Constants and quantities shown on the diagram are described in the text.

$$\frac{dS_1}{dt} = -(k_r + k_{nr} + k_{isom})S_1$$

$$\frac{dT}{dt} = k_{isom}S_1 - k_T T \quad \text{[VIII.1]}$$

$$\frac{dS_0}{dt} = (k_r + k_{nr})S_1 + \phi k_T T$$

where  $k_r$  is the radiative decay rate constant from  $S_1$ ,  $k_{nr}$  is the nonradiative decay rate constant,  $k_{isom}$  is the rate constant for crossing the excited state barrier,  $T$  is the twisted intermediate excited state,  $k_T$  is the decay rate constant for  $T$ , and  $\phi$  is the branching ratio for decay of  $T$  to either of the possible isomeric ground state structures. The integration of this series of coupled rate equations is straightforward, and has been reported before,<sup>[26]</sup>

$$S_1(t) = S_1(0) \exp(-k_\Sigma t)$$

$$T(t) = \frac{S_1(0)k_{isom}}{k_T - k_\Sigma} \left[ \exp(-k_\Sigma t) - \exp(-k_T t) \right]$$

[VIII.2]

$$S_0(t) = S_0(0) + S_1(0) \left\{ \begin{array}{l} \frac{k_r + k_{nr} + \phi k_{isom}}{k_\Sigma} + \frac{\phi k_{isom}}{k_T - k_\Sigma} \exp(-k_T t) \\ + \frac{k_r + k_{nr} - \phi k_T}{k_T - k_\Sigma} \exp(-k_\Sigma t) \end{array} \right\}$$

$$k_\Sigma = k_r + k_{nr} + k_{isom}$$

The implicit assumptions made in the solution of these equations are that excitation of  $S_1$  is instantaneous, there is insignificant population of the excited state isomer, and that exchange between the ground state isomers is negligible on the time scale of these relaxation processes. The first assumption is valid because of the short laser pulses we use. The second assumption is valid because we photoselect almost exclusively the so-

called "normal form" of DODCI by exciting at 595 nm. The absorption due to the photoisomer represents ~1% of the total absorption of DODCI at this wavelength.<sup>[7]</sup> The ground state barrier for DODCI has been measured to be 14 kcal/mol and thus the third assumption is valid.<sup>[3]</sup>

These equations predict that the stimulated emission response should decay as a single exponential and the ground state population should recover as a double exponential, with contributions from both direct  $S_1$  relaxation and relaxation through the twisted intermediate excited state. Our experimental data for DODCI in 1-propanol are shown in Figure VIII.3, and these data reveal a single exponential population decay of  $S_1$  and a double exponential recovery of  $S_0$ . The data for DODCI in ethylene glycol (not shown) are qualitatively the same, only with slightly different pre-exponential factors and decay time constants. The decay times and pre-exponential factors for DODCI in 1-propanol and ethylene glycol are presented in Table VIII.1. It is important to note that, for a given solvent, the slow ground state recovery time of DODCI is the same, to within the experimental uncertainty, as the stimulated emission decay time. This finding indicates that, for DODCI,  $k_{nr}$  is a direct relaxation process to  $S_0$ , *i.e.* there are no intermediate states involved in the nonradiative relaxation from  $S_1$ . Because of this agreement, we can assign the fast response to  $k_T$ , a quantity that is independent of solvent viscosity. For us to observe the ground state recovery signal, the DODCI molecule must rotate from its twisted conformation subsequent to relaxation from T. If intramolecular motion of the DODCI molecule was the rate limiting step in this relaxation, then we would observe a viscosity dependence to the fast relaxation. The absence of a discernible viscosity dependence of  $k_T$  shows that depopulation of the twisted intermediate excited state, T, and

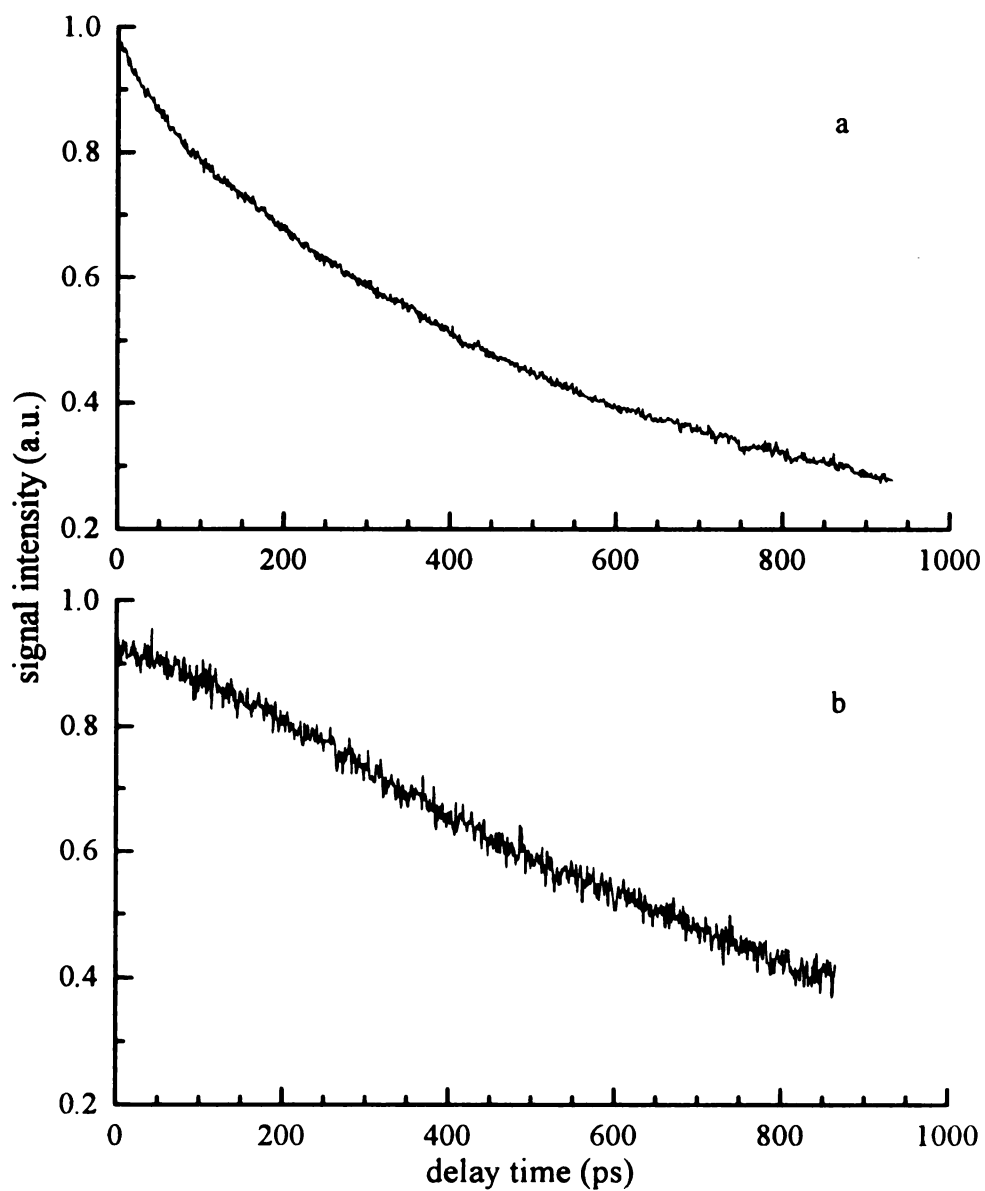


Figure VIII.3. (a) Ground-state recovery signal for DODCI in 1-propanol. (b) Stimulated emission decay signal for DODCI in 1-propanol. For both data sets the best fit parameters are given in Table VIII.1.

solvent	ground state recovery times (ps) and pre exponential factors		stimulated emission decay times (ps) and pre-exponential factors	
1-propanol	$\tau_1=144 \pm 48$ ps $a_1=0.20 \pm 0.07$	$\tau_2=917 \pm 95$ ps $a_2=0.79 \pm 0.07$	$\tau = 953 \pm 27$	N/A
ethylene glycol	$\tau_1=149 \pm 74$ ps $a_1=0.15 \pm 0.05$	$\tau_2=1016 \pm 65$ ps $a_2=0.85 \pm 0.07$	$\tau = 1040 \pm 40$	N/A

Table VIII.1. Ground state recovery times and stimulated emission decay times for DODCI in 1-propanol and ethylene glycol. The double exponential decay function is given by

$$f(t) = a_1 \exp\left(-t/\tau_1\right) + a_2 \exp\left(-t/\tau_2\right)$$

$$a_1 + a_2 = 1$$

The N/A listed for stimulated emission times indicates the best fit of these data is to a single exponential decay. These data represent averages of six individual determinations of each quantity. For each of the fits to the six determinations, the value of

$$\chi^2 = \frac{\sum_{i=1}^N (f(x_i) - y_i)^2}{N - n} \leq 10^{-4}.$$

not intramolecular rotation is the rate limiting step. It is possible that there is a weak viscosity dependence of the measured fast relaxation, but we can not discern it because of uncertainty in the experimental relaxation times.

### VIII.D.2. DTDCI

The population relaxation and recovery dynamics of DTDCI (Figure VIII.4 and Table VIII.2) are fundamentally different than those of DODCI. The most significant difference between DODCI and DTDCI lies in their excited state relaxation dynamics. We observe a single exponential decay from  $S_1$  for DODCI and a double exponential  $S_1$  population decay for DTDCI. In addition, the fast decay times measured for DTDCI depend on the solvent viscosity, in contrast to DODCI. The first question that must be addressed in understanding these data is whether or not the isomerization surfaces for DODCI and DTDCI bear any resemblance to one another. This question is difficult to answer solely on the basis of our experimental data because of the limited amount of information available from population relaxation and recovery measurements. For this reason we have attempted to answer this question through a series of calculations.

We have used semi-empirical Austin model 1 (AM1) calculations with configuration interaction to calculate the  $S_0$  and  $S_1$  torsional barriers for both DODCI and DTDCI.<sup>[22-24]</sup> In these calculations we have assumed that the isomerization is about one (or more) of the polyene chain bonds. We have considered the isomerization of conformers other than those with an all-*trans* polyene chain because, in solution there are likely to exist several stable conformers. Indeed, extensive work on  $\alpha,\omega$ -diphenylpolyenes has indicated the contribution of multiple conformers to both their static and transient

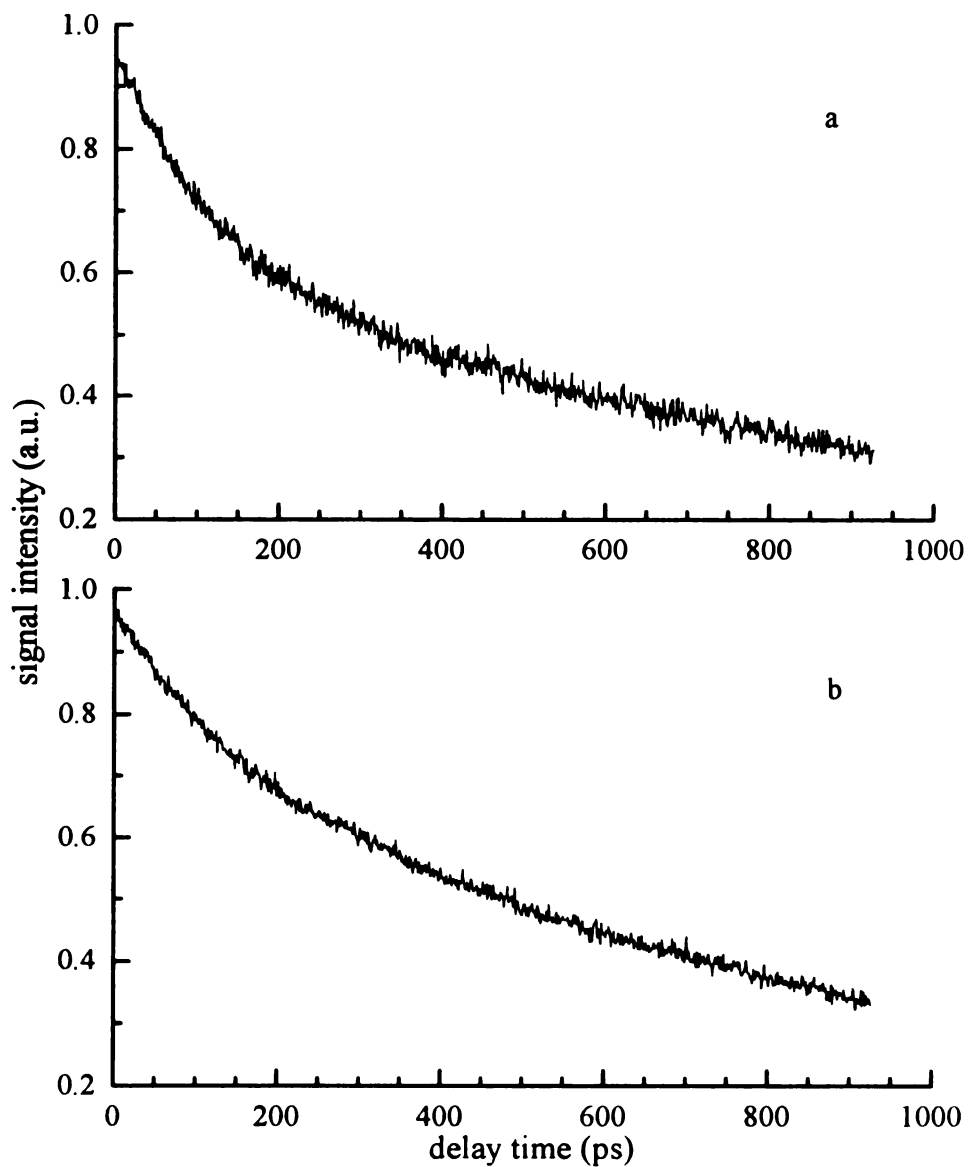


Figure VII.4. (a) Ground-state recovery signal for DTDCI in 1-propanol. (b) Stimulated emission decay signal for DTDCI in 1-propanol. For both data sets the best fit parameters are given in Table VII.2.

solvent	ground state recovery times (ps) and pre exponential factors		stimulated emission decay times (ps) and pre-exponential factors	
	1-propanol	$\tau_1=132 \pm 10$ ps $a_1=0.38 \pm 0.02$	$\tau_2=1416 \pm 66$ ps $a_2=0.62 \pm 0.02$	$\tau_1=144 \pm 21$ ps $a_1=0.24 \pm 0.02$
ethylene glycol	$\tau_1=255 \pm 19$ ps $a_1=0.47 \pm 0.02$	$\tau_2=1606 \pm 37$ ps $a_2=0.53 \pm 0.02$	$\tau_1=243 \pm 23$ ps $a_1=0.11 \pm 0.03$	$\tau_2=1185 \pm 32$ ps $a_2=0.89 \pm 0.03$

Table VIII.2. Ground state recovery times and stimulated emission decay times for DTDCI in 1-propanol and ethylene glycol. The double exponential decay function is the same as given in the caption to Table VIII.1.

optical responses.<sup>[27-29]</sup> We present in Figure VIII.5 our calculations of DODCI for sequential progressive rotation of the polyene chain single bonds, for both the  $S_0$  and the  $S_1$ . The bond rotation angle indexing axis is from  $0^\circ$  to  $540^\circ$ , as indicated in the figures. This total rotation angle represents sequential rotations from  $0^\circ$  to  $180^\circ$  for each of the three bonds rotated. For rotation about the two single bonds located within the polyene chain, we find that the ground state and excited state surfaces are in excellent semi-quantitative agreement with Rulliere's model,<sup>[3]</sup> with the ground state barrier calculated to be  $\sim 17$  kcal/mol (experimental:  $14.0 \pm 0.3$  kcal/mol),<sup>[3]</sup> and the excited state barrier calculated to be  $\sim 9$  kcal/mol (experimental:  $4.5 \pm 0.4$  kcal/mol).<sup>[3]</sup> For rotation about the bond connecting the polyene chain to the polar end group, we calculate both the  $S_0$  and  $S_1$  to exhibit a maximum at  $90^\circ$ . We attribute the maximum in the  $S_1$  to be a "sudden polarization" effect, and note that it is very sensitive to the torsion angle.<sup>[12-15]</sup> Barriers such as this have been predicted before for polyene chains, but experimental proof of their existence has been elusive. Our data for DODCI are consistent with isomerization about the polyene bonds where the energy surfaces are in agreement with Rulliere's model. We note that there are no  $S_1$  or  $S_0$  local minima in close angular proximity to the calculated  $S_1$  barrier, and thus it is not likely that this conformation contributes appreciably to the experimental distribution of DODCI isomers in solution. The calculated results for DTDCI (Figure VIII.6) are qualitatively similar to those for DODCI, with one crucial exception: There is a local energy minimum in both the  $S_0$  and  $S_1$  for DTDCI in close angular proximity to the calculated excited state barrier (indicated in Figure VIII.6). This subtle difference in the calculated surfaces provides an explanation for our experimental data.

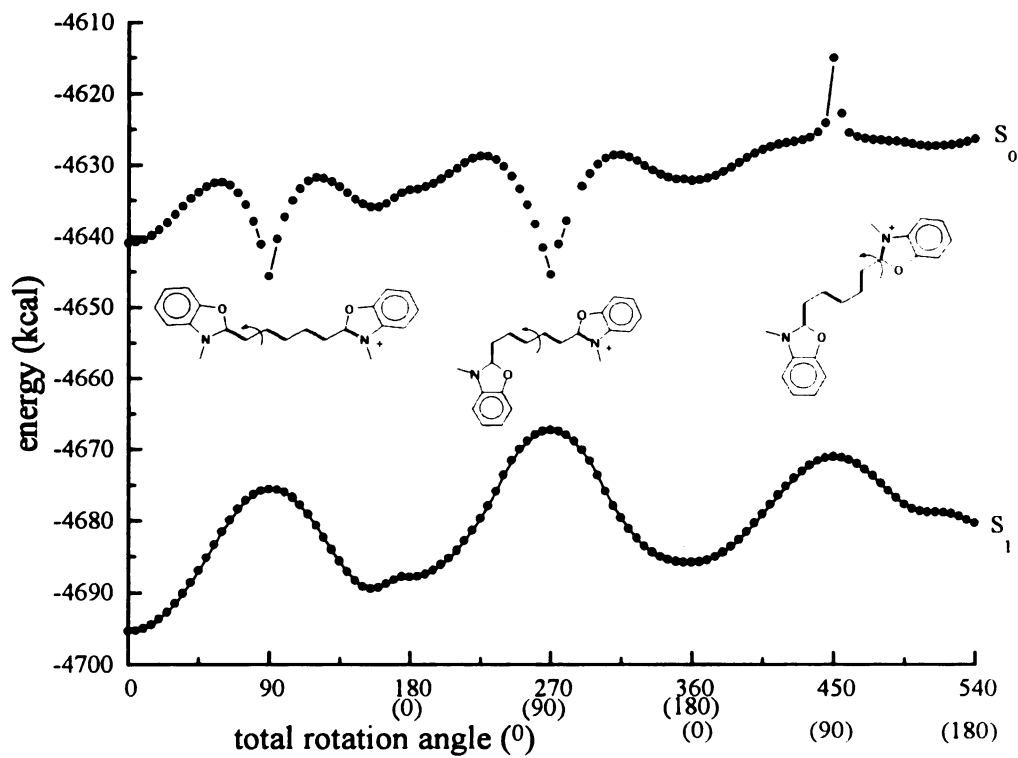


Figure VIII.5. Calculated isomerization surfaces for S<sub>0</sub> and S<sub>1</sub> DTDCI. Molecular structures indicate progressive isomerization about succeeding polyene bonds. The integrated rotation angle indicates the total extent of rotation, *i.e.*, the sum of the rotation angles for the rotated bonds. For each bond rotated, 180° was the maximum rotation, and the indices for each bond are indicated in parentheses.

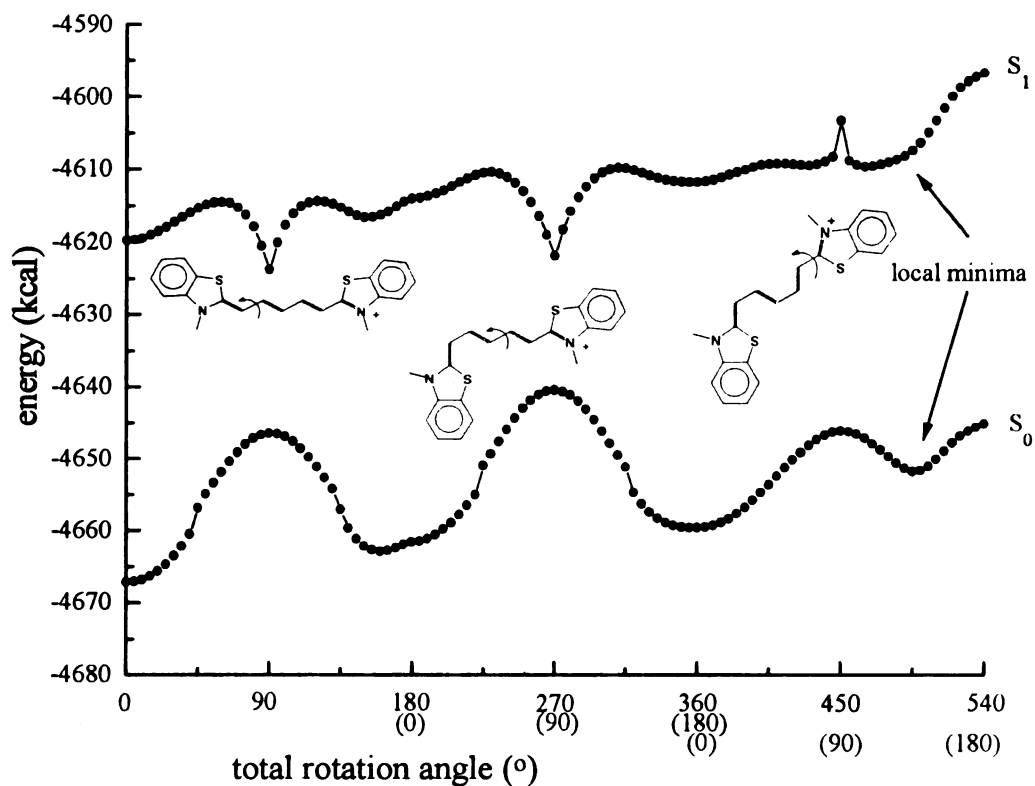


Figure VIII.6. Calculated isomerization surfaces for S<sub>0</sub> and S<sub>1</sub> DTDCI. Molecular structures indicate progressive isomerization about succeeding polyene bonds. The integrated rotation angle indicates the total extent of rotation, *i.e.*, the sum of the rotation angles for the rotated bonds. For each bond rotated, 180° was the maximum rotation, and the indices for each bond are indicated in parentheses. We indicate the local minima on the two potential surfaces that are responsible for the second component of the DTDCI stimulated emission decay.

The presence of a double exponential excited state population decay in DTDCI necessarily implies the simultaneous excitation of more than one conformer. Excited state decay, within the Rulliere model, for a given single conformation will be a first order process and therefore will decay in time as a single exponential. The presence of two conformers that do not interconvert efficiently, can, however, produce a double exponential stimulated emission decay, with one decay arising from each conformer. This mechanism is in contrast to that for DODCI, where the decay processes arise from a strongly coupled system. For DTDCI, we propose that the multiple exponential decays observed for  $S_1$  relaxation arise from effectively *uncoupled* relaxation processes. For DODCI, all of the stable ground state conformers are calculated to be approximately planar, while the same is not true for DTDCI. We calculate a local energy minimum for both  $S_0$  and  $S_1$  DTDCI in close angular proximity to the excited state barrier. Within our model, a fraction of the stimulated emission response arises from excitations and relaxations of molecules existing within these local minima, while the remainder of the stimulated emission response for DTDCI is contributed by conformers that follow the Rulliere model. The molecules not "trapped" in these local minima exhibit kinetic responses similar to DODCI. We attempt to distinguish these contributions based on the fractional contribution from the trapped conformer to the optical response. The fast ground state recovery and stimulated emission relaxation times are the same for DTDCI in a given solvent. Within the framework of our model, the fast stimulated emission decay arises from relaxation of the trapped conformer. We expect this (twisted) form to have a shorter lifetime than that of a planar conformer, and the viscosity-dependence of this lifetime can be understood in terms of the structural rigidity of the trapped conformer on

the time scale of the relaxation. This signal is 24% of the total stimulated emission response at  $t = 0$  in 1-propanol and 11% at  $t = 0$  in ethylene glycol. Within our uncertainty, the corresponding fast ground state recovery times are the same, but their fractional contribution to the total ground state recovery is 38% at  $t = 0$  in 1-propanol and 47% at  $t = 0$  in ethylene glycol. If the DTDCI data were simply two temporally overlapped single exponential decay processes, the pre-exponential factors for the ground state and excited state responses would be the same. The fact that they are different implies the contribution of an added decay process to the fast ground state response. The Rulliere model, as discussed above, predicts a double exponential recovery of  $S_0$ , with contributions from  $S_1$  and T. We believe that the contribution from T to the DTDCI ground state recovery data is obscured by the response of the trapped conformer. In principle, we could discern this contribution by fitting our data to three exponentials, but the uncertainty in our data would render results from such a fit virtually meaningless. The slow responses seen for DTDCI also contain important information. The slow ground state recovery time of DTDCI is longer than its stimulated emission decay time in both 1-propanol and ethylene glycol. For DTDCI,  $k_{nr}$  must therefore proceed through an intermediate state. The non-radiative decay from  $S_1$  DTDCI involves more steps than in DODCI.

### VIII.E. Conclusions

We have measured the transient population kinetics of two cyanine analogs in polar viscous solvents, and find that simple heterocyclic substitution gives rise to substantially different relaxation processes. We have calculated the  $S_0$  and  $S_1$

isomerization barriers for DODCI and DTDCI and find them to be largely similar, with an excited state barrier predicted for one particular conformation of each molecule. A possible explanation for the presence of this barrier is that it is a sudden polarization effect. The fundamental reason for the measured difference in population relaxation kinetics of DODCI and DTDCI lies in the presence of this sudden polarization barrier in close angular proximity to local  $S_0$  and  $S_1$  energy minima in DTDCI, and the absence of corresponding local minima on the DODCI isomerization surfaces. The observed population kinetics of DODCI can be explained in terms of a series of coupled relaxation steps. The data for DTDCI are consistent with the simultaneous response of multiple independent species. The reason for the energetic minimum at a  $\sim 45^\circ$  tilt of the polar end group in DTDCI is likely the larger physical size and orbital volume of the sulfur compared to oxygen, and its consequent interaction with a polyene chain proton.

#### VIII.F. References

1. Fleming, G. R.; Chemical Applications of Ultrafast Spectroscopy, Oxford University Press, 1986.
2. Walworth, V. K.; Mervis, S. H.; *Imaging Processes and Materials*, Ed. by J. Sturge, V. Walworth and A. Shepp, Van Nostrand Reinhold (1989).
3. Rulliere, C.; *Chem. Phys. Letters*, **43**, 303 (1976).
4. Zhu, X. R.; Harris, J. M.; *Chem. Phys.*, **142**, 301 (1989).
5. Velsko, S. P.; Waldeck, D. H.; Fleming, G. R.; *J. Chem. Phys.*, **78**, 249 (1983).
6. Fleming, G. R.; Knight, A. E. W.; Morris, J. M.; Robbins, R. J.; Robinson, G. W.; *Chem. Phys. Letters*, **49**, 1 (1977).
7. Baumler, W.; Penzkofer, A.; *Chem. Phys.*, **140**, 75 (1990).

8. Henrichs, P. M.; Gross, S.; *J. Am. Chem. Soc.*, **98**, 7169 (1976).
9. Duchowicz, R.; Scaffard, L.; Tocho, J. D., *Chem. Phys. Letters*, **170**, 497 (1990).
10. Baumler, W.; Penzkofer, A.; *Chem. Phys.*, **142**, 431 (1990).
11. Baumler, W.; Penzkofer, A.; *Chem. Phys. Letters*, **150**, 315 (1988).
12. Bonacic-Koutecky, V.; *J. Am. Chem. Soc.*, **100**, 396 (1978).
13. Salem, L.; *Acc. Chem. Res.*, **12**, 87 (1979).
14. Malrieu, J. P.; *Theoret. Chim. Acta*, **59**, 251 (1981).
15. Lam, B.; Johnson, R. P.; *J. Am. Chem. Soc.*, **105**, 7479 (1983).
16. Blanchard, G. J.; *J. Chem. Phys.*, **95**, 6317 (1991).
17. Hambir, S. A.; Jiang, Y.; Blanchard, G. J.; *J. Chem. Phys.*, **98**, 6075 (1993).
18. Blanchard, G. J.; *J. Chem. Phys.*, **87**, 6802 (1987).
19. Bado, P.; Wilson, S. B.; Wilson, K. R.; *Rev. Sci. Instrum.*, **53**, 706 (1982).
20. Andor, L.; Lorincz, A.; Siemion, J.; Smith, D. D.; Rice, S. A.; *Rev. Sci. Instrum.*, **55**, 64 (1984).
21. Blanchard, G. J.; Wirth, M. J.; *Anal. Chem.*, **58**, 532 (1986).
22. Dewar, M. J. S.; Zoebisch, E. G.; Healy, E. F.; Stewart, J. J. P.; *J. Am. Chem. Soc.*, **107**, 3902 (1985).
23. Dewar, M. J. S.; Dieter, K. M.; *J. Am. Chem. Soc.*, **108**, 8075 (1986).
24. Stewart, J. J. P.; *J. Comp. Aided Molec. Design*, **4**, 1 (1990).
25. Iwata, K.; Weaver, W. L.; Gustafson, T. L.; *J. Phys. Chem.*, **96**, 10219 (1992).
26. Alberty, R. A.; Miller, W. G.; *J. Chem. Phys.*, **26**, 1231 (1957).
27. Saltiel, J.; Sears, Jr., D. F.; Sun, Y.-P.; Choi, J.-O.; *J. Am. Chem. Soc.*, **114**, 3607 (1992).
28. Wallace-Williams, S. E.; Moller, S.; Hanson, K. M.; Goldbeck, R. A.; Kliger, D. S.; , W. A.; *Photochem. Photobiol.*, **56**, 953 (1992).

29. Wallace-Williams, S. E.; Moller, S.; Hanson, K. M.; Goldbeck, R. A.; Yee, W. A.; Kliger, D. S.; *J. Phys. Chem.*, **97**, 9587 (1993).

## IX. OVERVIEW

### IX.A. Conclusion

Up to this point, vibrational energy transfer measurements of perylene, 1-methylperylene, and tetracene have focused on the  $1370\text{cm}^{-1}$  ring breathing mode of these species. Additional studies that will further develop the understanding of the donor and acceptor species local organization and serve as a guide in developing theories of energy transfer may include measuring vibrational energy transfer efficiency for these probes at the  $1620\text{cm}^{-1}$  resonances, an energy that is close to degenerate water and carbonyl vibrations in selected ligands and solids. The carbonyl functional group is common to many biological systems such as membranes. The local organization of the membrane and proteins may be characterized by measuring changes in the Raman and IR frequencies as a function of temperature.<sup>[1,2]</sup> The phospholipids that comprise the membrane have three distinct regions because of their amphipathic nature; a hydrophilic zone, an interfacial zone, and hydrophobic zone.<sup>[3]</sup> In relation to the vibrational energy transfer efficiency of large chromophores reported in this thesis it is the interfacial region of the phospholipid that contains the carbonyl functional group. Thus, characterizing the vibrational energy transfer efficiency at the carbonyl resonance an understanding of the membrane structure in relationship to its functions may be developed.

In order to gain insight into the organization of the liquid state, the dependence of

vibrational energy transfer on solvent chain length, acceptor density, molecular alignment, multipolar interactions, and detuning effects have been investigated. My studies of each of these factors show that any theory of vibrational energy transfer<sup>[4]</sup> must take into account local ordering of the solvent about the solute. Since the Förster model<sup>[4,5]</sup> fails to do so, it may be inappropriate to apply it to the liquid phase when the critical radius of transfer ( $R_0$ ) is sufficiently small that an incomplete distribution of solvent orientations is sampled by the coupling process. Further study of the local order in solution, and the development of theories which take this order into account would be helpful in understanding the interactions of dissimilar molecules.

## **BIBLIOGRAPHY**

**BIBLIOGRAPHY**

1. Ira W. Levin, *Advances in Infrared and Raman Spectroscopy*, **11**, 1 (1984).
2. Burton J. Litman, E. Neil Lewis, Ira W. Levin, *Biochemistry*, **30**, 313 (1991).
3. S. J. Singer and G. L. Nicolson, *Science*, **175**, 720 (1972).
4. Yardley, J. T.; Introduction to Molecular Energy Transfer, Academic, New York, 1980.
5. Förster, Th; *Ann. Phys. Leipzig*, **2**, 55 (1948).